SRI International

Final Report • August 1994

MAGNETOSPHERIC–IONOSPHERIC POYNTING FLUX

Jeffrey P. Thayer, Research Physicist
Geoscience and Engineering Center

SRI Project 2432

Prepared for

National Aeronautics and Space Administration
Goddard Space Flight Center
Greenbelt, Maryland 20771

Attention: Gilbert Bullock
Contracting Officer's Technical Representative

Contract NAS5-31214

• Fax (415) 326-5512 • Telex

Final Report • August 1994

MAGNETOSPHERIC–IONOSPHERIC POYNTING FLUX

Jeffrey P. Thayer, Research Physicist
Geoscience and Engineering Center

SRI Project 2432

Prepared for

National Aeronautics and Space Administration
Goddard Space Flight Center
Greenbelt, Maryland 20771

Attention: Gilbert Bullock
Contracting Officer's Technical Representative

Contract NAS5-31214

Approved:

James F. Vickrey, Director
Geoscience and Engineering Center

Murray J. Baron, Vice President
Advanced Development Division

SRI International 333 Ravenswood Avenue • Menlo Park, CA 94025-3493 • (415) 326-6200 • FAX: (415) 326-5512 • Telex: 334486

1 SUMMARY OF RESULTS

Over the past three years of funding, SRI, in collaboration with the University of Texas at Dallas, has been involved in determining the total electromagnetic energy flux into the upper atmosphere from DE-B electric and magnetic field measurements and modeling the electromagnetic energy flux at high latitudes, taking into account the coupled magnetosphere–ionosphere system. This effort has been very successful in establishing the DC Poynting flux as a fundamental quantity in describing the coupling of electromagnetic energy between the magnetosphere and ionosphere. The DE-B satellite electric and magnetic field measurements were carefully scrutinized to provide, for the first time, a large data set of DC, field-aligned, Poynting flux measurements. Investigations describing the field-aligned Poynting flux observations from DE-B orbits under specific geomagnetic conditions and from many orbits, were conducted to provide a statistical average of the Poynting flux distribution over the polar cap. The theoretical modeling effort has provided insight into the observations by formulating the connection between Poynting's theorem and the electromagnetic energy conversion processes that occur in the ionosphere. Modeling and evaluation of these processes has helped interpret the satellite observations of the DC Poynting flux and improve our understanding of the coupling between the ionosphere and magnetosphere. One result of this effort is the generation of four manuscripts: two published and two submitted for publication. The titles for these manuscripts are given in Section 4 of this report, with the full manuscripts included as appendices. Highlights from these manuscripts are given in the following section.

2 PROJECT HIGHLIGHTS

2.1 NUMERICAL EXPERIMENT

Initial project efforts concerned the role of the ionospheric parameters on the electrodynamics, particularly the neutral wind. We performed a numerical experiment to determine whether the neutral wind at high latitudes could potentially influence the exchange of electromagnetic energy between the ionosphere and magnetosphere. The experiment examined the individual contribution to the high-latitude electrodynamics by evaluating separately the power per unit area generated by the neutral wind dynamo and the magnetospheric dynamo connected to the same load. From this analysis we found that the neutral winds contribute significantly to the high-latitude energetics in the polar cap and near the dawn and dusk sectors. Near the region of the magnetospheric convection reversal, the amount of electromagnetic energy flux from the

neutral wind can exceed that provided by the magnetospheric dynamo making the neutrals a dominant contributor to local electrodynamics. These results emphasize that care should be exercised in attributing features of high-latitude electrodynamics solely to magnetospheric and solar wind conditions.

2.2 DE-B POYNTING FLUX OBSERVATIONS: CASE STUDY

Work at the University of Texas at Dallas by J.B. Gary and R.A. Heelis involved the careful determination of the electric field and perturbation magnetic field from the DE-B satellite measurements. Significant effort was involved in determining the magnetometer baseline in an automated and physically defensible manner. The results from this effort led to the development of a routine processor for evaluating the field-aligned Poynting flux from the DE-B measurements. This was a necessary step toward determining unambiguously the Poynting flux from the DE-B satellite measurements. J. F. Vickrey and J. P. Thayer contributed to the early developments of the DE-B calculations and provided consultation on the interpretation of the measurement. The Poynting flux case study of a few chosen DE-B orbits illustrated that:

- The field-aligned Poynting flux is directed mainly downward into the high-latitude ionosphere with typical magnitudes of a few tens of mW/m^2 in the auroral zone and from zero to 10 mW/m^2 inside the polar cap.
- Regions of upward Poynting flux were observed over localized regions with magnitudes averaging less than 2 mW/m^2.

2.3 ELECTRODYNAMIC MODEL

Work at SRI involved modeling the exchange of electromagnetic energy between the ionosphere and magnetosphere to help interpret the DE-B Poynting flux observations. To describe the electrical properties of the high-latitude ionosphere, we constructed a numerical model, from the framework provided by the Vector Spherical Harmonic (VSH) model, that determines the ionospheric currents, conductivities, and electric fields including both magnetospheric inputs and neutral wind dynamo effects. This model development grew from the earlier question of whether an electrical energy source in the ionosphere was capable of providing an upward Poynting flux. The model solves the steady-state neutral wind dynamo equations and the Poynting flux equation to provide insight into the electrodynamic role of the neutral winds. The VSH model is based on a spectral representation of the output fields from NCAR Thermosphere/Ionosphere General Circulation Model (TIGCM) simulations. The NCAR-TIGCM is a time-dependent, three-dimensional model that solves the fully coupled, nonlinear, hydrodynamic, thermodynamic, and continuity equations of the neutral gas self-consistently with the ion energy, ion momentum, and ion continuity equations. A simulation is uniquely determined by the input parameters to the model (that is, EUV and UV fluxes, auroral particle precipitation, high-latitude ionospheric convection, and lower thermospheric tides).

During a model run, the particle fluxes and the cross polar cap potential may be specified to remain fixed throughout the 24-hour model simulation. This type of model simulation is referred to as a diurnally-reproducible state where the "UT effects" associated with the diurnal migration of the geomagnetic pole about the geographic pole are incorporated. Although the diurnally-reproducible state may not actually occur in nature (due to shorter term variations in the solar wind/magnetosphere interaction), the model simulation does provide a description of the global, UT-varying thermosphere–ionosphere system during a particular geophysical situation. A set of NCAR-TIGCM runs has been expanded into VSH model coefficients that can be used to represent a range of geophysical conditions.

Two conditions of the magnetospheric boundary are imposed. The first condition assumes the magnetosphere acts as a voltage generator. The neutral wind contribution to the ionospheric current is determined in this analysis. The second condition assumes the magnetosphere acts as a current generator so that any divergence in the ionospheric current due to the neutral wind sets up polarization electric fields in the high-latitude ionosphere. Under this condition, the neutral wind dynamo contribution to the polarization electric field can be determined. The calculation of the Poynting flux is not influenced by these approximations as it describes the flux of electromagnetic energy resulting from both the current and electric field patterns.

The modeling effort to determine the high-latitude energy flux has been able to reproduce many of the large-scale features observed in the Poynting flux measurements made by DE-2. Because the Poynting flux measurement is an integrated result of energy flux into or out of the ionosphere, we investigated the ionospheric properties that may contribute to the observed flux of energy measured by the spacecraft. The results are summarized in the appended manuscript, Appendix D: during steady state the electromagnetic energy flux, or DC Poynting flux, is equal to the Joule heating rate and the mechanical energy transfer rate in the high-latitude ionosphere. Although the Joule heating rate acts as an energy sink, transforming electromagnetic energy into thermal or internal energy of the gas, the mechanical energy transfer rate may be either a sink or source of electromagnetic energy. In the steady state, it is only the mechanical energy transfer rate that can generate electromagnetic energy and result in a DC Poynting flux that is directed out of the ionosphere.

The model simulation led to a number of conclusions.

- The electromagnetic energy flux is predominantly directed into the high-latitude ionosphere, with greater input in the morning sector than the evening sector by a factor of three.
- The Joule heating rate accounts for much of the electromagnetic energy deposited in the ionosphere, with the conductivity-weighted neutral wind contributing significantly to the Joule heating rate and thus to the net electromagnetic energy flux in the ionosphere.

- On average, the mechanical energy transfer rate contributes about 20% to the net electromagnetic energy flux in the dawn, dusk, and polar cap regions, acting as a sink of electromagnetic energy flux in the dawn and dusk sectors and a source of electromagnetic energy flux in the polar cap.
- An upward electromagnetic energy flux is found in the regions near the convection reversal boundaries. This flux is due to the mechanical energy transfer rate exceeding the Joule heating rate. The upward electromagnetic energy flux was found to be small partly due to the relationship of the conductivity-weighted neutral wind to the imposed electric field and partly due to the Joule heating rate increasing irrespective of the source of electromagnetic energy flux.

2.4 DE-B POYNTING FLUX OBSERVATIONS: STATISTICAL STUDY

Using DE-B data of ion drift velocities and magnetic fields, the field-aligned Poynting flux for 576 orbits over the satellite lifetime were calculated. The data was sorted for interplanetary magnetic field conditions (northward and southward IMF) and geomagnetic activity ($K_p \leq 3$ and $K_p > 3$) and binned by invariant latitude and magnetic local time. In general, it was found that the average Poynting flux is directed into the ionosphere over the entire polar cap indicating electric fields of magnetospheric origin generally dominate. The dawnside auroral zone generally has the largest Poynting flux values in the polar cap, exceeding 6 mW/m^2. We also investigated the distribution of upward Poynting flux and found it never exceeded 3 mW/m^2 over the entire polar cap. An interesting feature in the DE-B data set is the significant occurrence and magnitude of upward Poynting flux in the predawn sector during periods of southward IMF and high K_p conditions.

3 RECOMMENDATIONS

Project results have led to a number of recommendations concerning future modeling efforts and satellite measurements. We demonstrated that the measurement of the electromagnetic energy flux is fundamental in studying the electrodynamic coupling between the magnetosphere and ionosphere at high latitudes. Thus, future satellite missions designed to investigate high-latitude electrodynamics should be equipped with the proper instrumentation to determine the electric field and perturbation magnetic field so that routine measurements can be made of this quantity. These measurements inherently account for the electromagnetic contributions made by the neutral wind and conductivity to the overall electrodynamics. However, the measurements are limited to one dimension along the satellite track and therefore assume the horizontal divergence in the Poynting flux is negligible. This assumption and the steady-state condition must be a consideration when making the evaluation. The determination of accurate

perturbation magnetic field vectors is the major procedural obstacle to methodically establishing the Poynting flux from satellite data. The perturbation magnetic field is susceptible to spacecraft attitude errors and errors in the background magnetic field used to determine the perturbation field.

A better description of the Poynting flux, particularly when upward, is necessary to properly model the coupling between the ionosphere and magnetosphere. The modeling effort performed under this project described in detail the interplay of the ionosphere with the magnetospheric inputs but lacks the feedback to the magnetosphere, mainly due to the limited understanding of the generator characteristics of the magnetosphere. This aspect should be pursued further to provide more realistic boundary conditions and to improve the understanding of how the ionosphere may influence the response of the magnetosphere.

4 SCIENTIFIC REPORTS

A paper describing the initial modeling effort of the influence of the neutral winds on the high-latitude energetics has been published: Thayer, J.P., and J.F. Vickrey, "On the Contribution of the Thermospheric Neutral Wind to High-Latitude Energetics," *Geophys. Res. Lett.*, 19, No. 3, 265-268, 1992. (See Appendix A.)

A paper describing the technique and giving examples of Poynting flux measurements from DE-2 has been published: Gary, J.B., R.A. Heelis, W.B. Hanson, and J.A. Slavin, Field-Aligned Poynting Flux Observations in the High-Latitude Ionosphere, *J. Geophys. Res.*, 87, 11417-11427, 1994. (See Appendix B.)

A paper describing the distribution of the Poynting flux measurements from DE-2 has been submitted: "Summary of Field-Aligned Poynting Flux Observations From DE 2," by J.B. Gary, R.A. Heelis, and J.P. Thayer. (See Appendix C.)

A paper describing the numerical results for the modeling study of the Poynting flux has been submitted: "Interpretation and Modeling of the High-Latitude Electromagnetic Energy Flux," by J.P. Thayer and J.F. Vickrey. (See Appendix D.)

APPENDIX A

Thayer, J.P., and J.F. Vickrey, "On the Contribution of the Thermospheric Neutral Wind to High-Latitude Energetics," *Geophys. Res. Lett.*, 19, No. 3, 265-268, 1992

Geophysical Research Letters

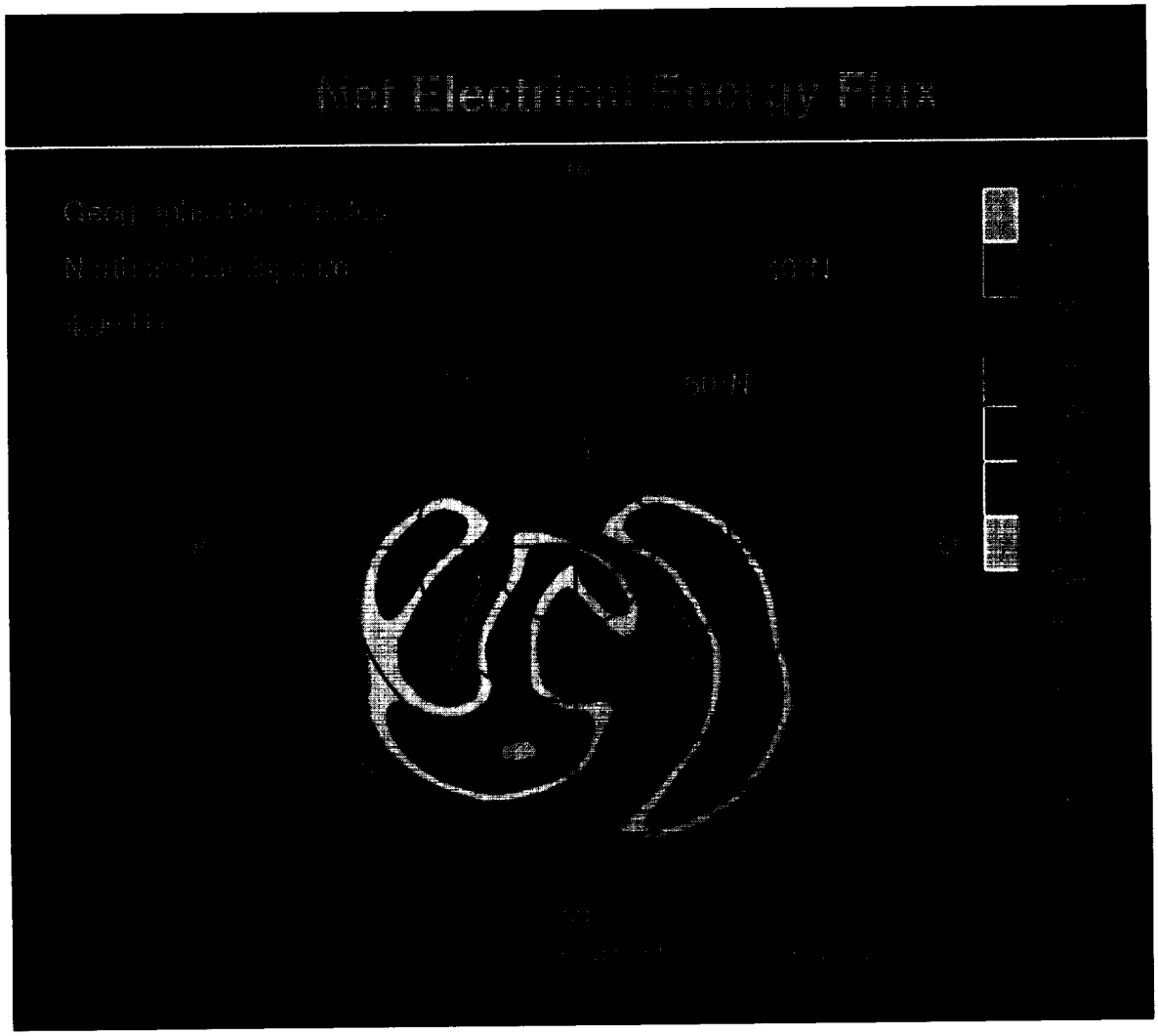

FEBRUARY 7, 1992

Volume 19 Number 3

AMERICAN GEOPHYSICAL UNION

Geophysical Research Letters

* * *

The Editors of **Geophysical Research Letters** welcome short, interesting contributions of broad geophysical interest. GRL Letters should be written in a style that makes their meaning and content clear to scientists from diverse geophysical disciplines. Ideally, the abstract and introduction should be easily understood by a beginning graduate student.

To submit a Letter, send 5 copies of the manuscript to one of the editors listed below. The covering letter should include the author's telephone number and the names, addresses, and telephone numbers of five potential referees.

Enrique Banda, Institute Jaume Almera CSIC, Marti i Franques S/N, 08028 Barcelona, SPAIN; telephone 011-34-3-3302716; FAX 011-34-3-4110012

James L. Burch, Geophysical Research Letters, Southwest Research Institute, P.O. Drawer 28510, San Antonio, TX 78228-0510 USA; telephone (512) 522-2526; telex 244846 . *Editorial Assistant:* William S. Lewis (512) 522-5261

K. D. Cole, La Trobe University, Bundoora, Victoria, 3083 AUSTRALIA; telephone 011-61-03-479-1111; FAX 011-61-03-478-5814

Jeff Dozier, Geophysical Research Letters, Earth Science Support Office, 600 Maryland Ave., SW, Suite 440, Washington, DC 20024 USA

Editorial Assistant: Deborah Critchfield (202) 479-0360; FAX (202) 479-2743

Friedrich Heller, Institut fur Geophysik, ETH-Honggerberg, CH-8093 Zurich, SWITZERLAND; telephone 011-41-1-377-4411; FAX 011-41-1-371-1864

Hiroshi Matsumoto, Radio Atmospheric Science Center, Kyoto University, Uji, Kyoto 611, JAPAN; FAX 011-81-774-31-8463

Peter L. Olson, Geophysical Research Letters, Department of Earth and Planetary Sciences, The Johns Hopkins University, Baltimore, MD 21218 USA

Editorial Assistant: Shirley Johnson (410) 516-7680; FAX (410) 516-7933

Robert M. Owen, Geophysical Research Letters, University of Michigan, Department of Geological Sciences, 1006 C.C. Little Building, Ann Arbor, MI 48109–1063 USA; telephone (313) 764-4278

Editorial Assistant: Maria M. Burdett (313) 764-4278

David Rees, Atmospheric Physics Laboratory, University College London, 67-73 Riding House Street, London W1P 7PP, UK: telephone 71-436-7614; FAX 71-436-7615

Manuscript Preparation. To expedite publication and hold down page charges, papers submitted to GRL are strictly limited to 4 printed pages, and Comments and Replys to 2 pages ordinarily.

GRL contributions first undergo the usual review process. Authors send papers to the editors as double-spaced typescript. Including text, title, abstract, references, tables and all graphics, these should be the equivalent (or less) of 16 double-spaced pages.

After acceptance, camera-ready copy must be sent to AGU as single-spaced typewriting or typesetting to these widths: for single columns 10.4 cm (4⅛ in.) maximum & 9.8 cm (3⅞ in.) minimum; for double columns 21.6 cm (8½ in.); and for broadside tables and figures 29.8 cm (11¾ in.). Words and illustrations together cannot exceed 239 cm (94 in.) in depth. Sans serif typefaces are unacceptable.

If any previously published figures are to be reproduced in GRL, the AGU office must have written permission from the copyright holder. Copies of these permissions must accompany the figures. Moreover, AGU cannot process or publish any camera-ready copy until a signed copyright transfer form is received at AGU.

Publications Office. For assistance with accepted manuscripts, color charges, typographic or typewriter specifications, or AGU publication policy, contact: Cynthia A. Duck, *Production Coordinator,* (202) 462-6900.
TWX 710-822-9300 FAX 202-328-0566

Judy C. Holoviak, *Director of Publications*

Publication Charges. Author's institutions are requested to pay a publication charge of $90 per journal page, which entitles them to 100 reprints.

Microform Publications. To help meet the stri page limit for GRL, supporting material, su as data tables, lengthy mathematical deriv tions, and extended discussion, can with tl editor's approval, be microfiched. (Photograp with a wide tonal range are not suitable.)

This supplemental material is included GRL's microfiche editions which are archiv by libraries. Individuals may order microfic supplements separately for a small char from AGU.

Subscriptions. AGU members may subscribe GRL in printed or microfiche editions for the personal use at an annual rate of $50 (U. members) and $69 (non-U.S. members). St dent members may subscribe at reduced rate Contact AGU for special rates for libraries ar other multiple-use institutions. Individu nonmembers interested in subscribing to GR for personal use should contact AGU. Singl issue prices are available on request.

Claims and Changes of Address. Send addre changes to AGU Customer Service Depar ment with at least 5 weeks' advance notic Claims due to insufficient notice of addre change or for such reasons as "missing fro files" cannot be serviced. For the U.S., lost ma should be reported within 90 days of the la day of the month of publication; for oth countries, within 150 days.

POSTMASTER: Send address changes t **Geophysical Research Letters,** American Geo physical Union, 2000 Florida Avenue, N.W Washington, D.C. 20009 USA.

Geophysical Research Letters (ISSN 0094 8276) is published twice a month for $50 pe year for members' personal use by the Amer ican Geophysical Union from 2000 Florid Avenue, N.W., Washington, D.C. 20009. Sec ond-class postage paid at Washington, D.C and additional offices.

2/7/9

GEOPHYSICAL RESEARCH LETTERS, VOL. 19, NO. 3, PAGES 265-268, FEBRUARY 7, 1992

ON THE CONTRIBUTION OF THE THERMOSPHERIC NEUTRAL WIND TO HIGH-LATITUDE ENERGETICS

J. P. Thayer and J. F. Vickrey

SRI International, Menlo Park, California

Abstract. Although the neutral wind's contribution to ionospheric electrodynamics is well-established at low latitudes, this electrical energy source has been largely ignored at high latitudes, owing to the assumed dominance of the magnetospheric dynamo contribution. Yet, the potential for exchange of electrical energy between the neutral wind dynamo and the magnetospheric dynamo is a direct consequence of the coupling between the two regions by highly conducting magnetic field lines. The integral nature of this coupling precludes the direct separation of the neutral wind and solar wind contributions to the observed electrodynamics. Therefore, to gain some insight into their relative importance, we have performed a simple numerical experiment in which the two dynamos are individually connected to a fixed load and their energetics evaluated separately. To determine the electrical energy flux supplied by the magnetosphere, we treat it as a voltage generator and the ionosphere as a resistive load. The available electrical energy flux generated by the neutral wind dynamo is determined from the mechanical energy stored within an established neutral wind field. This exercise has led to a number of conclusions, including: i) The neutral wind dynamo contributes significantly to high-latitude energetics, particularly in the central polar cap; and ii) In the region near the plasma convection reversal boundary, the amount of energy flux available from the neutral wind dynamo can exceed that provided by the magnetospheric dynamo.

1. Introduction

The solar wind interaction with the earth's magnetosphere generates electric fields and currents that flow from the magnetosphere to the ionosphere at high latitudes. Consequently, the high-latitude neutral atmosphere is subject to the dissipation and conversion of electrical energy to thermal and mechanical energy through Joule heating and Lorentz forcing. As a result of the mechanical energy stored within the neutral wind (caused in part by Lorentz- and pressure gradient-forces setup by the magnetospheric flux of electrical energy), currents can be generated in the ionosphere through the neutral wind dynamo mechanism.

The neutral wind dynamo has been largely ignored in most studies of high-latitude electrodynamics. Consequently, measurements of electrodynamic features, such as ion drifts in the F region, have been interpreted in terms of the interaction of the magnetosphere with the solar wind. However, the F region plasma drift is caused by an electric field that is the integrated result of all contributions to electrical energy along the magnetic flux tube. Thus, any polarization electric fields established by the neutral wind dynamo must be self-consistently combined with the magnetosphere contribution to the electric field. Similarly, any field-aligned currents generated by neutral dynamo action must feedback on the magnetospheric current system. Yet, the integral nature of these processes precludes the neutral wind contribution from being directly separable from the net electric field and current. By the same token, the characteristics resulting solely from the magnetospheric dynamo cannot be separately determined from observations of the plasma drift and field-aligned current patterns alone.

In this paper, we describe a numerical experiment in which the two dynamos are individually connected to a fixed load and their energetics evaluated separately. This approach compares the power per unit area of two separate generators, as shown schematically in Figure 1a,b. Here, the available electrical energy flux contained in the neutral wind dynamo is calculated assuming current generator properties, i.e., Figure 1b. The electrical energy flux provided by the magnetospheric dynamo is calculated assuming voltage generator properties, i.e., Figure 1a. A comparison of the available electrical energy flux stored in the neutral gas motion with that provided by the magnetospheric dynamo indicates the maximum influence that the ionospheric dynamo can have on high-latitude energetics. This simple approach accounts for all the available electrical energy that could be provided by the neutral wind, but avoids the more difficult task of determining the current and electric field distributions generated by the neutral wind when the dynamos are coupled with realistic magnetospheric boundary conditions.

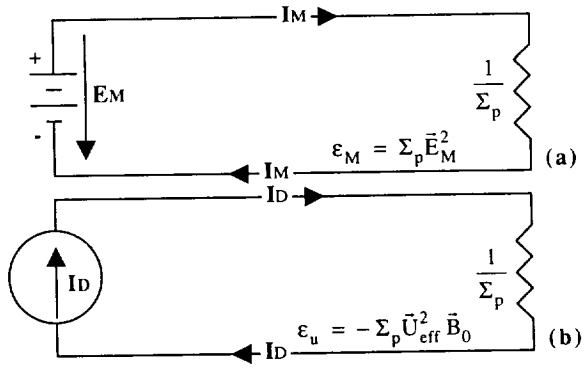

Fig. 1. Schematic circuit diagrams of the (a) magnetospheric and (b) neutral wind dynamos used in our analysis.

In the following section, we discuss the electrodynamic interaction at high latitudes in terms of the exchange of electrical energy between the ionosphere and magnetosphere. The subsequent section describes the analysis technique used to determine separately the flux of electrical energy provided by the neutral wind and solar wind dynamos. A discussion section addressing these calculations is followed by a conclusion section.

Paper number 91GL02868
0094-8534/92/91GL-02868$03.00

2. Approach

Because this investigation of ionospheric electrodynamics deals with the interactive coupling of the thermosphere, ionosphere, and magnetosphere, we approach the problem from an electrical energy viewpoint for the entire system. We use an MHD approach, because we are concerned with the total energy of the system, rather than the internal redistribution of energy among individual particles.

Following the energy conservation law for electromagnetic fields (e.g., Bittencourt, 1986), the local time rate of change of the electromagnetic energy density, W, stored in a system is given as

$$\frac{\partial W}{\partial t} + \iiint_V \nabla \cdot \left(\frac{\vec{E} \times \vec{B}}{\mu_0} \right) dV + \iiint_V \left(\vec{j} \cdot \vec{E} \right) dV = 0 \qquad (1)$$

where $\vec{E}$ is the electric field, $\vec{B}$ is the magnetic field, μ_0 is the permeability of free space, and $\vec{j}$ is the current density. The second term is the divergence of the electromagnetic energy (Poynting) flux within the volume, while the third term is the volume energy transfer rate. For the case where the sources remain constant and the stored electromagnetic energy within the volume is unchanged, the volume integral of the divergence in the Poynting flux provides a valuable measure of energy flow *into* or *out of* the system. For this case, Eq. (1) may be written using Gauss' law as

$$-\iiint_V \nabla \cdot \left(\frac{\vec{E} \times \vec{B}}{\mu_0} \right) dV = \iint_S \vec{P} \cdot \hat{n} \, ds = \iiint_V \vec{j} \cdot \vec{E} \, dV \qquad (2)$$

where $\vec{P}$ is the Poynting flux, $\hat{n}$ is a unit vector normal to the surface of the volume directed positive inward, $\vec{j}$ is the total current density, and $\vec{E}$ is the total electric field. Thus, for steady-state conditions, the net Poynting flux of energy across the surface of the volume (parallel to $\hat{n}$) must be equal to the energy transfer rate within the volume.

Recently, Knudsen (1990) and Kelley et al. (1991) have used measurements from the HILAT satellite to determine the divergence in the magnetospheric Poynting flux. While such measurements do not separate the various electrical contributions from the individual dynamo systems, they do provide an indication of whether the flux of electrical energy is *into* or *out of* the ionosphere. In this regard, a measurement of energy flux out of the ionosphere signifies the dominance of the neutral wind dynamo. Knudsen (1990) and Kelley et al. (1991) have presented such satellite observations of net *outward* Poynting flux.

The energy transfer rate determines the rate of electrical energy conversion, dissipation, or generation within the volume. If electrical energy is generated within the volume, $\vec{j} \cdot \vec{E}$ is negative and, therefore, the divergence of the Poynting flux is positive. If electrical energy is dissipated as heat or converted to mechanical energy within the volume, $\vec{j} \cdot \vec{E}$ is positive and, therefore, the divergence of the Poynting flux is negative. To further elucidate this point, the energy transfer rate within the volume can be written as,

$$\iiint_V \vec{j} \cdot \vec{E} \, dV = \iiint_V \left\{ \vec{j} \cdot \vec{E}' + \vec{u}_n(z) \cdot \left(\vec{j}(z) \times \vec{B}_0 \right) \right\} dV \qquad (3)$$

where the first term on the RHS is the Joule heating rate and the second term on the RHS is the mechanical energy conversion rate. Brekke and Rino (1978) also used the MHD energy equation to derive the relationship given in equation 3. The Joule heating rate is a positive definite quantity which determines the rate at which electrical energy is dissipated as heat in the neutral gas. The mechanical energy conversion rate can be of either sign depending on whether electrical energy is converted to mechanical energy (positive), or mechanical energy is converted to electrical energy (negative). Thus, from Eq. (2), a positive divergence in the Poynting flux in the ionosphere *requires* that the neutral wind have a component directed opposite to Ampere's $\vec{j} \times \vec{B}$ force.

3. Analysis

Herein, we analyze separately and independently the electrical energy flux provided to the ionosphere by the magnetospheric dynamo and that available from an already established neutral wind field. The established neutral wind field is determined by the time-dependent, three-dimensional NCAR Thermosphere/Ionosphere General Circulation Model (NCAR-TIGCM) which solves the full, coupled, nonlinear, hydrodynamic, thermodynamic, and continuity equations of the neutral gas coupled to an aeronomic scheme of the ionosphere (Roble et al., 1988). In the TIGCM formulation, the magnetosphere is treated as a generator delivering a fixed voltage to the ionosphere, i.e., Figure 1a. There is no electrodynamic feedback to the magnetospheric electric field by the thermospheric neutral wind generated during the simulation. As a result, the electrical energy flux provided by the magnetosphere can be determined given the ionospheric conductivity distribution. Owing to the lack of electrodynamic feedback in the model, electrical energy is stored as mechanical energy in the "established" neutral wind.

The model is run until the output reaches a diurnally-reproducible state, providing output at 25 different pressure levels (ranging in altitude from approximately 100 - 500km) on a 5° geographic grid. For this study, a specific model run has been chosen to simulate solar maximum, summer solstice conditions with a cross-polar-cap potential of 90 kV and a hemispheric power of 33 GW. The Vector Spherical Harmonic (VSH) model of Killeen et al. (1987), originally designed to make the NCAR-TIGCM output more manageable, is used to provide the output variables from the model run. Calculations of the power per unit area, or the electrical energy flux, for each dynamo connected to the same load are performed at each grid point to elucidate their relative importance in high-latitude energetics as a function of latitude and local time.

The magnetospheric electric field is determined directly from the Heelis ion convection model (Heelis et al., 1982) and used in the magnetospheric electrical energy flux calculation. In determining the respective magnetospheric and ionospheric electrical energy fluxes, the conductivity profile is held constant with latitude and local time so that the results can be unambiguously related to the neutral wind and magnetospheric dynamos. The conductivity profile is determined from a double Chapman layer with an F layer centered at 300 km with a peak density of 1.0×10^6 cm^{-3} and an E layer at 130 km with a peak density of 1.0×10^5 cm^{-3}. The neutral atmosphere model used for the conductivity calculation is MSIS-86 for conditions of solar maximum, summer solstice, moderate activity at 4:00 UT.

The electrical energy flux supplied by the magneto-

spheric dynamo to the high-latitude ionosphere can be determined by assuming this source to be a voltage generator connected via highly conducting magnetic field lines to an ionospheric load (Fig 1a). Under these conditions, the expression describing the electrical energy flux from the magnetospheric dynamo is

$$\varepsilon_m = \Sigma_p \vec{E}_m^2 = \Sigma_p \vec{V}_I^2 \vec{B}_0^2 \quad (4)$$

where Σ_p is the height-integrated Pedersen conductivity and $\vec{E}_m$ is the externally imposed magnetospheric dynamo electric field described by the Heelis model, $\vec{V}_I$ is the $\vec{E}_m \times \vec{B}_0$ drift velocity, and $\vec{B}_0$ is the background geomagnetic field.

A neutral wind dynamo acts (initially, at least) as a current generator (Fig 1b). The available electrical energy flux from the ionospheric dynamo is contained in the mechanical energy term of equation (3):

$$\varepsilon_u = \int_z \vec{u}_n(z) \bullet \left(\vec{j}(z) \times \vec{B}_0\right) dz = -\int_z \vec{j}(z) \bullet \left(\vec{u}_n(z) \times \vec{B}_0\right) dz \quad (5)$$

Accounting for only the neutral wind contribution to the current, Ohm's law can be written

$$\vec{j}(z) = \sigma_p(z)\left(\vec{u}_n(z) \times \vec{B}_0\right) + \sigma_h(z)\hat{b} \times \left(\vec{u}_n(z) \times \vec{B}_0\right) \quad (6)$$

Substituting this form of Ohm's law into equation 5, the available electrical energy flux generated solely by neutral motion in a conducting ionosphere can be expressed as

$$\varepsilon_u = -\int_z \sigma_p(z)\left(\vec{u}_n(z) \times \vec{B}_0\right)^2 dz \quad (7)$$

This equation can be expressed in a form similar to equation 4 by applying the mean value theorem to the height integration, since σ_p is positive definite. The square of the effective neutral wind follows as

$$\vec{U}_{eff}^2 = \frac{\int_z \sigma_p(z)\, \vec{u}_n^2(z)\, dz}{\int_z \sigma_p(z)\, dz} \quad (8)$$

Importing these results into equation 7, we have

$$\varepsilon_u = -\Sigma_p \vec{U}_{eff}^2 \vec{B}_0^2 \quad (9)$$

which is helpful when comparing the electrical energy flux of the neutral wind dynamo to that of the magnetospheric dynamo.

4. Discussion

In our analysis, we have defined a volume which extends from 110 to 500 km in altitude. We consider this volume to consist of individual vertical magnetic flux tubes, each enclosing a 5° × 5° latitude/longitude bin. The volume is in geographic coordinates extending from the pole to the 40°N latitude circle. The energy flux (power per unit area) calculations are performed at each grid point assuming horizontal uniformity of the parameters within each 5° bin.

The electrical energy flux calculation for the magnetospheric dynamo is performed using the Heelis convection model and the previously described conductivity profile. This calculation determines the amount of electrical energy provided by the magnetospheric dynamo that is converted into thermal and mechanical energy in the ionosphere. The magnetospheric electrical energy flux is directed downward into the ionosphere. The result of this calculation is displayed in Figure 2 on a geographic latitude/local solar time grid extending in latitude from 40°N to the geographic pole at 4:00 UT. The contour interval is 2 mW/m^2 or 2 ergs/cm^2 sec. Significant downward (positive) electrical energy flux is confined to the high-latitude region with maxima coinciding with the dusk/dawn sunward convection, as well as with the antisunward polar cap convection. Two distinct minima in the electrical energy flux are evident which coincide with the reversal boundaries in the ion convection.

For the ionospheric dynamo, the maximum amount of electrical energy flux due to neutral gas motion that is available in the ionosphere is expressed in equation 9. The height integration is performed at each grid point over the altitude range from 110 to 500 km. The simulated neutral

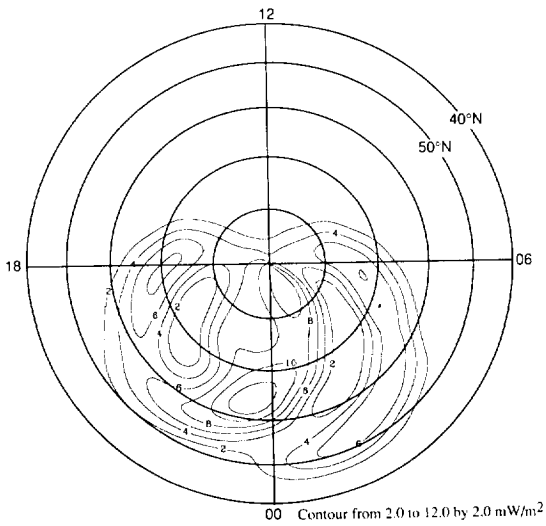

Fig. 2. Electrical energy flux into the ionosphere due to the magnetospheric dynamo displayed on a geographic latitude / local time grid extending from 40°N to the geographic pole at 4:00 UT with a contour interval of 2 mW/m^2.

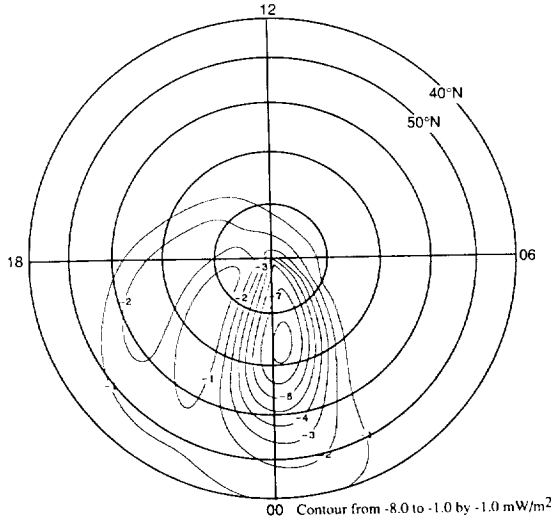

Fig. 3. Maximum electrical energy flux available in the ionosphere due to the neutral wind dynamo with the same format as Figure 2, except the contour interval is –1 mW/m^2.

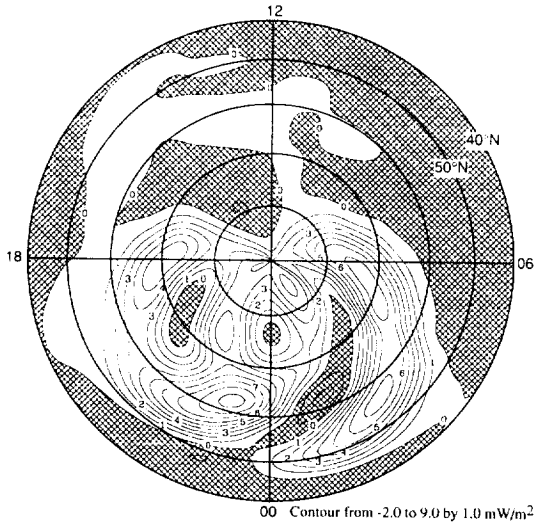

Fig. 4. Net electrical energy flux resulting from the addition of the two generators (same format as the earlier figures) with a contour interval of 1 mW/m^2. "Negative" energy flux is shaded, "positive" energy flux is shown in white.

winds are a result of pressure gradient forces (partly generated by Joule heating) and ion drag forces setup by the imposed convection field, as well as other hydrodynamic forces included in the NCAR-TIGCM. The available ionospheric electrical energy flux is negative if connected to a magnetospheric load. Herein, we connect the two generators to the same load but retain the sign convention to facilitate the comparison of their energetics. The negative electrical energy flux, determined from the effective neutral wind, is given in Figure 3 in the same format as Figure 2, except the contour interval is –1 mW/m^2 or -1 erg/cm^2 sec. This energy flux has a strong maximum in the high-latitude midnight sector and a weaker maximum in the dusk sector.

To assess the potential for either of these dynamos to dominate the energetics of the system, we can compare their magnitudes as a function of space. The energy fluxes from the two sources are added together in Figure 4. The positive net energy flux is shown by the white areas, while the negative net energy flux is depicted by the gray areas. The contour interval is 1 mW/m^2 or 1 erg/cm^2 sec. As one would expect, the high-latitude region has a net energy flux that is directed downward, indicating that the magnetospheric dynamo dominates globally and that electrical energy is being converted to other forms of energy in the ionosphere. However, there are two distinct areas where the neutral wind-ionospheric dynamo can dominate locally. These regions coincide with the reversal area in the externally-driven ion convection pattern. Thus, in the vicinity of externally-imposed electric field reversals, the neutral wind is capable of providing a significant source of electrical energy, which can, in principal, dominate the plasma electrodynamics. From these simple energy calculations alone, we cannot say how the electrical energy from the neutral wind will be manifested, i.e., whether it modifies the current system, the polarization electric field, or both. To do so requires specific boundary conditions and detailed information on the magnetospheric "load." Nonetheless, it is clear from Figure 4 that the ionospheric electrodynamics are strongly influenced by neutral motion in the thermosphere.

5. Conclusions

We have addressed the significance of the neutral wind dynamo as a contributor to ionospheric energetics at high latitudes. Our approach was to determine separately the electrical energy flux from the magnetospheric dynamo and the maximum electrical energy flux available due to the neutral wind dynamo, neglecting the natural feedback processes between the two. For the conditions considered here, the following conclusions have been reached:

- The neutral wind dynamo contributes significantly to the flux of energy exchanged between the magnetosphere and thermosphere, particularly in the central polar cap.
- In the region of the magnetospheric convection reversal, the amount of available energy flux from the neutral wind dynamo can exceed that provided by the magnetospheric dynamo making the neutrals a dominant contributor to local electrodynamics.
- For the above reasons, care should be exercised in attributing features of high-latitude electrodynamics solely to magnetospheric and solar wind conditions.

Acknowledgments. This work was supported by NASA Contract NAS5-31185, by NSF Cooperative Agreement ATM-88-22560, and by the Air Force Geophysics Laboratory under Contract F19628-90-K-0036. We would like to thank Dr. Rod Heelis for extremely helpful discussions and Dr. Tim Killeen and Rob Raskin for the VSH model code. We also appreciate the extensive effort and helpful suggestions made by both referees in evaluating this paper.

References

Bittencourt, J. A., *Fundamentals of Plasma Physics*, Pergamon Press, New York, 1986.

Brekke, A., and C.L. Rino, High-resolution altitude profiles of the auroral zone energy dissipation due to ionospheric currents, *J. Geophys. Res.*, 83, A6, 2517-2524, 1978.

Heelis, R.A., J.K. Lowell, and R.W. Spiro, A model of the high-latitude ionospheric convection pattern, *J. Geophys. Res.*, 87, 6339-6345, 1982.

Kelley, M.C., D.J. Knudsen, and J.F. Vickrey, Poynting flux measurements on a satellite: a diagnostic tool for space research, *J. Geophys. Res.*, 96, A1, 201-207, 1991.

Killeen, T.L., R.G. Roble, and N.W. Spencer, A computer model of global thermospheric winds and temperatures, *Adv. Space Res.*, 7, 207-215, 1987.

Knudsen, D. J., Alfven waves and static fields in magnetosphere/ionosphere coupling: in-situ measurements and a numerical model, Ph. D. thesis, Cornell University, 1990.

Roble, R.G., E.C. Ridley, A.D. Richmond, and R.E. Dickinson, A coupled thermosphere/ ionosphere general circulation model, *Geophys. Res. Lett.*, 15, 1325-1328, 1988.

(Received April 29, 1991
revised October 4,1991
accepted November 5, 1991)

APPENDIX B

Gary, J.B., R.A. Heelis, W.B. Hanson, and J.A. Slavin, Field-Aligned Poynting Flux Observations in the High-Latitude Ionosphere, *J. Geophys. Res.*, 87, 11417-11427, 1994

JOURNAL OF GEOPHYSICAL RESEARCH, VOL. 99, NO. A6, PAGES 11,417–11,427, JUNE 1, 1994

Field-aligned Poynting flux observations in the high-latitude ionosphere

J. B. Gary, R. A. Heelis, and W. B. Hanson

Center for Space Sciences, Physics Programs, University of Texas at Dallas, Richardson

J. A. Slavin

Laboratory for Extraterrestrial Physics, NASA Goddard Space Flight Center, Greenbelt, Maryland

Abstract. We have used data from Dynamics Explorer 2 to investigate the rate of conversion of electromagnetic energy into both thermal and bulk flow particle kinetic energy in the high-latitude ionosphere. The flux tube integrated conversion rate $\mathbf{E}\cdot\mathbf{J}$ can be determined from spacecraft measurements of the electric and magnetic field vectors by deriving the field-aligned Poynting flux, $S_{||}=\mathbf{S}\cdot\hat{B}_o$, where $\hat{B}_o$ is in the direction of the geomagnetic field. Determination of the Poynting flux from satellite observations is critically dependent upon the establishment of accurate values of the fields and is especially sensitive to errors in the baseline (unperturbed) geomagnetic field. We discuss our treatment of the data in some detail, particularly in regard to systematically correcting the measured magnetic field to account for attitude changes and model deficiencies. $S_{||}$ can be used to identify the relative strengths of the magnetosphere and thermospheric winds as energy drivers and we present observations demonstrating the dominance of each of these. Dominance of the magnetospheric driver is indicated by $S_{||}$ directed into the ionosphere. Electromagnetic energy is delivered to and dissipated within the region. Dominance of the neutral wind requires that the conductivity weighted neutral wind speed in the direction of the ion drift be larger than the ion drift, resulting in observations of an upward directed Poynting flux. Electromagnetic energy is generated within the ionospheric region in this case. We also present observations of a case where the neutral atmosphere motion may be reaching a state of sustained bulk flow velocity as evidenced by very small Poynting flux in the presence of large electric fields.

Introduction

The study of coupling processes between the Earth's magnetosphere and ionosphere is frequently aided by an examination of the energy flow between these regions. Poynting vectors determined from in situ electric and magnetic field measurements have been frequently used in the study of magnetospheric wave phenomena associated with micropulsations of the magnetic field. *Cummings et al.* [1978] performed such an analysis using ATS 6 data from geosynchronous orbit to establish the presence of standing hydromagnetic waves along the magnetic field. *Mauk and McPherron* [1980], again with ATS 6 data, used calculated Poynting vectors in their analysis of possible Alfven/ion cyclotron waves originating in the equatorial magnetosphere. More recently, *Erlandson et al.* [1990], *LaBelle and Truemann* [1992], and *Fraser et al.* [1992] calculated Poynting vectors from satellite data to establish the presence of electromagnetic ion cyclotron waves similar to those discussed by Mauk and McPherron [1980].

The use of Poynting flux determined from satellite measurements in an analysis of very large scale, high-latitude ionospheric activity was first proposed by *Knudsen* [1990] and shortly thereafter by *Kelley et al.* [1991]. These authors described in some detail the application of global Poynting flux determination from in situ measurements to the geophysical system comprised of the coupled magnetosphere and ionosphere. Using the principle of conservation of electromagnetic energy (Poynting's theorem), they demonstrated the possibility of determining the rate of energy conversion taking place in a volume extending from the satellite orbit down to the base of the ionosphere by examining the vertical component of the Poynting vector. The energy conversion rate $\mathbf{E}\cdot\mathbf{J}$ is related to the Joule heating rate of the plasma and the rate of momentum transfer between the ions and the neutral gas in the lower ionosphere. They also included results of such an analysis

Paper number 93JA03167.
0148-0227/94/93JA-03167$05.00

using data from the HILAT satellite at 800 km altitude. Our approach to the technique is similar to theirs with the exceptions that the volume to which Poynting's theorem is applied is a single flux tube in our case and we determine the field-aligned component of the Poynting vector rather than approximate it using the vertical component. We refer the reader to the Appendix of *Kelley et al.* [1991] for further details. The major assumption in applying Poynting's theorem to determine the rate of electromagnetic energy conversion using in situ measurements is the assumption that steady state conditions prevail. This ignores possible contributions from wave phenomena which are likely to be present in the high latitude ionosphere but which are likely to present a signature at DE 2 altitudes below the minimum scale size that we are considering in the present work (tens of kilometers).

The electric fields and currents which link the magnetosphere and ionosphere are generated by the dynamo action of plasma flowing through the ambient magnetic field. Electromagnetic energy in the high latitude ionosphere can come from two sources, one originating from the interaction of the solar wind and magnetosphere and the other originating in the ionosphere. The magnetospheric source can be considered as a dynamo directly connected to the polar cap at the highest magnetic latitudes which, under most conditions in the ionosphere, magnetosphere, and solar wind, will drive energy into the lower regions of the earth's atmosphere where the circuit is closed through the ionosphere. In these circumstances, the ionosphere acts as a resistive load to the magnetospheric generator, although it is not a passive resistive element in this circuit. The effect of the ionosphere on the global circuit is determined by the ionospheric conductivity and on the behavior of the neutral wind. Electromagnetic energy can also be produced within the high latitude ionosphere via the action of a neutral wind dynamo, principally in the E region. In this region the neutral atmosphere motion may be driven by solar heating but, more importantly, energy is "stored" in the neutral atmosphere at lower ionospheric altitudes through frictional coupling between the magnetosphere-driven plasma and the neutral gas in which it is embedded. Electric fields mapped from the magnetosphere impose a circulation pattern on the ions in the ionosphere. During prolonged times of strong interplanetary magnetic field (IMF) conditions, this circulation is transferred to the neutrals through collisions. If the IMF then changes its orientation, say from southward to northward, then the ions can be driven by electric fields in a different direction from that in which the neutrals are moving. The resulting ion motion will then be determined by the relative strengths of the newly established electric fields from the magnetosphere and the inertial and viscous effects of the neutral wind. If the electric field in the frame of reference of the neutral particles is small, then the ions may be driven by the neutral wind dynamo along the previously established convection pattern. Conceptually, these are the anticipated circumstances under which an upward directed Poynting flux may be observed in a reference frame corotating with the Earth.

The initial motivations behind an effort to calculate the large scale Poynting vector in the Earth's ionosphere have been to provide observations of the action of a neutral wind dynamo. *Lyons et al.* [1985] proposed a neutral wind dynamo as a current source in the polar cap during times of stagnant ion convection. Modeling efforts of neutral wind phenomenon have been carried out recentiy by *Deng et al* [1991] and by *Thayer and Vickrey* [1992]. These efforts have suggested the existence of regions of outward directed electromagnetic energy flux in the polar cap. *Fejer* [1983] also described a neutral wind dynamo effect, termed a disturbance dynamo, as an electric field driver at sub-auroral latitudes following the onset of geomagnetic storms. The dominance of these dynamos would be readily identifiable with field-aligned Poynting flux observations of sufficient accuracy.

Measurements from DE 2

A measurement of the Poynting vector is critically dependent on accurate measurements of the electric field and the magnetic field perturbation vectors. Accordingly, the bulk of the technical work involved in this research involves an analysis of the absolute magnitudes of the measured quantities, as well as their uncertainties, and the development of suitable techniques to render accurate calculations of the Poynting vector over the widest possible range of acquired DE 2 data.

We have taken some care to provide the highest quality derivation of the drift velocities. This is particularly important in the derivation of the ion drift velocity along the spacecraft x axis (ram) which involves a least squares analysis of the ion energy distribution measured by the retarding potential analyzer (RPA). A planar retarding potential analyzer was flown on DE 2 and this instrument is described in detail by *Hanson et al.* [1981]. Substantial variations in the spacecraft potential, $\phi_{s/c}$, are known to occur, for example, as the vehicle traverses regions of elevated electron temperature, which affect the derived ion velocities in a manner not generally compensated for in the RPA analysis [Anderson *et al*, 1994]. Changes in $\phi_{s/c}$ can alter the baseline values for the ram drift by 100 m/s or more, and we have modified the RPA analysis to account for these changes.

The components of the ion drift velocity perpendicular to the direction of the spacecraft velocity vector were measured using an ion drift meter, described by *Heelis et al.* [1981]. This measurement is also sensitive to $\phi_{s/c}$, although less so than the RPA, and changes in the ion arrival angle produced by a changing spacecraft potential are taken into account in determining the ion drift velocity vector. The ion drifts are then used to calculate the electric field under the assumption that $\mathbf{E} = -\mathbf{V} \times \mathbf{B}$. Comparisons between the values of the electric field measured directly by the Vector Electric Field Instrument and those derived from the ion drift

have shown generally very good agreement [Hanson *et al.*,1993].

Magnetic field measurements from DE 2 were made using a triaxial flux gate magnetometer, which has been described in detail by *Farthing et al.* [1981]. For determination of the Poynting vector, it is the perturbation magnetic field vector produced by currents in the system that must be known. The perturbation magnetic field $\delta\mathbf{B}$ is defined as the difference between the measured ambient magnetic field $\mathbf{B}$ and a vector spherical harmonic model of the Earth's unperturbed field $\mathbf{B_O}$ which incorporates satellite measurements from the MAGSAT magnetic field mapping mission [*Langle and Estes*, 1985]: $\delta\mathbf{B} = \mathbf{B}\text{-}\mathbf{B}_o$. The determination of accurate perturbation magnetic field vectors is the major procedural obstacle to methodically establishing the Poynting vector from satellite data. This difficulty is mostly a reflection of the uncertainty in our knowledge of the actual spacecraft attitude, that is, its orientation relative to the unperturbed field $\mathbf{B_O}$. Efforts to reduce this error have been made by many spacecraft magnetometer investigators in the past, and their approaches have ranged from estimating the attitude error using complicated functions involving spacecraft attitude and position [e.g., *McDiarmid et al.*, 1978] to simple endpoint matching [e.g., *Doyle et al.* [1981].

The magnitude of the attitude error between that derived from the spacecraft horizon sensors and the magnetometer may be several tenths of a degree and variable over the course of a polar pass. For this reason, it is not unusual for the perturbation magnetic fields to be biased by several hundred nanoTesla due to these attitude errors. Compensations for these errors can be made if it is assumed that (1) the total attitude error changes slowly over a polar pass, and (2) the natural perturbation magnetic field below about 50 deg invariant latitude is small. The first assumption generally appears to be true in that while a single attitude correction made at the beginning of a polar pass is not sufficient to "level" the magnetic field base line at the end of the pass, the error appears to grow steadily over the course of the pass. The second assumption also appears to be reasonable in that the sum of the magnetic fields associated with the magnetopause currents, the tail current systems and the Sq currents should not be any larger than several tens of nanoTesla at mid-latitudes. We therefore determine a new base line for the magnetic field perturbations by fitting a cubic spline to the magnetometer output with four anchor points located at invariant latitudes sufficiently below the auroral oval to escape influences from field-aligned currents on both the entering and departing sections of the high-latitude pass. This curve is now assumed to be a realistic base line for the intrinsic magnetic field, since it takes into account possible inaccuracies in both spacecraft orientation and in the model field. We typically choose the anchor points as near to 40 deg invariant latitude as the data allows. The difference between the measured field and the spline fit in these regions is less than 50 nT, and we have no reason to expect this uncertainty to increase in the high latitude region where the Poynting flux is being determined.

In assessing the total uncertainty in our results, we must examine the combined effect of our uncertainties in determining the magnetic and electric fields. If we denote the uncertainty in the perturbation magnetic field as β and the uncertainty in the electric field as ϵ, then the true (as opposed to measured) Poynting vector can be written as

$$\mathbf{S_{True}} = \frac{1}{\mu}(\mathbf{E} \pm \epsilon) \times (\delta\mathbf{B} \pm \beta). \tag{1}$$

Combining all terms containing ϵ and β we can arrive at the following estimate for the maximum uncertainty in the magnitude of $\mathbf{S}_{True}$ (ΔS) :

$$\Delta S = \frac{1}{\mu}(E\beta \pm \delta B\epsilon \pm \beta\epsilon). \tag{2}$$

Our uncertainty in the field-aligned Poynting flux depends not only on the product of the uncertainties ϵ and β but on their product with E and δB as well. In order to gain some intuition as to the relative size of the uncertainty, we can take the ratio of ΔS to our calculated value of $\mathbf{S} = \frac{1}{\mu}(\mathbf{E} \times \delta\mathbf{B})$:

$$\frac{\Delta S}{S} = \pm\frac{\beta}{\delta B} \pm \frac{\epsilon}{E} \pm \frac{\epsilon\beta}{E\delta B}. \tag{3}$$

For the perturbation magnetic field, we estimate 50 nT to be the maximum cumulative uncertainty, while for the electric field we take 2 mV/m to be the cumulative uncertainty. The sensitivity of the Poynting flux to the measured data is immediately apparent, especially to the determination of the perturbation magnetic field, and allows us to place confidence bounds on our analysis. As an illustration, a calculated Poynting flux of

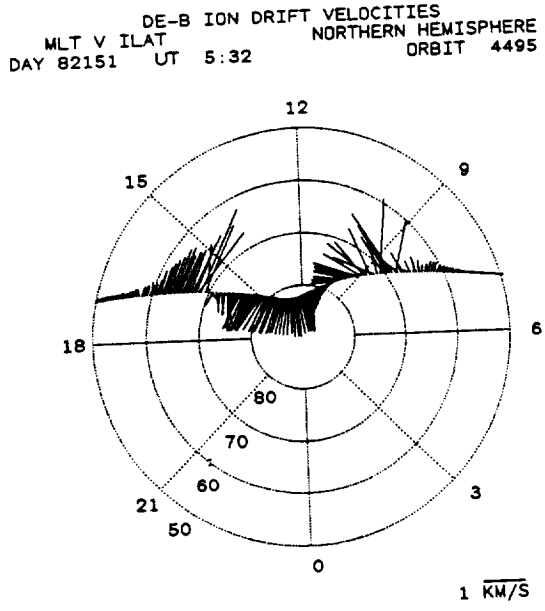

Figure 1. Polar plot of horizontal ion drift velocities for orbit 4495.

1 mW/m^2 corresponding to $\delta B = 200$ nT and E = 6.3 mV/m gives $\frac{\Delta S}{S} \sim 0.60$, that is, a possible error of 60 percent, whereas typical auroral zone values of S $\sim$ 20 mW/m^2 with $\delta B = 500$ nT and E = 50 mV/m lead to an uncertainty of about 14 percent.

Data Analysis

We have selected six high latitude passes of Dynamics Explorer 2 to illustrate the variation in the large scale Poynting flux along the spacecraft track and the role that this parameter may play in revealing the conditions under which energy exchange between the ionosphere and the magnetosphere can be drastically different. The chosen passes lie approximately along the dawn-dusk meridian. We have chosen a coordinate system in which the positive x direction is always along the spacecraft velocity vector (ram direction or meridional), positive y is always upward (out of the ionosphere), z makes up the remaining (zonal) component of the right-handed system. For each orbit we present the magnetometer data used in the calculations before and after the base line alterations, together with the spline curve taken as the new base line. The field-aligned Poynting flux is shown together with the horizontal ion drift velocities.

Poynting's theorem for steady state conditions applied to a single flux tube bounded by the satellite at top and the base of the ionosphere at bottom reads

$$\int \mathbf{S}_{\parallel} \cdot \hat{n} da = -\int \mathbf{E} \cdot \mathbf{J} dV, \qquad (4)$$

which relates the surface integral of the field-aligned

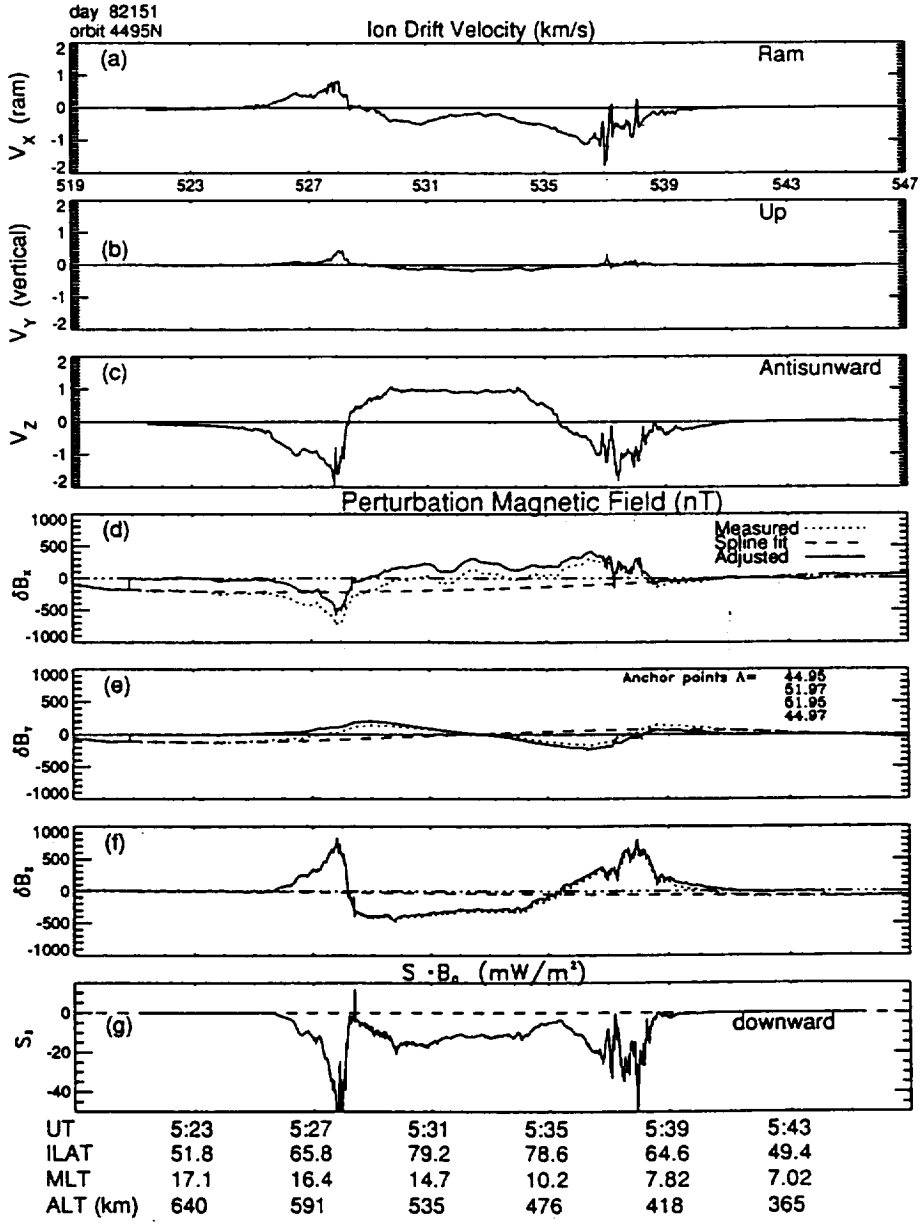

Figure 2. Ion drift velocity components for orbit 4495 : (a) ram, (b) vertical, and (c) cross-track; (d-f) perturbation magnetic field components as measured and after spline fit; and (g) field-aligned Poynting flux $S_{\parallel} = \mathbf{S} \cdot \hat{\mathbf{B}}_o$. All quantities are in spacecraft coordinates.

Poynting flux $S_\parallel$ across the boundary to the energy conversion rate within the volume. With $\hat{n}$ pointing outward everywhere, and assuming that no energy flows out the bottom of the region, a measurement of $S_\parallel$ at the top of the region is equal to minus the rate of energy conversion below [*Kelley, et al.*, 1991].

The right-hand side of (4) can be written [e.g., *Thayer and Vickrey*, 1992] as

$$\int \mathbf{E}\cdot\mathbf{J}dV = \int \mathbf{E}'\cdot\mathbf{J} + \mathbf{U}\cdot(\mathbf{J}\times\mathbf{B})dV, \qquad (5)$$

where $\mathbf{E}'$ is the electric field in the frame of the neutrals and is related to the measured electric field $\mathbf{E}$ by the transformation $\mathbf{E}' = \mathbf{E} + \mathbf{U}\times\mathbf{B}$. This equation may be further examined by decomposing the current density $\mathbf{J}$ into Hall and Pedersen components, after which (5) becomes

$$\int \mathbf{E}\cdot\mathbf{J}dV = \int [\sigma_P \mathbf{E}'^2 - \sigma_P \mathbf{U}\cdot(\mathbf{E}'\times\mathbf{B}) + \sigma_H B\mathbf{U}\cdot\mathbf{E}']dV. \qquad (6)$$

Equation (6) makes explicit the interplay between the electric field $\mathbf{E}'$ typically originating in the magnetosphere and the neutral wind velocity $\mathbf{U}$, as well as the weighting of the energy conversion rate by the conductivities. It is interesting that there is a term weighted by the Hall conductivity, a fact often neglected in assessments of $\mathbf{E}\cdot\mathbf{J}$.

The first term in (6) gives the contribution to the energy conversion rate from frictional heating between the ions and the neutrals, leading to elevated temperatures from increased thermal motion. This may also be termed the Joule heating rate or Joule dissipation rate, although there is a certain lack of consistency in the widespread usage of these terms. The second and third terms in (6) describe the rate of change of kinetic energy of the neutral gas due to collisions with the ions.

Given that our assessment of the field-aligned Poynting flux is correct, we see that there must be three general cases of interest in looking at the data: $S_\parallel < 0$ (into the ionosphere, ionospheric load), $S_\parallel > 0$ (out of the ionosphere, ionospheric generator), and $S_\parallel = 0$ (no net energy conversion). Equation (6) demonstrates the requirements for these conditions, and we see that the direction of the field-aligned Poynting flux is principally dependent upon the relative orientations of $\mathbf{U}$ and $\mathbf{E}'$. Observationally, we take the ion drift velocity $\mathbf{V}$ to be indicative of the overall nature of $\mathbf{E}'$ since, in the F region where our measurements are made, $\mathbf{E}' = (\mathbf{U}-\mathbf{V})\times\mathbf{B}$. While we are unable to discriminate between the effects of the individual terms in (6), we can make some statements from the more general equation (5). Whenever the height-integrated quantity $\mathbf{U}\cdot(\mathbf{J}\times\mathbf{B})$ is positive, the entire quantity $\mathbf{E}\cdot\mathbf{J}$ is positive and electromagnetic energy is being converted into particle thermal and kinetic energy within the volume. Electromagnetic energy generation within the volume requires that $\mathbf{U}$ oppose the $\mathbf{J}\times\mathbf{B}$ force and that the flux tube-integrated magnitude of $\mathbf{U}\cdot(\mathbf{J}\times\mathbf{B})$ be greater than that of $\mathbf{E}'\cdot\mathbf{J}$ ($=\Sigma_P E'^2$), signifying the dominance of the neutral wind over the magnetosphere as the driver of the energy flow. The conditions for $S_\parallel < 0$ are perhaps best exemplified during times of southward IMF where a well defined two-cell convection pattern generally forms in the ionosphere. The large scale electric field is generally imposed from the magnetosphere as indicated by the organized ion drifts. We can expect $S_\parallel < 0$ in the polar cap, where both $\mathbf{V}$ and $\mathbf{U}$ are generally antisunward with $V > U$, and in the auroral zone where $\mathbf{V}$ and $\mathbf{U}$ are oppositely directed. We present two cases which are typical of these conditions and in which the sunward and antisunward ion drift velocities exceed 1 km/s, much larger than we would expect neutral wind velocities to be.

The first case presented is orbit 4495 from May 31, 1982. The satellite passes through the dayside northern high latitude summer ionosphere, moving from dusk to dawn at altitudes descending from 640 to 365 km. The ion drift velocities, seen in the polar dial of Figure 1 and as separate components in Figures 2a-2c, show a characteristic two-cell convection pattern associated with a steady southward IMF, suggesting that the magnetosphere is in firm control of the circulation in the ionosphere. Hourly averaged values of the IMF indicate that the IMF was in fact steady, although not strongly, southward during this time.

Figures 2d-2f show the three components of the magnetic field perturbation measured from DE 2 together with the corrected perturbations obtained by establishing a new base line for the measurement. The originally measured perturbations are indicated by the dotted curve. It can be seen that substantial perturbations exist at invariant latitudes below 50° where we would expect such perturbations to be small. The dashed curve shows the cubic spline base line determined by requiring the perturbation to be zero at 45° and 52°

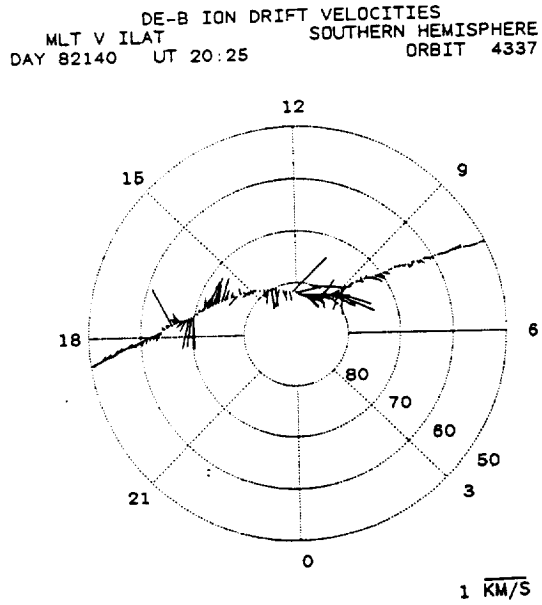

Figure 3. Polar plot of horizontal ion drift velocities for orbit 4337.

invariant latitude. The resulting magnetic field perturbations used in the calculation of the Poynting flux are shown by the solid curve. The result of this correction procedure has the most pronounced effect on δB_X with a maximum difference between corrected and uncorrected values of about 200 nT. Notice, however, that this correction procedure essentially preserves the gradients in δB from which field-aligned currents (FAC) would be determined. The presence of region 1 and region 2 FAC can be clearly seen in the horizontal components of the perturbation magnetic field, especially δB_Z (figure 2f). The satellite passed between the large scale current sheet on the duskside at roughly 0527 UT, with the region 1 current associated with the δ B gradients just poleward and the region 2 current sheet associated with the equatorward gradient [e.g., *Zanetti et al.*, 1983]. On the dawnside, the region 1 current was apparently spread over a larger extent as indicated by the smaller gradient, and is more structured than on the dusk side. The high degree of correlation between the horizontal components of the magnetic field perturbation δB_X and δB_Z suggest that the spacecraft is passing through an "infinite" field-aligned current sheet at the dusk side convection reversal. The quasi-sinusoidal signature evident in the vertical component (δB_Y) is indicative of the effect of the distant auroral electrojet [*Zanetti et al.*, 1983]. The cross-track components of V and δB have a correlation coefficient of 0.93 across the entire pass. This would be expected if the height-integrated Pedersen conductivity was uniform [*Sugiura et al.*, 1982], and for these data the E region below was sunlit.

As can be seen in Figure 2c, the horizontal ion drift across the polar cap is largely antisunward and of sufficient magnitude for us to conjecture that $|V| > |U|$ and that the electric field is primarily magnetospheric, consistent with our expectations for downward Poynting

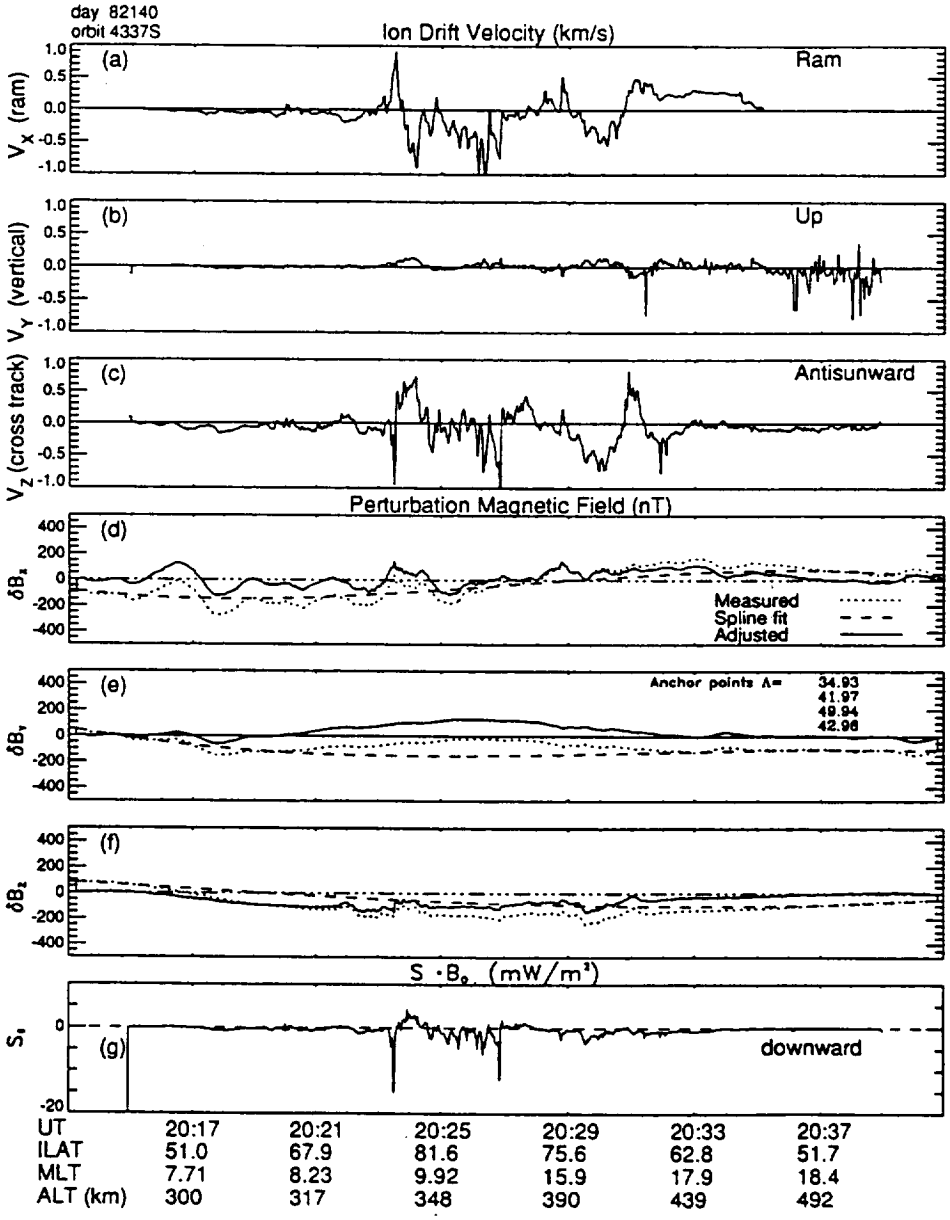

Figure 4. Data for orbit 4337 in the same format as Figure 2.

flux in the polar cap. In the auroral zone, the drift velocities are large and sunward. The observed Poynting flux is downward along the entire pass across the polar cap, averaging 6.29 mW/m^2 over the pass, with maximum values in the auroral zones of about 82 mW/m^2 on the dusk side and 40 mW/m^2 on the dawn side. This asymmetry is in accordance with the findings of *Foster et al.* [1983] and *Vickrey et al.* [1982] on the local time variation of Joule heating rates. The distribution of the field-aligned Poynting flux across the polar cap, from about 0528 UT to 0536 UT, supports the idea that appreciable region 1 current closes across the polar cap with resulting Joule dissipation and momentum transfer in the region of the lower ionosphere. This is consistent with previous interpretations of the horizontal perturbation magnetic field signature across the polar cap, with the antisunward/tailward extension of δB_z in that section of the pass indicating region 1 current closure across the polar cap [e.g., *McDiarmid et al.*, 1978]

As we have mentioned, the case of upward, or outward, Poynting flux is indicative of a neutral wind dynamo process. The criterion for a neutral wind dynamo is most likely to be satisfied during times of northward IMF when the ions are not being strongly driven by electric fields from the magnetosphere. It is also possible for there to be small regions of upward Poynting flux during southward IMF near the reversal boundaries where the ion drifts become comparable to the neutral wind velocities.

We now present a case for which the conditions necessary for upward Poynting flux are apparently met. Orbit 4337, day 82140, passed across the dayside southern winter ionosphere at an altitude of about 300 km roughly from dawn to dusk. The IMF was steadily northward for several hours preceding the pass with an hourly averaged B_z of 1.4 nT for the time of the orbit. Figure 3 and Figures 4a-4c show the structured ion drifts typical of northward IMF, winter conditions, and the perturbation magnetic field signatures seen in Figures 4d-4f do not indicate the presence of large scale field-aligned currents. The electrodynamic coupling between the magnetosphere and ionosphere is far weaker in this instance, having no well-defined convection patterns or large field-aligned current systems. The plot of $S_\parallel$ (Figure 4g) reveals two relatively large scale regions as well as a few isolated locations where the Poynting flux is directed upward. The regions of upward Poynting flux are well correlated with regions of antisunward ion drift velocities, as we expect from our earlier arguments. The largest region of upward $S_\parallel$, between 2023 and 2024 UT, spans 427 km along the satellite track with a peak value of 3.6 mW/m^2 and an average value of 1.54 mW/m^2. The second region, between 2027 and 2028 UT, represents a smaller energy conversion rate, with a maximum value across the 480 km stretch being only 1.55 mW/m^2 and an average value of only 0.57 mW/m^2. This weaker region marks the extreme edge of confidence in our ability to determine the field-aligned Poynting flux from DE 2 measurements with the cor-

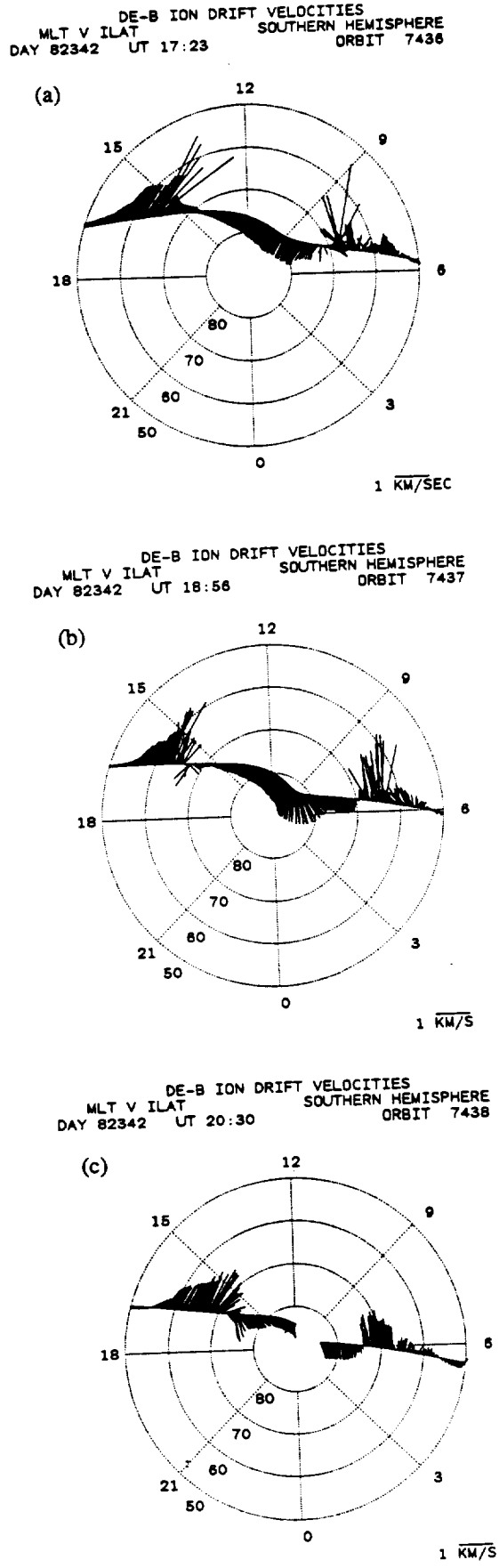

Figure 5. Polar plots of the horizontal ion drift velocities for orbits (a) 7436, (b) 7437, and (c) 7438.

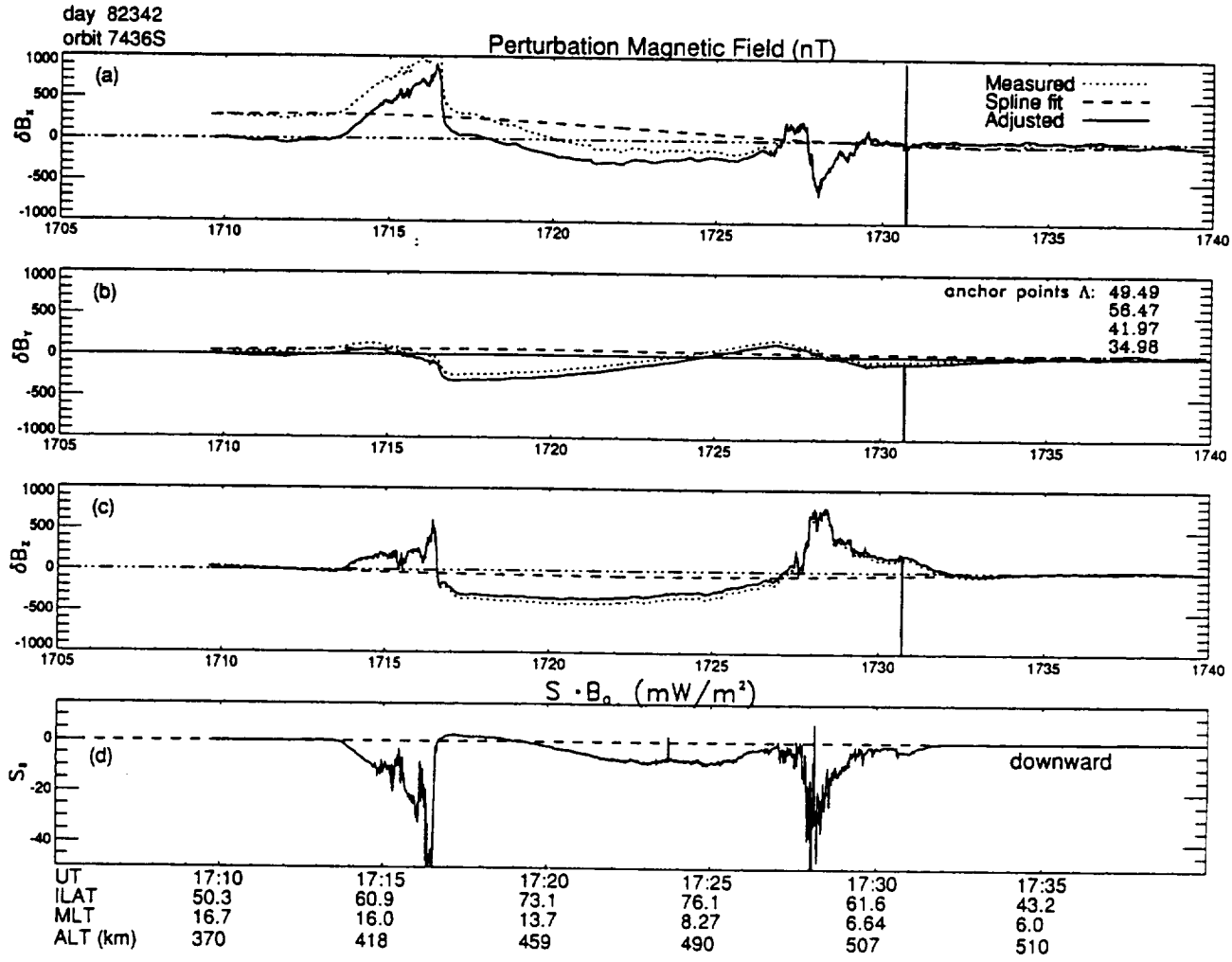

Figure 6. Perturbation magnetic field components in spacecraft coordinates and field-aligned Poynting flux for orbit 7436: (a) δB_x or ram, (b) δB_y or vertical, (c) δB_z or cross track, and (d) $S_{\parallel}$.

rection procedures we have described, with an average uncertainty determined from (1) of 55 percent.

The condition under which $S_{\parallel}$ may equal 0, implying that no net energy conversion is taking place in the flux tube volume, is for $\mathbf{E'}\cdot\mathbf{J} = -\mathbf{U}\cdot(\mathbf{J}\times\mathbf{B})$. $S_{\parallel}$ will also equal zero if the ion drift, and hence electric field, is zero. Note that this may be achieved by changing coordinates to a system that is moving with the ions, so that the Poynting flux is dependent on the choice of coordinate system. In the frame co-rotating with the Earth, however, this condition is unlikely to be met under steady state conditions in that while the electric field may change sign over a very short spatial scale, as in a shear reversal, there is no point where the ions are actually stationary. In general, $S_{\parallel} = 0$ indicates that the rate of frictional heating of the ions is balanced by the rate of bulk flow kinetic energy transfer between the ions and the neutrals due to collisions. This condition may mark the establishment of a sustained neutral wind "flywheel", where the neutral particles have been accelerated by the ions until they are moving at comparable speeds, thus in some sense storing the energy until the bulk ion flow changes in response to varying electrodynamic conditions. Observation of the development of such a situation requires consecutive data sets during a time of stable conditions.

The orbits shown in the polar dials of Figure 5 represent a sequence of three southern hemisphere summer dayside passes, all on day 82342 between 1700 UT and 2100 UT. The spacecraft measurements shown lie entirely in daylight and the conductivities in the polar cap ionosphere are dominated by ionization produced by solar UV radiation. Under these conditions, we may assume that the principal differences between orbits in the sequence are attributable to variations in the electromagnetic energy driver rather than in the conductivity of the ionosphere, at least on the global scale which we are considering here. Therefore changes in the ionospheric energy conversion rate are more a reflection of changes in IMF conditions and in the motion of the neutral wind.

The IMF was strongly southward for at least two hours before the beginning of the sequence and continued to be so until around 2000 UT. Hourly averages for B_z during this interval range from -7.4 to -10.0 nT, after which B_z began to swing northward. The hourly average for B_z during the third orbit was near zero, and reached 3.6 nT in the following hour. The ion drift

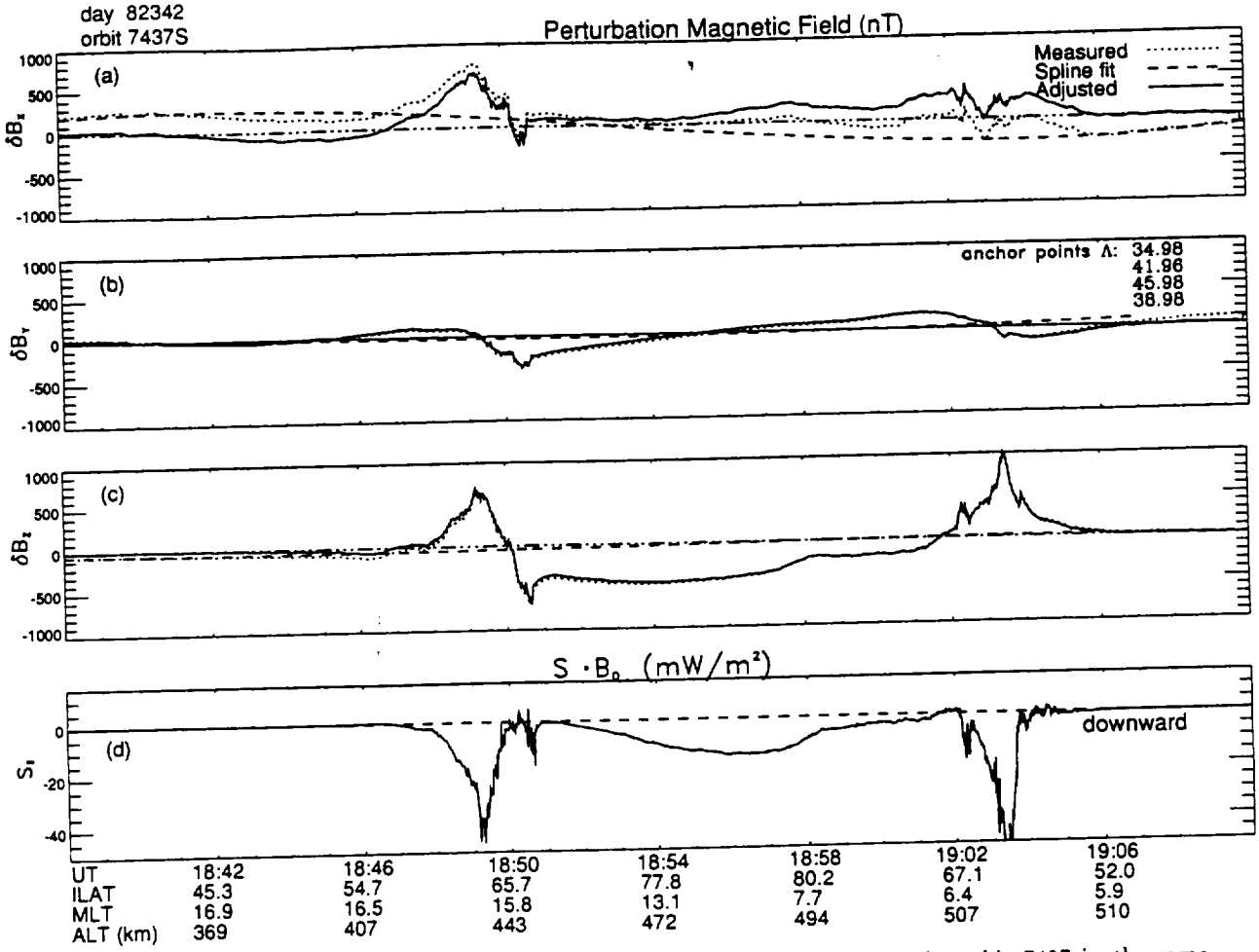

Figure 7. Perturbation magnetic field and field-aligned Poynting flux for orbit 7437 in the same format as Figure 6.

velocities in all three cases suggest a strong two-cell convection pattern, with the drifts increasing from the first orbit to the second and then decreasing between the second and final orbits. In all three orbits, the perturbation magnetic field signature contains well defined region 1 and region 2 field-aligned currents. The field-aligned Poynting flux in each case is almost everywhere directed into the ionosphere and is of smaller magnitude in the polar cap than in the auroral zones.

For the first orbit in the sequence, orbit 7436, $S_\parallel$ across the polar cap is dominantly downward and has an average value of 3.7 mW/m^2. There is a region of upward Poynting flux poleward of the duskside convection reversal boundary, as seen in figure 6d, centered near 1715 UT. The average value for $S_\parallel$ across this region is 1.4 mW/m^2, and it spans about 1050 km along the satellite track. Orbit 7437 took place near the conclusion of the period of strongly southward B_z, and it can be seen in the polar plot (figure 5b) that there is a substantial increase in ion drift velocity from the previous orbit, implying that the ions are being more strongly driven by the magnetosphere. The observed values for $S_\parallel$ across the polar cap are consistent with this interpretation, with an average value of 8.7 mW/m^2. The region 1 and region 2 current signatures in δB seen in Figures 7a-7c in this case are consistent with substantial field-aligned current closing across the polar cap, as evidenced by the very sharp gradient in δB_z on the duskside.

In the final orbit, 7438, the ion drifts have slowed (Figure 5c) and $S_\parallel$ across the polar cap has an average value of only 1.37 mW/m^2. Comparison with the plots of $S_\parallel$ for the three orbits (Figures 6c, 7c and 8c) clearly demonstrates the marked decrease in the energy conversion rate. This observation, combined with the decrease in B_z to near zero, leads us to conclude that the ions and neutrals must be moving at very nearly the same speed, representing an "undriven" ionosphere in the polar cap. Examination of the δB signature suggests that the large scale field-aligned currents have greatly diminished in magnitude from the previous orbit, and that much of the region 1 current could be closing through the neighboring region 2 current rather than across the polar cap as indicated by the small values of $S_\parallel$.

Conclusions

We have undertaken an examination of the electromagnetic energy conversion rate in the earth's ionosphere by determination of the Poynting vector at points along the trajectory of a polar orbiting satellite. In so doing, we have presented a systematic approach to es-

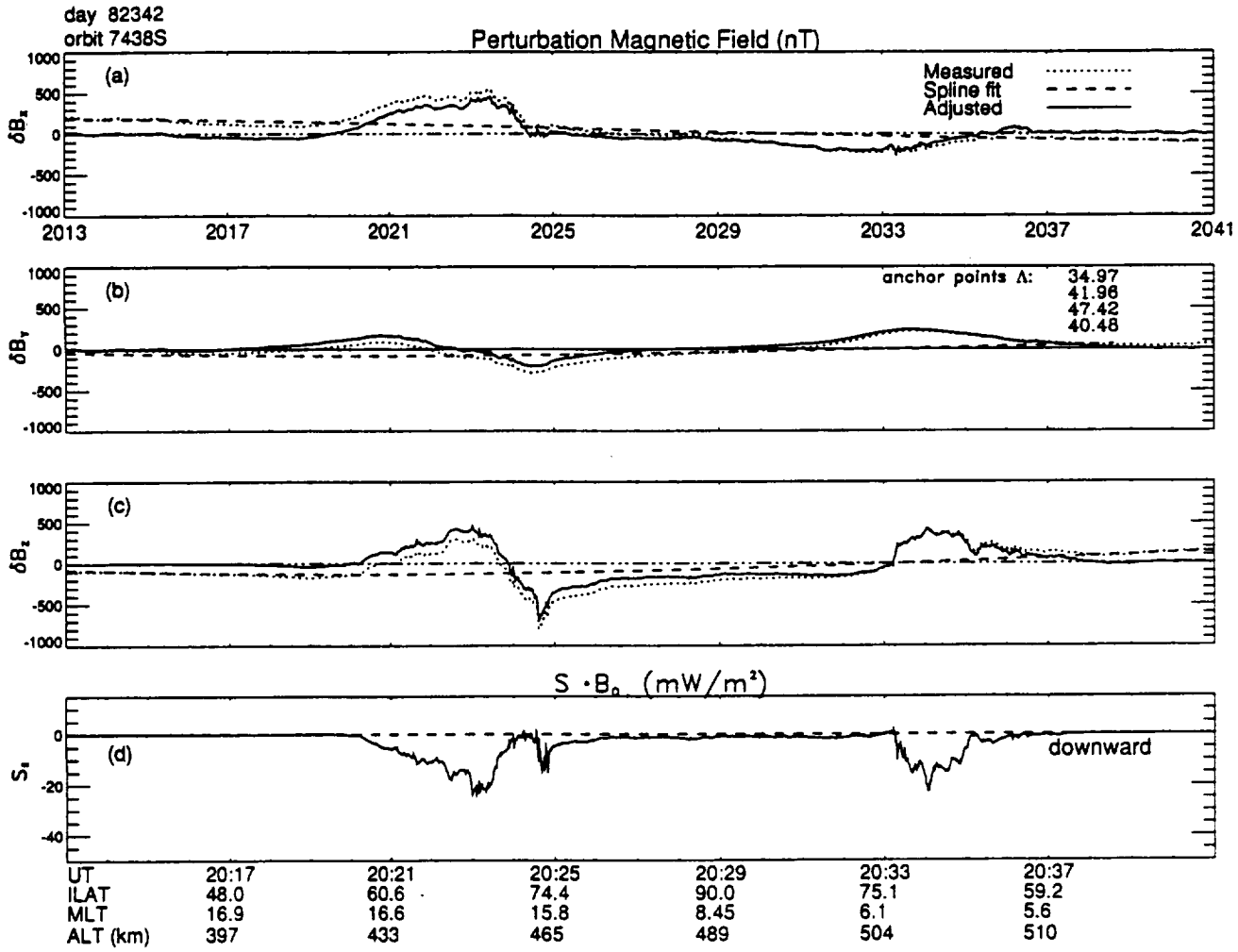

Figure 8. Perturbation magnetic field and field-aligned Poynting flux for orbit 7438 in the same format as Figure 6.

tablishing the magnitudes of the electric field and perturbation magnetic field, as well as providing error estimates for each quantity and the cumulative uncertainty of our results. The electromagnetic energy flux is equivalent to the sum of the rates at which kinetic energy is transferred to the neutral atmosphere via Lorentz ($\mathbf{J} \times \mathbf{B}$) forcing and at which the atmosphere is heated by Joule dissipation. Poynting's theorem, applied to a magnetic flux tube segment bounded at the top by the satellite and at the bottom by the base of the ionosphere, allows the field-aligned energy flux measured at the satellite altitude to be equated to the rate of electromagnetic energy conversion taking place in the volume.

The ionosphere often acts as an active load in the global high latitude ionosphere-magnetosphere circuit with energy deposited from the magnetosphere into the ionosphere. Energy is delivered to the lower ionosphere when the neutral wind is in the direction of the $\mathbf{J} \times \mathbf{B}$ force, and it is transported from the region when this component of the neutral wind velocity is larger than the ion drift and oppositely directed to the $\mathbf{J} \times \mathbf{B}$ force. Hence we expect that in the auroral zones, where the ion drift and neutral wind are generally oppositely directed, the Poynting flux will be downward and dominated by the frictional heating rate. Upward Poynting flux, indicative of a dynamo process, may be expected in the polar cap at times when the neutral wind velocity may exceed the ion drift velocity. We have presented observations indicative of each of these drivers, including a sequence demonstrating the approach of a steady state neutral wind pattern.

Downward directed Poynting flux with magnitudes of a few tens of mW/m^2, typical of our observations, are consistent with a Pedersen conductivity near 10 Mhos and ion drifts of the order of 1 km/s. It is important to emphasize that the adjustments to the measured data as described here can easily alter the zero line for the derived Poynting flux by a few tens of mW/m^2. The automated correction procedure that we have outlined may be of value to investigators interested in the absolute magnitude of the perturbation magnetic field or any quantity, such as the Poynting flux, which is proportional to this magnitude. Such corrections, or lack thereof, may change observations of the downward Poynting flux by 50 percent, which may be considered unimportant to some investigations. However, such ad-

justments can change the magnitude of upward Poynting flux by several hundreds of percent, and even the inferred direction, which may lead to significant interpretive misunderstandings. Assuming that the large scale neutral wind velocity in the E region will not exceed a few hundreds of meters per second, we should not expect upward directed Poynting flux to exceed 10 mW/m^2 over large spatial scales.

Acknowledgments. This work is supported at the University of Texas at Dallas by NASA grants NAG 5-305 and NAG 5-306, and by Air Force Geophysics Directorate contract F19628-90-K-0001. The authors wish to acknowledge the extremely helpful input from F.S. Johnson of UTD, Jeff Thayer of SRI, Menlo Park, and Reuben Edgar of SwRI, San Antonio. The Editor thanks J. C. Samson and J. F. Vickrey for their assistance in evaluating this paper.

References

Anderson, P. C., W. B. Hanson, W. R. Coley, and W. R. Hoegy, Spacecraft potential effects on the Dynamics Explorer 2 satellite, *J. Geophys. Res., 99*, 3985, 1994.

Cummings, W.D., S.E. DeForest, and R. L. McPherron, Measurements of the Poynting vector of standing hydromagnetic waves at geosynchronous orbit, *J. Geophys. Res., 83*, 697, 1978.

Deng,W., T.L. Killeen, A.G. Burns, and R.G. Roble, The flywheel effect:Ionospheric currents after a geomagnetic storm, *Geophys. Res. Lett, 18*, 1845 , 1991.

Doyle, M.A., F.J. Rich, W.J. Burke, and M. Smiddy, Field-aligned currents and electric fields observed in the region of the dayside cusp, *J. Geophys. Res., 86*, 5656, 1981.

Erlandson, R.E., L.J. Zanetti, T.A. Potemra, L.P. Block, and G. Holmgren, Viking magnetic and electric field observations of Pc 1 waves at high latitudes, *J. Geophys. Res., 95*, 5941, 1990.

Farthing, W.H., M. Sugiura, and B.G. Ledley, Magnetic field observations on DE-A and -B, *Space Sci. Instrum., 5*, 551, 1981.

Fejer, B.G., M.F. Larsen, and D.T. Farley, Equatorial disturbance dynamo electric fields, *Geophys. Res. Lett., 10*, 537, 1983.

Foster, J.C., J.-P. St.-Maurice, and V.J. Abreu, Joule Heating at hight latitudes, *J. Geophys. Res., 88*, 4885, 1983.

Fraser, B.J., J.C. Samson, Y.D. Hu, R.L. McPherron, and C.T. Russell, Electromagnetic ion cyclotron waves observed near the oxygen cyclotron frequency by ISEE 1 and 2, *J. Geophys. Res., 97*, 3063, 1992.

Hanson, W.B., R.A. Heelis, R.A. Power, C.R. Lippincott, D.R. Zuccaro, B.J. Holt, L.H. Harmon, and S. Sanatani, The retarding potential analyzer for Dynamics Explorer-B, *Space Sci. Instrum., 5*, 503, 1981.

Hanson, W.B., W.R. Coley, R.A. Heelis, N.C. Maynard, and T.L. Aggson, A comparison of in Situ Measurements of E and -V×B from Dynamics Explorer 2, *J. Geophys. Res., 98*, 21493, 1993.

Heelis, R.A., W.B. Hanson, C.R. Lippincott, D.R. Zuccaro, L.H. Harmon, B.J. Holt, J.E. Doherty, and R.A. Power, The ion drift meter for Dynamics Explorer-B, *Space Sci. Instrum., 5*, 511, 1981.

Kelley, M.C., D.J. Knudsen, and J.F. Vickrey, Poynting flux measurements on a satellite: A diagnostic tool for space research., *J. Geophys. Res., 96*, 201-207, 1991.

Knudsen, D.J., Alfven waves and static fields in magnetosphere/ionosphere coupling: In-situ measurements and a numerical model, Ph.D. thesis, Cornell Univ., Ithaca, N. Y., 1990.

LaBelle, J., and R.A. Treumann, Poynting vector measurements of electromagnetic ion cyclotron waves in the plasmasphere, *J. Geophys. Res., 97*, 13,789, 1992.

Langle, R.A., and R.H. Estes, The near-Earth magnetic field at 1980 determined from Magsat data, *J. Geophys. Res., 90*, 2495, 1985.

Lyons, L.R., T.L. Killeen, and R. L. Waltersheid, The neutral wind "flywheel" as a source of quiet-time, polar-cap currents, *Geophys. Res. Lett., 12*, 101, 1983.

Mauk, B.H., and R.L. McPherron, An experimental test of the electromagnetic ion cyclotron instability within the Earth's magnetosphere, *Phys. Fluids, 23*, 2111, 1980.

McDiarmid, I.B., J.R. Burrows and Margaret D. Wilson, Comparison of Magnetic Field perturbations at high latitudes with charged particle and IMF measurements, *J. Geophys. Res., 83*, 681, 1978.

Sugiura, M., N.C. Maynard, W.H. Farthing, J.P.H.G. Ledley, and J.L.J. Cahill, Initial results on the correlation between the magnetic and electric fields observed from the DE-2 satellite in field-aligned current regions, *Geophys. Res. Lett., 9*, 985, 1982.

Thayer, J.P., and J.F. Vickrey, On the contribution of the thermospheric neutral wind to high-latitude energetics, *Geophys. Res. Lett., 19*, 265, 1992.

Vickrey, J.F., R.R. Vondrak, and S.J. Matthews, Energy deposition by precipitating particles and Joule dissipation in the auroral ionosphere, *J. Geophys. Res., 87*, 5184, 1982.

Zanetti, L.J., W. Baumjohann, and T.A. Potemra, Ionospheric and Birkeland current distributions inferred from the MAGSAT magnetometer data, *J. Geophys. Res., 88*, 4875, 1983.

J. B. Gary, R. A. Heelis, and W. B. Hanson, Center for Space Sciences, M.S. FO22, University of Texas at Dallas, P. O. Box 830688, Richardson, TX 75083.(e-mail: Internet.gary@utdallas.edu; Internet.heelis@utdallas.edu; SPAN.utspan::utadnx::utdssa::cssmail)

J. A. Slavin, Laboratory for Extraterrestrial Physics, NASA Goddard Space Flight Center, Greenbelt, MD 20771. (e-mail: Internet.slavin@lepjas.gsfc.nasa.gov)

(Received May 17, 1993; revised August 30, 1993; accepted October 28, 1993.)

APPENDIX C

"Summary of Field-Aligned Poynting Flux Observations From DE 2," by J.B. Gary, R.A. Heelis, and J.P. Thayer

Summary of Field-Aligned Poynting Flux Observations from DE 2

J. B. Gary [1] and R. A. Heelis
University of Texas at Dallas, Richardson

J. P. Thayer
SRI International, Menlo Park, California

Received _____; accepted _____

To appear in *Geophysical Research Letters*, 1994.

Short title:

[1]Now at Applied Physics Laboratory, Laurel, Maryland.

Abstract. Using DE 2 data of ion drift velocities and magnetic fields, we have calculated the field-aligned Poynting flux ($S_{||}$) for 576 orbits over the satellite lifetime. This represents the first broad application over an extended data set of Poynting flux observations from in situ measurements. This data has been sorted by interplanetary magnetic field conditions (northward or southward IMF) and geomagnetic activity (Kp$\leq$3 and Kp >3) and binned by invariant latitude and magnetic local time. Our general results may be summarized as 1) the averaged $S_{||}$ is everywhere directed into the ionosphere, indicating that electric fields of magnetospheric origin generally dominate, and 2) the distribution of $S_{||}$ for southward IMF can be well explained in terms of an average two cell convection pattern, while for northward IMF a four cell convection pattern may be inferred. We have addressed the interesting question of the distribution of upward Poynting flux by binning only upward observations and found that average upward Poynting flux of less than 3 mW/m^2 may occur anywhere across the high latitude ionosphere. We have also observed a region at high latitudes in the predawn sector where the average upward Poynting flux is of significant size and occurrence frequency during southward IMF and high Kp conditions. This region corresponds to a feature modeled by *Thayer and Vickrey* [1992] and indicates that a neutral wind dynamo may dominate the magnetospheric generator where field lines extend deep into the magnetotail.

Introduction

Several studies of large scale energy dissipation in the high latitude ionosphere have been conducted in the past. They have either involved radar observations [e.g., *Vickrey et al.*, 1982 and included references] or satellite measurements [e.g., *Heelis and Coley*, 1988, *Foster et al.*, 1983] of plasma densities and electric fields together with models of the height-integrated conductivities to estimate the Joule heating rate as $\Sigma_P E^2$, where Σ_P is the height-integrated Pedersen conductivity and E is the electric field in the ionosphere. The use of field-aligned Poynting flux ($S_{||}$) derived from satellite observations of electric fields and perturbation magnetic fields as proposed by *Kelley et al.* [1991] has recently been added as a method for determining the large scale energy conversion, or transfer, rate $\mathbf{E}\cdot\mathbf{J}$ in the ionosphere.

There are two advantages to using $S_{||}$ over electric field and energetic particle observations that are related to the inclusion of neutral wind effects and an independence from modeled conductivities. Computations of the Joule heating rate cannot take into account the height-integrated effects of the electric field, conductivities, and neutral wind motions [e.g., *Banks*, 1977, *Heelis and Coley*, 1988] whereas the Poynting flux is directly dependent on these parameters. *Thayer and Vickrey* [1992] and *Deng et al.* [1993] have recently used models of thermospheric circulation to estimate the magnitude of the electromagnetic energy generated by neutral wind dynamo actions and have related this to possible observations of the Poynting flux.

Data Presentation

In a previous work [*Gary et al.*, 1994], we have described our technique for determining $S_{||}$ from DE 2 observations of the ion drift velocity ($\mathbf{V}$) and perturbation magnetic field ($\delta\mathbf{B}$). Of the several thousand orbits during the satellite lifetime, only about 1300 passes over the high latitude region are available which are suited to our purposes. Determination of $S_{||}$ requires near continuous data between middle

latitudes ($\Lambda \leq 50$ deg.) on each side of a high latitude crossing in order to establish a perturbation magnetic field baseline as described in Gary *et al.* [1994]. In addition to this requirement, we have inspected each pass to ensure that the final calculation of $S_{||}$ is made using reliable data. Ultimately, 576 passes met our criteria for the production of reliable $S_{||}$. These orbits range over all DE 2 altitudes, from about 300 km to 1000 km, and represent passes from both hemispheres. As described by *Heelis and Coley* [1988], the 90 deg. inclination orbit of the DE 2 satellite causes coverage of season to be linked to the local time coverage with dawn-dusk passes occurring predominantly in summer/winter and noon-midnight passes near the equinoxes. It should also be mentioned that the lifetime of DE 2 occurred during a period of very high solar activity. Interpretations of our data need to be made with these points in mind.

We have binned the data by invariant latitude (Λ) and magnetic local time (MLT) and sorted according to Kp and IMF B_z conditions when possible. Each bin covers 5 deg in Λ and 1 hour in MLT. Kp sorting separates low geomagnetic activity ($0<Kp\leq3$) and high activity ($Kp>3$), and IMF sorting separates northward from southward IMF. The results are shown in polar dials representing the high latitude region above 50 deg invariant latitude using a color coded intensity scale to indicate the magnitude of $S_{||}$. Bins which contain diamonds represent regions where we have less than 75 observations, which we have taken to be the limit for undersampling. The choice of 75 as a limit ensures that at least two passes are included, as one pass may contribute as many as 70 observations in a single bin. Bins which have no shading and no diamond represent regions for which we have no observations. IMF data is available for only 302 of the 576 orbits used in this study, thus reducing the statistics considerably when we examine the distributions under different IMF and Kp conditions. In this work we will continue to use the sign convention where downward directed Poynting flux is negative ($S_{||} < 0$) and indicates electromagnetic energy being converted into particle kinetic energy in the flux tube below the satellite, and upward Poynting flux ($S_{||} > 0$) indicates the generation of

electromagnetic energy below the satellite.

Observations for all IMF

The results of our binning procedure for all IMF and Kp conditions are presented in Figure 1. The averaged $S_{||}$ is everywhere downward with the largest values occurring near dusk, dawn, and local noon. The highest energy transfer rates are observed between 65 and 80 deg invariant latitude. These regions are generally colocated with the auroral zone, indicating that on average most of the Birkeland currents close locally in region 1/region 2 current sheet pairs. It is easily seen in Figure 1 that the total energy transferred into the ionosphere is greater on the dayside of the dawn-dusk meridian than on the nightside. For the variety of IMF and Kp conditions which we have investigated, the dayside integrated values exceed the nightside values by 20% to 50%.

Across the dayside between 70 and 85 deg there is a region of relatively large $S_{||}$. Part of this region can be associated with cusp currents as well as with the average convection patterns. A region of high average electric field was observed in our results near 70 deg between 0900 MLT and 1200 MLT. This overlaps a region of enhanced magnetic field perturbation producing the "cusp" signature in $S_{||}$ at the same location. There is a bay of smaller valued $S_{||}$ in the premidnight sector which corresponds to relatively small values of $\mathbf{E}$ and $\delta\mathbf{B}$ in the premidnight hours. The premidnight sector showed consistently lower values of $S_{||}$ throughout our analysis, for all IMF and Kp conditions. Comparison between some of the published studies on ion drifts [*Kelley*, 1989, and included references] and neutral winds [*McCormac et al.*, 1991, *Kelley*, 1989] as well as model results [e.g., *Thayer and Killeen*, 1993] indicate that the general circulation of the ions and the neutrals is quite similar in this region. For low Kp, the same asymmetries about the noon-midnight and dawn-dusk meridians exist as for high Kp, but the magnitudes of both $\mathbf{E}$ and $\delta\mathbf{B}$, and thus $S_{||}$, are smaller. The low Kp distribution of $S_{||}$ is dominated by the region of elevated activity near noon. The auroral

zone is well defined across the nightside in the $S_{||}$ data as a narrow belt between 65 and 70 deg.

Observations for northward and southward IMF

Figures 2(a) and 2(b) show the results of our sorting the data by the sign of IMF B_z and for high and low Kp, with Figure 2(a) showing the case of southward IMF at high Kp and Figure 2(b) the case of northward IMF at low Kp. Many features of the distribution of $S_{||}$ can be fairly easily reconciled with typical convection patterns associated with northward and southward IMF, and the values at high Kp can be generally described as being larger than, and located at lower latitudes from, those at low Kp. For southward IMF, the average $S_{||}$ exhibits elevated values along the dusk and dawn convection boundaries, or auroral zones, reaching a maximum of about 12 mW/m^2 as seen in Figure 2(a). Note also a region of enhanced $S_{||}$ extending to higher latitudes between 1000 and 1200 MLT. This region, previously identified with enhanced electric fields in the cusp, is more easily identified when the orientation of the IMF is included in the data selection. The largest bin average is between 1500-1600 MLT and 60-65 deg, and is primarily composed of five southern hemisphere orbits that occurred during magnetic storms. *Deng et al.* [1993] described some of these orbits in their study of the response of the neutral atmosphere to geomagnetic storms. The bin averaged $S_{||}$ is quite large above 60 deg invariant latitude, peaking between 65 and 75 deg.

The interaction between the IMF and geomagnetic field for northward IMF leads to much weaker driving of the ions from magnetospheric electric fields, and the northward IMF results in Figure 2(b) show little variation below 70 deg. The largest values are about $7.3mW/m^2$ and occur across the dayside in the regions where typical four-cell convection patterns might exist and the general motion of the ions would oppose that of the neutrals. The regions of $S_{||}$ above the background near dawn and dusk are also consistent with a four-cell convection pattern.

Observations of upward Poynting flux

Several authors have addressed the ability of neutral wind motion to generate electromagnetic energy in the lower ionosphere. This energy would be transported along magnetic field lines into the magnetosphere. As discussed in e.g., *Kelley et al.* [1991], this would result in observations of upward $S_{||}$. We have not observered any locations in the high-latitude ionosphere which exhibited upward Poynting flux over a relatively long term average. However, we have taken all observations of upward $S_{||}$ and performed the same binning and sorting of the data as was applied to the overall observations in order to report on the distribution and occurrence of upward Poynting flux. Some of these results are presented in Figure 3. Perhaps the most obvious point to be made from the figure is that the average magnitude of upward Poynting flux is quite small under all conditions, with no single bin greater than 2.25 mW/m^2 . Such small average values are in line with the modelling of *Thayer and Vickrey* [1992] and *Deng et al.* [1993]. All of our observations above the nominal uncertainty level of 0.5 mW/m^2 occur above 65 deg. invariant latitude.

Figure 3 depicts the distribution of upward $S_{||}$ for all IMF and high Kp. The largest bin averages occur on the dawnside of the noon-midnight meridian, and are almost entirely composed of southward IMF observations. On the duskside, the occurrences are of smaller magnitude and seem to be sporadically located. There are no significant observations above 85 deg, few below 65 deg, and observations of upward $S_{||}$ near noon are noticeably absent. For low Kp, observations of substantial ($> 1 mW/m^2$) upward $S_{||}$ averages all but vanish. The early morning hours which show the largest upward $S_{||}$ at high Kp exhibit insignificant average values at low Kp.

It is apparent that, while observations of upward $S_{||}$ occur over most of the high latitude ionosphere, they are not widely significant in an average sense. Bin averages greater than 0.5 mW/m^2 are rare, and it is possible that most could vanish if a substantially larger data set was employed. A likely exception would be the region

between 70-80 deg near 0300 MLT. We have examined the frequency of occurrence of upward $S_{||}$ greater than 0.5 mW/m^2 , and in this region it exceeds 20% for southward IMF. The occurrence frequency is determined by taking the ratio of the number of observations for which $S_{||} > 0.5$ mW/m^2 to the total number of observations in each bin. Detailed examination of the binned orbits in this region does not suggest that the upward Poynting flux observations are suspect. Few regions show an occurrence frequency greater than 10%, but even this frequency is somewhat remarkable. Examination of separate orbits reveals that the regions of appreciable upward Poynting flux are associated with field-aligned currents in the polar cap which are distinctly smaller in scale size than the large scale region 1 and region 2 current distributions. Such field-aligned currents are likely to arise from divergences in the horizontal ionospheric currents which should exist whenever the thermospheric winds become the dominant driver of electromagnetic energy.

We could perhaps have predicted the existence of this region of upward Poynting flux by considering the electrical connection between the ionosphere, magnetosphere, and solar wind, together with the bulk motion of the ions and neutrals in the predawn polar cap. The field lines connecting the predawn ionosphere to the magnetosphere and beyond during southward IMF extend far into the magnetotail, where the magnetosheath plasma is super-Alfvenic. This argues for a weak connection along open field lines between the magnetospheric electric field driver and the ionospheric load. In addition, the neutral gas obtains its highest velocities during southward IMF and high Kp conditions in just this region. The combination of relatively rapid moving neutral particles traveling in the same direction as weakly magnetospheric driven ions is exactly the requirement for a significant large scale neutral wind dynamo. In their work on assessing the role of the neutral wind dynamo in high latitude energy generation, *Thayer and Vickrey* [1992] predicted this general location to be dominated by the neutral wind.

Conclusion

Our work in determining the distribution of the energy transfer rate in the high latitude ionosphere using observations of the field-aligned Poynting flux $S_{||}$ has produced the following results:

1) $S_{||}$ is downward everywhere on average;

2) for southward IMF, a two-cell convection pattern is evidenced with the greatest $S_{||}$ occurring in the auroral zones at dawn and dusk, with an "offset" cusp region at higher latitudes just before noon;

3) for northward IMF, a four-cell convection pattern is evidenced with the greatest $S_{||}$ occurring near noon where we might expect the ion and neutral gas bulk flows to have opposite directions;

4) upward Poynting flux may be observed at all locations but at generally small values, averaging to less than 1 mW/m^2 , and never with sufficient frequency to dominate a long term average;

5) there is a region of significant upward Poynting flux generated in the predawn polar cap with an average of greater than 2 mW/m^2 , although the net $S_{||}$ is downward when all observations are averaged. Observations of upward $S_{||}$ account for more than 20% of the total observations for southward IMF with Kp>3 in this region;

This work is supported at the University of Texas at Dallas by NASA contract No. NAGW-3508 and by Air Force Geophysics Directorate contract F19628-93-K-0008, and at SRI International by NASA contract No. NAS5-31214.

References

Banks, P. M., Observations of Joule and particle heating in the auroral zone, *J. Atmos. Terr. Phys.*, *39*, 179, 1977.

Deng, W., T. L. Killeen, A. G. Burns, R. G. Roble, J. A. Slavin, and L. E. Wharton, The effects of neutral inertia on ionospheric currents in the high latitude thermosphere following a geomagnetic storm, *J. Geophys. Res.*, *98*, 7755-7790, 1993.

Foster, J. C., J.-P. St-Maurice, and V. J. Abreu, Joule heating at high latitudes,*J. Geophys. Res.*, *88*, 4885-4896, 1983.

Gary, J. B., R. A. Heelis, W. B. Hanson, and J. A. Slavin, Field-aligned Poynting flux observations in the high latitude ionosphere, *J. Geophys. Res.*, *99*, 11417-11427, 1994.

Heelis, R. A., and W. R. Coley, Global and local Joule heating effects seen by DE 2, *J. Geophys. Res.*, *96*, 7551-7557, 1988.

Kelley, M. C., *The Earth's Ionosphere*, Academic Press, New York, 1989.

Kelley, M. C., D. J. Knudsen, and J.F. Vickrey, Poynting flux measurements on a satellite: A diagnostic tool for space research., *J. Geophys. Res.*, *96*, 201-207,1991.

McCormac, F. G., T. L. Killeen, and J. P. Thayer, The influence of IMF B_y on the high-latitude thermospheric circulation during northward IMF, *J. Geophys. Res.*, *96*, 115-128,1991.

Thayer, J. P., and T. L. Killeen, A kinematic analysis of the high-latitude thermospheric neutral circulation pattern, *J. Geophys. Res.*, *98*, 11,549-11,565, 1993.

Thayer, J. P. and J. F. Vickrey, On the contribution of the thermospheric neutral wind to high-latitude energetics, *Geophys. Res. Lett.*, *19*, 265, 1992.

Vickrey, J. F., R. R. Vondrak, and S. J. Matthews, Energy deposition by precipitating particles and Joule dissipation in the auroral ionosphere, *J. Geophys. Res.*, *87*.

5184-5196, 1982.

This manuscript was prepared with the AGU LaTeX macros v3.0.

Figure 1. Polar dial showing the distribution of the average field-aligned Poynting flux ($S_{||}$) in magnetic local time (MLT) and invariant latitude (Λ) above Λ=50°. The bins used in the averaging cover 1 hour in MLT and 5 degrees in Λ. The data are for all IMF orientations and Kp values, averaged over 570 DE 2 high latitude passes.

Figure 2. Results of sorting the bin averaged $S_{||}$ data by southward and northward IMF for high and low Kp, in the same format as Figure 1 but with a different scale. Bins with no data are not colored. Bins with fewer than 75 measurements are shown with a diamond. (a) results for southward IMF and Kp>3, representing data from 92 high latitude passes. (b) results for northward IMF and Kp<3, representing data from 117 passes.

Figure 3. Results of the bin averaged upward Poynting flux in the same format as Figure 1. Only measurements of $S_{||}$ >0 have been included in the averages, for Kp>3.

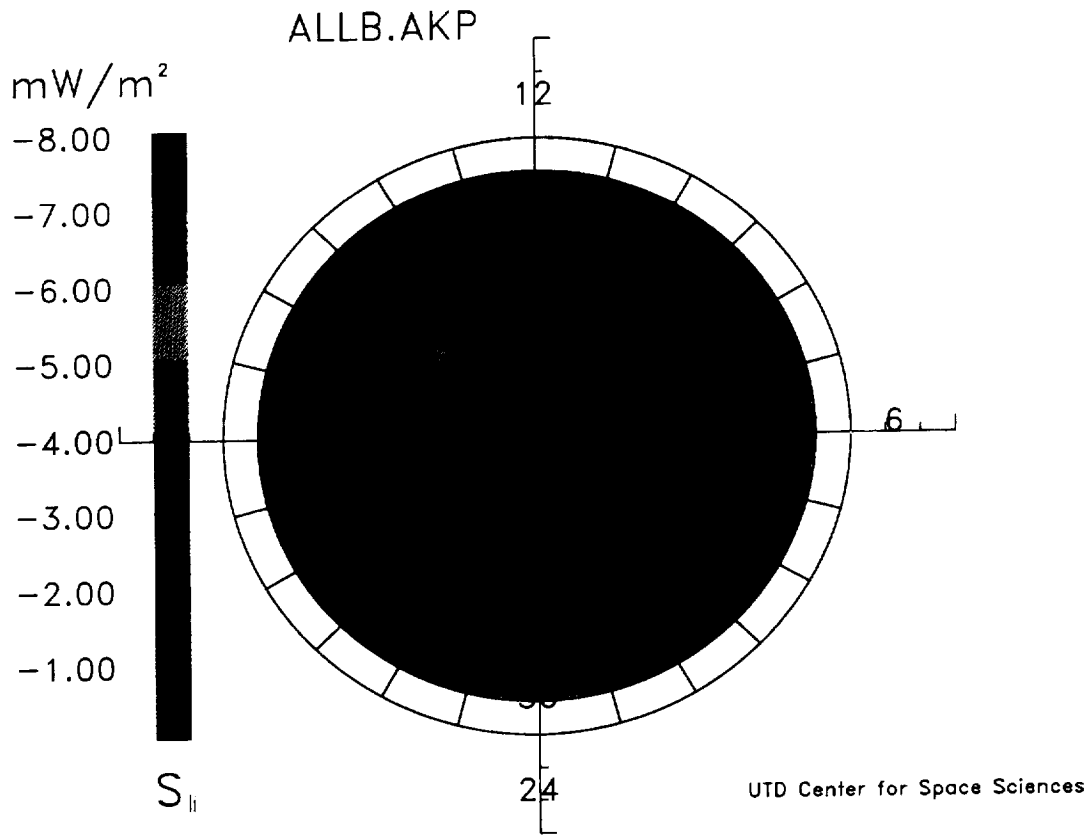
ALLB.AKP
mW/m²
-8.00
-7.00
-6.00
-5.00
-4.00
-3.00
-2.00
-1.00
12
6
24
UTD Center for Space Sciences

Fig. 1

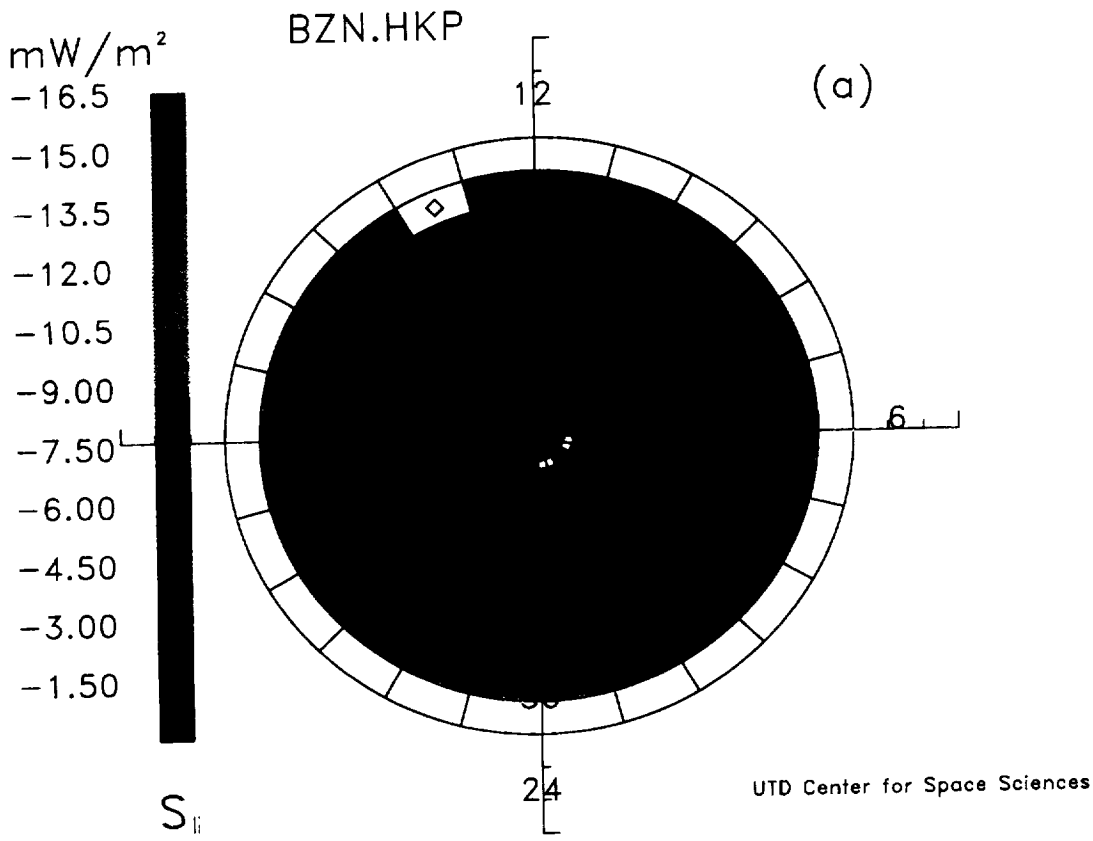
BZN.HKP
mW/m²
−16.5
−15.0
−13.5
−12.0
−10.5
−9.00
−7.50
−6.00
−4.50
−3.00
−1.50
12
6
24
(a)
UTD Center for Space Sciences

Fig. 2a

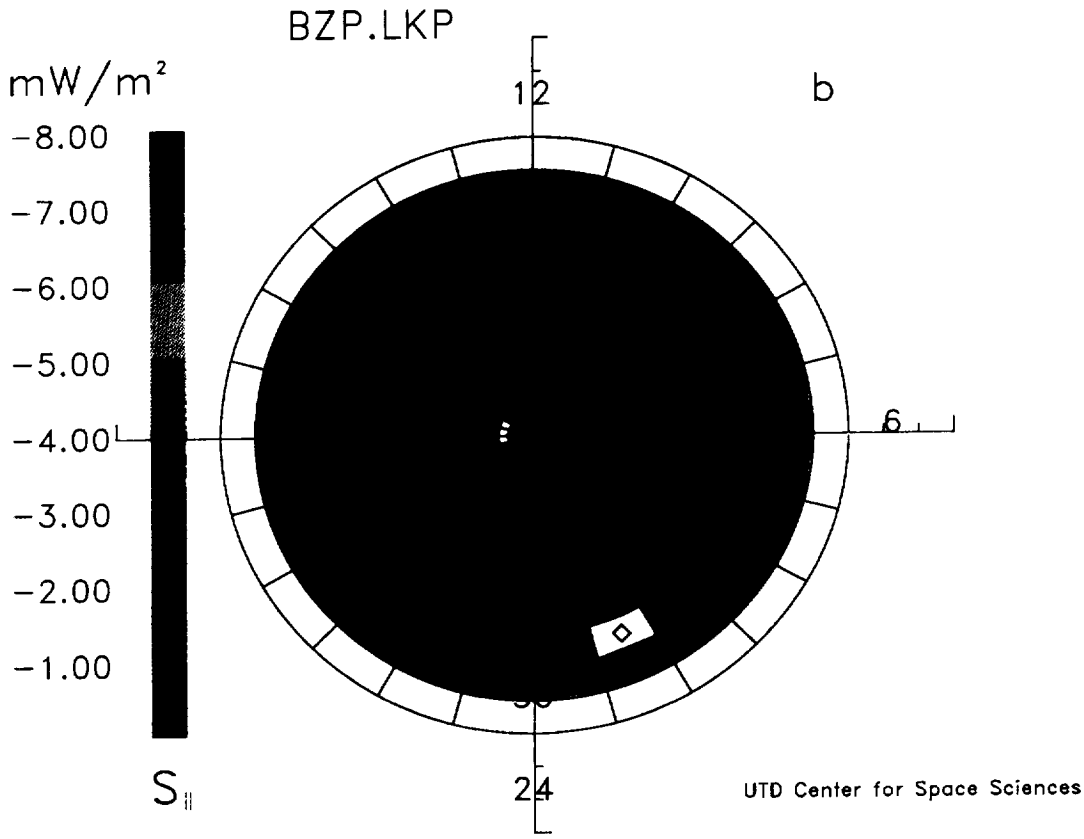
BZP.LKP
mW/m²
-8.00
-7.00
-6.00
-5.00
-4.00
-3.00
-2.00
-1.00
S∥
12
b
6
24
UTD Center for Space Sciences

Fig. 2b

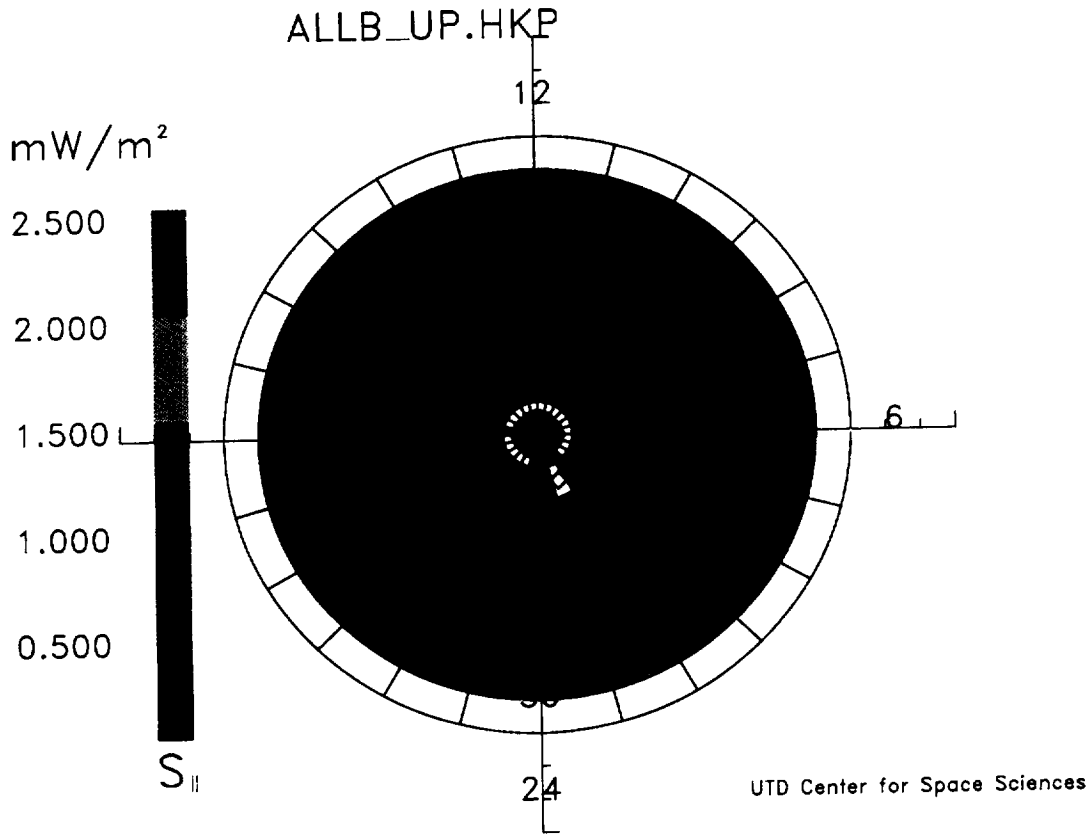
ALLB_UP.HKP
12
mW/m²
2.500
2.000
1.500
1.000
0.500
6
24
S
UTD Center for Space Sciences

Fig. 3

APPENDIX D

"Interpretation and Modeling of the High-Latitude Electromagnetic Energy Flux," by J.P. Thayer, J.F. Vickrey, R.A. Heelis, and J.B. Gary

INTERPRETATION AND MODELING OF THE HIGH-LATITUDE ELECTROMAGNETIC ENERGY FLUX

J.P. Thayer and J.F. Vickrey

SRI International, Menlo Park, California

R.A. Heelis, and J.B. Gary

Center for Space Science, Physics Program, University of Texas at Dallas, Richardson

For submission to the *Journal of Geophysical Research*

September 1994

ABSTRACT

An interpretation of the electromagnetic energy flux at high latitudes under steady-state conditions is presented and analyzed through modeling of the large-scale coupling between the high-latitude ionosphere and magnetosphere. In this paper we demonstrate that during steady state the electromagnetic energy flux (divergence of the DC Poynting flux), is equal to the Joule heating rate and the mechanical energy transfer rate in the high-latitude ionosphere. Although the Joule heating rate acts as a sink (transforming electromagnetic energy into thermal or internal energy of the gas), the mechanical energy transfer rate may be either a sink or source of electromagnetic energy. In the steady state, it is only the mechanical energy transfer rate that can generate electromagnetic energy and result in a DC Poynting flux that is directed out of the ionosphere. To evaluate the electromagnetic energy flux at high latitudes and interpret the role of the ionosphere, we employ the Vector Spherical Harmonic model, which is based on the NCAR Thermosphere–Ionosphere General Circulation Model, to provide the steady-state properties of the thermosphere–ionosphere system under moderate to quiet geomagnetic activity.

We conclude that 1) the electromagnetic energy flux is predominantly directed into the high-latitude ionosphere with greater input in the morning sector than the evening sector. 2) The Joule heating rate accounts for much of the electromagnetic energy converted in the ionosphere, with the conductivity-weighted neutral wind contributing significantly to the Joule heating rate and thus to the net electromagnetic energy flux in the ionosphere. 3) On average, the mechanical energy transfer rate contributes about 20% to the net electromagnetic energy flux in the dawn, dusk, and polar cap regions, acting as a sink of electromagnetic energy flux in the dawn and dusk sectors and a source of electromagnetic energy flux in the polar cap. 4) An upward electromagnetic energy flux is found in the regions near the convection reversal boundaries. This flux is due to the mechanical energy transfer rate exceeding the Joule heating rate. The upward electromagnetic energy flux was found to be small partly due to the relationship of the conductivity-weighted neutral wind to the imposed electric field and partly due to the Joule heating rate increasing irrespective of the source of electromagnetic energy flux.

1 INTRODUCTION

The magnetosphere–ionosphere (M–I) system at high latitudes can exhibit a diverse character in the distribution of currents and electric fields and in the population and energy of plasma particles. These features help to define the various regions of the M–I system. These regions are coupled through the exchange of energy between the electromagnetic field and the plasma. The energy exchange involved in this process can be described in terms of Poynting's theorem,

$$\iiint_V \frac{\partial}{\partial t}\left(\frac{B^2}{2\mu_0} + \frac{\varepsilon_0}{2}E^2\right) dV + \iiint_V \frac{\nabla \circ \left(\vec{E} \times \vec{B}\right)}{\mu_0} dV + \iiint_V \vec{j} \circ \vec{E}\, dV = 0 \quad , \tag{1}$$

where the first term is the electromagnetic energy density within the volume, the second term is the divergence of the electromagnetic (Poynting) energy flux within the volume, and the third term is the volume energy transfer rate. The derivation of Poynting's theorem comes directly from Maxwell's equations using the identity $\nabla \circ \left(\vec{E} \times \vec{B}\right) \equiv \vec{B} \circ \left(\nabla \times \vec{E}\right) - \vec{E} \circ \left(\nabla \times \vec{B}\right)$. For magnetospheric–ionospheric applications, the magnetic field energy density, to a very good approximation, greatly exceeds the electric field energy density. Poynting's theorem, given by (1), can then be written as

$$\iiint_V \frac{\partial}{\partial t}\left(\frac{B^2}{2\mu_0}\right) dV + \iiint_V \frac{\nabla \circ \left(\vec{E} \times \delta\vec{B}\right)}{\mu_0} dV + \iiint_V \vec{j} \circ \vec{E}\, dV = 0 \quad , \tag{2}$$

with $\delta\vec{B}$ representing the perturbation magnetic field due to the large-scale ionospheric current system (see Kelley et al. [1991]).

Poynting's theorem has been used to provide a general description of the energy exchange between the solar wind and magnetosphere [e.g., Hill, 1983; Cowley, 1991], for the interpretation of time-varying electromagnetic fields [e.g., Fraser, 1985], and, more recently, for the evaluation and interpretation of large-scale energy transfer in the ionosphere [e.g., Cowley, 1991; Kelley et al., 1991; Thayer and Vickrey, 1992; Gary et al., 1994a]. For investigations concerned with high-latitude ionospheric energetics, the electromagnetic energy flux described by Poynting's theorem is a fundamental quantity because it describes the electromagnetic energy

exchange between the magnetosphere and ionosphere. Joule heating and the bulk motion of the neutral gas in the high-latitude ionosphere are a direct result of this energy exchange. It is this more recent use of Poynting's theorem that will be developed further in our modeling study.

In a steady state, the net energy exchange between the electromagnetic field and the plasma is zero. As stated by Cowley [1991], Poynting's theorem in the steady state demonstrates that any increase in plasma energy that occurs in one region of space must be at the direct expense of the loss of plasma energy in another, where the two regions are connected by a current tube. Thus, source regions where energy is transferred from the plasma to the electromagnetic field ($\vec{J} \circ \vec{E}$ negative) must be balanced by sink regions of energy transfer from the electromagnetic field to the plasma ($\vec{J} \circ \vec{E}$ positive). Based on this premise and the magnetic coupling of the magnetosphere and ionosphere at high latitudes, source or sink regions of electromagnetic energy flux in the high-latitude ionosphere must be matched by sink or source regions in the magnetosphere. This approach is also used to derive the conventional view of energy flow in the open magnetosphere. On the dayside magnetopause, electromagnetic energy converges and energy is transferred to the plasma, accelerating it poleward. Poleward of the cusp, energy flow is directed from the plasma to the electromagnetic field forming the geomagnetic tail and maintaining the magnetic distortion and motion of the tail region. A fraction of this source energy is directed into the high-latitude ionosphere, where, in the simplest case, the ionosphere acts as a resistive load converting electromagnetic energy to thermal energy. In the tail current sheet, electromagnetic energy is converted back into plasma energy by reconnection, accelerating plasma toward and away from the earth.

This view, however, neglects the reactive nature of the high-latitude ionosphere due to the presence of neutral winds and their potential contribution to the electrodynamics. The neutral wind acts as a modifying influence on how much Poynting flux energy is required by the magnetosphere to power the dissipation processes in the high-latitude ionosphere and may potentially make the ionosphere a source of electromagnetic energy [Thayer and Vickrey, 1992]. In a study of the neutral wind contribution to the high-latitude energetics, Thayer and Vickrey [1992] expressed the influence of the neutral wind on the Poynting flux by writing the steady-state form of Poynting's theorem as

$$-\iiint_V \frac{\nabla \circ \left(\vec{E} \times \vec{B}\right)}{\mu_0} dV = \iiint_V \vec{j} \circ \vec{E}\ dV = \iiint_V \left\{ \vec{j} \circ \vec{E}' + \vec{u}_n \circ \left(\vec{j} \times \vec{B}_0\right) \right\} dV \quad , \tag{3}$$

where the divergence of Poynting flux is equal to the volume energy transfer rate which is equal to the Joule heating rate and the mechanical energy transfer rate. As a positive definite quantity, the Joule heating rate is a sink of electromagnetic energy flux in the ionosphere, while the mechanical energy transfer rate could be a sink or source depending on the height relationship among the neutral wind, conductivity, and electric field. By applying Gauss' theorem and following the arguments presented by Kelley et al. [1991], the divergence in the Poynting flux may be equated to the vertical, or field-aligned, Poynting flux.

Recently, Kelley et al. [1991] and Gary et al. [1994a] have shown through low-altitude, polar-orbiting satellite observations that the large-scale transfer of energy and momentum via the electromagnetic field between the solar wind-magnetosphere and the ionosphere-thermosphere at high latitudes can be determined by evaluating the DC component of the field-aligned Poynting flux. These derived results interpreted from observations have shown regions of electromagnetic energy flux into the ionosphere depicting the magnetospheric dynamo as the electrical source. However, electromagnetic energy flux out of the ionosphere over large scales has also been observed (see Gary et al. [1994a]). The outward directed energy flux can be interpreted as having a generator in the ionosphere, presumably through the neutral wind dynamo mechanism.

Thayer and Vickrey [1992] investigated the neutral wind contribution to the high-latitude energetics by assuming two uncoupled systems made up of a magnetospheric circuit and an ionospheric circuit. They then quantified the electrical energy contained in each system, separately, and demonstrated the importance of the neutral wind dynamo as a potential source of electrical energy at high latitudes. Deng et al. [1993] investigated the effects of the time dependent neutral wind dynamo on high-latitude ionospheric electrodynamics after a geomagnetic storm and found that the neutral winds contribute significantly to the ionospheric current system.

Therefore, it is important (and more accessible through measurement) to investigate the exchange of electromagnetic energy in the high-latitude ionosphere using this source–sink concept of Poynting's theorem to provide further insight into the M–I electrodynamic system. Here, we will pursue a modeling effort to treat the coupled aspects of the M–I system in evaluating the exchange of electromagnetic energy in the high-latitude ionosphere. In our approach, we develop further the relationship of Poynting's theorem to ionospheric studies of Joule heating and neutral wind dynamics to help elucidate the sources and sinks of electromagnetic energy in the high-latitude ionosphere.

2 THEORETICAL DEVELOPMENT

Equation 3 has important implications for studies of ionospheric electrodynamics that can be best understood by deriving the equation from basic principles using the MHD energy and momentum equations. A similar derivation is provided by Brekke and Rino [1978], however, the connection to Poynting's theorem is new.

The ionospheric energy equation describing the total energy of the gas using the MHD or single fluid approximation can be expressed as

$$\rho\frac{D}{Dt}(u) + \rho\frac{D}{Dt}\left(\frac{V^2}{2}\right) + \nabla\circ\left(\overline{\overline{P}}\circ\vec{V}\right) + \nabla\circ\vec{q} = \rho\vec{V}\circ\vec{g} + \rho Q + \vec{j}\circ\vec{E} \quad , \tag{4}$$

where the terms on the LHS are the time rate of change of the internal energy of the gas, the time rate of change of the kinetic energy of the gas, the divergence of the momentum flux vector, and the divergence of the heat flux vector. The terms on the RHS are the kinetic energy of the gas associated with gravity, the internal energy of the gas caused by chemical and radiative processes, and the electromagnetic energy transfer rate describing the rate of electrical energy conversion, dissipation, or generation within the gas.

Equation 4 describes the kinetic and internal energies of the gas. It is useful however, to have a separate equation to describe each of these forms of energy. The kinetic energy equation, derived by taking the inner product of the velocity with the MHD momentum equation, is expressed as

$$\rho\frac{D}{Dt}\left(\frac{V^2}{2}\right) + \vec{V}\circ\left(\nabla\circ\overline{\overline{P}}\right) = \rho\vec{V}\circ\vec{g} + \vec{V}\circ\left(\vec{j}\times\vec{B}\right) \quad , \tag{5}$$

where the first term is the time rate of change of kinetic energy of the gas, while the other terms represent the work done by mechanical and electrical forces on the gas. To describe only the internal energy of the gas, the kinetic energy equation can be subtracted from the total energy equation resulting in the expression,

$$\vec{j} \circ \vec{E} - \vec{V} \circ \left(\vec{j} \times \vec{B}\right) = \vec{j} \circ \vec{E}' = \rho \frac{D}{Dt}(u) + \nabla \circ \vec{q} - \rho Q + \overline{\overline{P}} : \nabla \vec{V} \quad . \tag{6}$$

This equation accounts for only the internal energy of the gas, with the new term $\vec{j} \circ \vec{E}'$ representing the Joule heating rate of the gas. The last term of (6) accounts for the internal energy of the gas caused by viscous heating and the expansion or contraction of the gas.

To a good approximation in the ionosphere, the center of mass velocity, $\vec{V}$, can be replaced by the neutral wind, $\vec{u}_n$, because the mass density of the neutrals is much greater than that of the ions. The Joule heating rate is then expressed in the more familiar form

$$\vec{j} \circ \vec{E}' = \vec{j} \circ \left(\vec{E} + \vec{u}_n \times \vec{B}\right).$$

Rearranging (6), the energy transfer rate can be written as $\vec{j} \circ \vec{E} = \vec{j} \circ \vec{E}' + \vec{u}_n \circ \left(\vec{j} \times \vec{B}\right)$ and substituted into (2) to obtain the relationship given in (3) between the divergence in the Poynting flux, the Joule heating rate, and the mechanical energy conversion rate. The expression $\vec{j} \circ \vec{E} = \vec{j} \circ \vec{E}' + \vec{u}_n \circ \left(\vec{j} \times \vec{B}\right)$ could have also been derived by a straightforward transformation of $\vec{j} \circ \vec{E}$ into the nonaccelerating reference frame of the neutral wind, $\vec{u}_n$. However, the full derivation provides more insight into the physical meaning of each of the terms in the expression.

3 APPROACH

Adopting the source-sink concept, we apply Poynting's theorem to the high-latitude ionosphere where the ionosphere is directly coupled to the magnetosphere through highly conducting field lines. Thus, electromagnetic energy flux is transferred between the source and sink regions of the magnetosphere and ionosphere via electric fields and field-aligned currents. To study the sources and sinks of electromagnetic energy in the high-latitude ionosphere under steady-state conditions, we use the expression for Poynting's theorem described in (3). To model this expression we use the Vector Spherical Harmonic (VSH) model of Killeen et al. [1987] to provide the necessary thermospheric and ionospheric parameters.

The VSH model is based on a spectral representation of the output fields from NCAR Thermosphere/Ionosphere General Circulation Model (TIGCM) simulations. The NCAR-TIGCM is a time-dependent, three-dimensional model that solves the fully coupled, nonlinear, hydrodynamic, thermodynamic, and continuity equations of the neutral gas self-consistently with the ion energy, ion momentum, and ion continuity equations (see Roble et al. [1988] and references therein). A simulation is uniquely determined by the input parameters to the model (i.e., EUV and UV fluxes, auroral particle precipitation, high-latitude ionospheric convection, and lower thermospheric tides). During a model run, the particle fluxes and the cross polar cap potential may be specified to remain fixed throughout the 24-hour model simulation. This type of model simulation is referred to as a diurnally reproducible state where the "UT effects" associated with the diurnal migration of the geomagnetic pole about the geographic pole are incorporated. Although the diurnally reproducible state may not actually occur in nature, due to shorter term variations in the solar wind/magnetosphere interaction, the model simulation does provide a description of the global, UT-varying thermosphere-ionosphere system during a particular geophysical situation. A set of NCAR-TIGCM runs have been expanded into VSH model coefficients that can be used to represent a range of geophysical conditions.

In the TIGCM formulation, the magnetosphere is treated as a generator delivering a fixed voltage to the ionosphere using the Heelis ion convection model [Heelis et al., 1982]. The parameterization of the ion convection pattern is tied to estimates of the total auroral hemispheric power input from the NOAA/TIROS particle flux measurements (H_p index). For the model simulation, any charge separation in the ionosphere due to neutral winds or gradients in conductivity are closed through field-aligned currents. Thus, for calculations of the

electromagnetic energy flux, the neutral winds contribute to the current system while the electric field originates in the magnetosphere. The electromagnetic energy flux calculations are coupled to the magnetosphere through the electric field, but no direct magnetospheric feedback is incorporated into the model to address how the processes in the ionosphere influence the magnetospheric response.

In this study, a model simulation providing a self-consistent description of the thermosphere-ionosphere system is used to study the coupled aspects of the M-I system at high latitudes. This approach differs from that used by Thayer and Vickrey [1992] in which the electrodynamic properties of the ionosphere and magnetosphere were evaluated separately to demonstrate the potential role the neutral winds could play in high-latitude electrodynamics. To make our calculations, we define a volume that covers the area from the geomagnetic pole to the 60°N magnetic latitude circle and extends in altitude from 110 to 400 km. We assume that the vertical magnetic flux tubes permeate this volume, each enclosing a 5°× 5° latitude / longitude bin. The calculations are performed at each grid point assuming horizontal uniformity of the parameters within each 5° bin. Applying these approximations to (3), the expression evaluated at each grid point in the modeling effort becomes

$$\int_z \vec{S} \circ \hat{n}\, dz = \int_z \vec{j} \circ \vec{E}\, dz = \int_z \left\{ \vec{j} \circ \vec{E}' + \vec{u}_n \circ \left(\vec{j} \times \vec{B}_0 \right) \right\} dz \quad , \tag{7}$$

where $\vec{S}$ is Poynting's vector, $\vec{E} \times \delta\vec{B}$, and $\hat{n}$ is the unit normal directed positive downward along magnetic field lines into the ionosphere. The coordinate system employed is right-handed with $\hat{x}$ directed positive northward, $\hat{y}$ directed positive eastward, and $\hat{z}$ directed positive downward.

The model simulation used in this study is representative of moderate to quiet geomagnetic activity (H_p index = 11 GW and cross-cap potential = 60 kV) and solar maximum conditions ($F_{10.7} = 220 \times 10^{-22}$ W m^{-2} sec^{-1}). Polar plots (from the model simulation for the December solstice in the northern hemisphere at 4 UT) of the height-integrated Pedersen conductivity in mhos and the electric field magnitude in mV/m are shown in Figure 1a and b on a magnetic latitude/magnetic local time grid extending in magnetic latitude from 60°N to the geomagnetic pole. The distribution of the height-integrated Pedersen conductivity is structured across the polar cap with enhanced values in the midnight and dawn sectors and a factor of three reduction in magnitude inside the polar cap. The enhanced regions of conductivity near midnight and in the dawn sector are due to the NCAR-TIGCM formulation for auroral particle precipitation. The

electric field shown in Figure 1 is representative of the typical two-cell ion convection pattern with its greatest values found inside the polar cap. Figure 1c and d is an altitude plot of the local Pedersen and Hall conductivity in mhos/m along the dawn-dusk magnetic meridian. The local Pedersen conductivity peaks near 130 km with enhancements in the dawn and dusk sectors of the E region and moderate conductivity values in the polar cap in both E and F regions. The local Hall conductivity is limited to the E region with peak values near 115 km and an asymmetric distribution across the polar cap with maxima found in the dawn sector. These parameters are important contributors to the net electromagnetic energy flux into the ionosphere and will be used in the evaluation of (7). The neutral wind contribution to (7) will be discussed in more detail in the following section. Due to the coarse $5° \times 5°$ grid of the NCAR-TIGCM, the model parameterizations, and the inherent smoothing of the spectral representation by the VSH model, the model output variables represent only the large-scale features of the system.

4 ANALYSIS

We begin the analysis by evaluating the height-integrated energy transfer rate, $\vec{J} \circ \vec{E}$, in the high-latitude ionosphere which, from (7), is equal to the height-integrated, field-aligned Poynting flux. The relationship of the energy transfer rate, or the electromagnetic energy flux, to the electric field, conductivity, and neutral wind can be shown by expanding (7) to give the expression

$$\int_z \vec{j} \circ \vec{E}\, dz = \Sigma_p \vec{E}^2 + \vec{E} \circ \int_z \sigma_p \left(\vec{U}_n \times \vec{B}\right) dz + \vec{E} \circ \int_z \sigma_h \vec{U}_n \left|\vec{B}\right| dz \quad , \tag{8}$$

where σ_p and σ_h are the Pedersen and Hall conductivity and Σ_p is the height-integrated Pedersen conductivity. The height-integrated electromagnetic energy flux calculated from (8) for the model run described in the approach section is displayed in Figure 2 on a magnetic latitude/magnetic local time grid in units of milliWatts per square meter for the northern winter hemisphere at 4 UT. The distribution of electromagnetic energy flux over the polar cap shown in Figure 2 is representative of the field-aligned Poynting flux directed into (positive) and out of (negative) the high-latitude ionosphere. The electromagnetic energy flux is predominantly directed into the entire polar ionosphere with only weak regions of upward energy flux near the convection reversal boundaries. If integrated over the area of the polar cap, 90° to 60° magnetic latitude, the total electromagnetic power into the ionosphere is approximately 3.5×10^{11}W which is about 5% of the total power generated in the tail magnetopause [Hill, 1983]. Figure 2 also shows an asymmetry in the electromagnetic energy flux across the noon-midnight meridian with more electromagnetic energy flux directed into the ionosphere in the morning sector (00 - 12 MLT) than in the evening sector (12 - 00 MLT) by factors of two and three.

Recently, Gary et al. [1994b] provided statistical averages of the field-aligned DC Poynting flux determined from DE 2 for the entire polar cap, albeit with mixed hemispheres and geomagnetic conditions, that illustrate similar features to the model results shown in Figure 2. The magnitude of the modeled electrical energy flux is underestimated within the auroral oval compared with that determined from the observations by Gary et al. [1994b]. This may be due to an underestimate of auroral features in the model or to the geomagnetic conditions of the model simulation of quiet to moderate not being representative of the data set presented by Gary et al.

[1994b]. Weak regions of negative electrical energy flux or upward Poynting flux are determined from the model and are located in the regions of the ion convection reversals. These features of negative electrical energy flux are caused by the electrical contribution of the neutral wind as will be discussed in the following section.

Figure 3 illustrates the distribution along the dawn-dusk plane of each of the height-integrated terms given in (8) to demonstrate their relative contributions to the total electromagnetic energy flux shown in Figure 2. The total electromagnetic energy flux is given by the solid line in Figure 3 and shows the asymmetric distribution of energy flux between the dawn and dusk sectors. The first term on the RHS of (8), Term 1, is a positive definite quantity and, as shown by the dashed line in Figure 3, the dominate term contributing to the positive or downward flux of electromagnetic energy into the ionosphere. Term 1 peak values of 2 mW/m^2 occur in the polar cap with nearly equal enhancements of 1.5 mW/m^2 located in the dawn and dusk sectors. The other two terms in (8) tend to reduce the net flux of electromagnetic energy. Term 2 is the main contributor to the reduction in the downward energy flux, as shown by the dotted line in Figure 3, with peak values in the polar cap of -1.7 mW/m^2 and values of -0.7 mW/m^2 and -0.3 mW/m^2 in the dusk and dawn sectors, respectively. Strong ionospheric coupling between the neutral wind and the electric field in the dusk and polar cap regions and weak coupling in the dawn sector accounts for the asymmetry in the dawn-dusk distribution of Term 2 and is responsible for the asymmetric distribution of the total electromagnetic energy flux. Term 3 is subsidiary with values in the dawn sector of about 0.2 mW/m^2 and -0.1 mW/m^2 in the polar cap.

To illustrate the height dependencies in evaluating the integrals in (8), model calculations are made for each term along the dawn-dusk plane at 5 km increments from 110 to 400 km. Figure 4 is a plot of the altitude distribution for each term integrated in (8) and displayed in Figure 3. Figure 4a represents the distribution in altitude of Term 1 along the dawn-dusk plane. The main contribution to this positive definite term comes from the E region with enhancements in the dawn, dusk, and polar cap regions. The enhancement in the polar cap is due to the presence of strong electric fields in this region, while enhancements in the dawn and dusk sector are due primarily to enhancements in the conductivity (with greater conductivity in the dawn sector than in the dusk sector). Lesser contributions made by altitudes above the E region are also limited to dawn, dusk, and polar cap regions. A noticeable contribution to Term 1 from the F region can be seen in the polar cap region where soft particle precipitation enhances the Pedersen conductivity (see Figure 1c).

The altitude distribution of Term 2 is illustrated in Figure 4b. This term accounts for the coupling between the electric field and the Pedersen-weighted neutral wind. Throughout all altitudes this term is predominantly negative, with most of the contribution coming from altitudes above 140 km. As illustrated by the integrated result for Term 2 in Figure 3, the main contributions come from the dawn, dusk, and polar cap regions with peak contributions from F region and E region altitudes. The greatest contribution to Term 2 comes from the polar cap at F-region altitudes, where the neutral winds are strongly coupled to the electric field. The magnitude of Term 2 with increasing altitude is quite uniform in both the dawn and dusk sectors as a reduction in Pedersen conductivity is countered by an increase in the neutral wind and its improved coupling to the electric field. The dawn and dusk sectors illustrate the asymmetric pattern seen in the integrated result throughout all altitudes.

Term 3, describing the coupling between the electric field and Hall-weighted neutral wind, is displayed in Figure 4c showing its altitude distribution to be isolated to the lower E region and concentrated in the dawn and polar cap sectors. The height distribution is limited by the Hall conductivity, as was shown in Figure 1d, while the distribution along the dawn-dusk plane is attributable to the relationship between the electric field and the neutral wind. The neutral winds in the E region are a factor of three to four lesser in magnitude than winds in the F region. The E region neutral wind pattern is also rotated counter clockwise by a couple of hours compared to the F region circulation and favors a more cyclonic neutral wind circulation. These variations in the neutral wind with height are a result of the complex interaction between tidal forcing and magnetospheric forcing in the E region as is discussed by Mikkelsen and Larsen [1991]. Because of the counter clockwise rotation of the wind pattern, the winds in the polar cap are in opposite direction to the imposed dawn-dusk electric field, resulting in a negative energy flux. However, due to the more cyclonic behavior of the E-region winds, the electric field and winds in the dawn sector are in the same direction, resulting in a positive energy flux. Because this term does not contribute to the Joule heating rate, a positive energy flux is representative of electrical energy being converted to mechanical energy, while a negative energy flux is representative of mechanical energy converted to electrical energy. This term is less important after height integration, yet, it represents a contribution that is typically not accounted for in studies of electrodynamics at high latitudes.

The altitude distribution of the electromagnetic energy flux per meter along the dawn-dusk plane is displayed in Figure 4d. The greatest contribution to the electrical energy flux comes from the E region where Term 1 dominates. The dawn-dusk distribution of positive

electromagnetic energy flux per meter in the E region is skewed toward the dawn sector as Term 3 and Term 1 contribute positively in this sector. In the E-region dusk sector, positive electromagnetic energy flux per meter is reduced due to Term 2. In the F region, the electrical energy flux per meter is negative due to the dominating negative contribution from Term 2.

5 DISCUSSION

In the previous section we demonstrated that the neutral wind contributes significantly to the DC field-aligned Poynting flux in the ionosphere, particularly in the polar cap and dusk sector. If it is assumed that the magnetic field is independent of height over our altitude range, an effective neutral wind can be determined to describe the height-integrated neutral wind profile weighted by the conductivity.

$$\vec{U}_{eff} = \frac{\int_z \sigma_P \vec{U}_n \, dz + \int_z \sigma_h \hat{b} \times \vec{U}_n \, dz}{\Sigma_P} \quad . \tag{9}$$

The effective neutral wind from (9) for the model simulation used above is displayed in Figure 5. The resultant effective neutral wind has a pattern similar to that of the F region (see Thayer and Killeen [1993]) with speeds reduced by approximately 50%. There is also a small counter clockwise twist of the pattern due to the contribution from E region altitudes (see discussion by Mikkelsen and Larsen [1991]). The weighting of the neutral wind with height by the ionospheric conductivity results in a combined influence of neutral wind dynamics and conductivity variations with altitude.

Using (9), the volume energy transfer rate may be written in a more informative way as

$$\int_z \vec{j} \circ \vec{E} \, dz = \Sigma_P \left[\vec{E}^2 - \vec{U}_{eff} \circ \left(\vec{E} \times \vec{B} \right) \right] \quad . \tag{10}$$

Expressed in this form, the effective neutral wind acts as a modifying influence on how much Poynting flux energy is required by the magnetosphere to power the dissipation processes in the high-latitude ionosphere, as discussed previously. However, the neutral wind's influence may make the ionosphere a source of electromagnetic energy ($\vec{J} \circ \vec{E}$ negative) if the effective neutral wind has a component in the $\vec{E} \times \vec{B}$ direction that exceeds the $\vec{E} \times \vec{B}$ plasma drift velocity. The negative or upward Poynting flux regions illustrated in Figure 2 are located near the convection

reversal boundaries where the effective neutral wind in the $\vec{E} \times \vec{B}$ direction exceeds the plasma drift velocity. At the convection reversal boundaries there is no Poynting flux, because the electric field is zero.

It is the component of the effective neutral wind in the direction of the electric field that is significant in the electrodynamics, not the effective neutral wind itself. The influence of the effective neutral wind coupled to the electric field is illustrated in Figure 3 by combining the results of Term 2 and Term 3 from (8). Referring to Figure 3, the enhancement of negative energy flux in the polar cap is a result of the effective neutral wind having a strong component in the $\vec{E} \times \vec{B}$ direction. The asymmetry in the negative electromagnetic energy flux from Term 2 and 3 between the dawn and dusk sectors reflects the dawn-dusk asymmetry demonstrated by the effective neutral wind pattern shown in Figure 5. This asymmetry has also been observed in the F region neutral circulation pattern [e.g., Thayer and Killeen [1993]. Thayer and Killeen [1993] demonstrated that an ion convection pattern with dawn and dusk cells of equal and opposite potential results in an asymmetric neutral circulation pattern with the dawn cell less organized than the dusk cell. Gundlach et al. [1988] explain this asymmetry in terms of the disparate balance of hydrodynamic forces between the dusk and dawn sectors. In Figure 3, the higher values of the net electrical energy flux (solid line) in the dawn sector demonstrate that the effective neutral wind is less coupled to the electric field in the dawn sector than in the dusk sector. Overall, the neutral wind contribution to the energy flux in the ionosphere is significant, particularly in the polar cap and dusk sector (as was concluded by Thayer and Vickrey [1992]).

We have shown that the neutral wind contributes significantly to the overall electrical energy flux in the high-latitude ionosphere. However, we have not determined how much the neutral wind is contributing to the Joule heating of the gas or to the mechanical energy of the gas. The partitioning of electromagnetic energy flux into its sinks (kinetic and internal energy of the gas) and sources (electrical energy caused by the neutral wind dynamo) can be addressed by evaluating separately the Joule heating rate and mechanical energy transfer rate described in (3).

Joule Heating Rate

The Joule heating rate is a positive definite quantity acting purely as a sink of electromagnetic energy in the ionosphere as electrical energy is transferred to the internal energy of the gas as heat. The height-integrated Joule heating rate can be obtained without approximation given the height distribution of the neutral wind, electric field, and conductivity as described by the expression

$$\int_z \vec{j} \circ \vec{E}' \, dz = \int_z \vec{j} \circ \left(\vec{E} + \vec{U}_n \times \vec{B}\right) dz = \int_z \sigma_p \left(\vec{E} + \vec{U}_n \times \vec{B}\right)^2 dz \quad . \qquad 11)$$

An illustration of the height-integrated Joule heating rate for the simulation described in the previous sections is given in Figure 6. The main features of the Joule heating pattern are enhanced regions of Joule heating in the auroral oval with maxima in the dawn and post-midnight sectors and relatively weak enhancements in the dusk sector and inside the polar cap. The Joule heating rate displays an asymmetric pattern in the auroral zone with the Joule heating rate in the dawn sector a factor of three greater than in the dusk sector. Comparing these results with the electromagnetic energy flux calculations given in Figure 2, we find that the magnitude and pattern of the Joule heating rate is very similar to the electromagnetic energy flux. Thus, most of the electromagnetic energy flux directed into the ionosphere is dissipated as heat under the conditions of this simulation. That is not to say that the neutral winds contribute insignificantly to the distribution of the energy flux at high latitudes, as was shown above, but that the winds are contributing most to the Joule heating rate of the gas (either positively or negatively).

To elucidate the impact of the neutral wind on the Joule heating rate at high latitudes, a calculation of the Joule heating rate neglecting the neutral wind is shown in Figure 6b. Neglecting the neutral wind has its greatest impact in the dusk sector and central polar cap where the Joule heating rate is overestimated by as much as a factor of three. This makes the point that, although the conductivity may be enhanced in this region, the neutral winds are also strongly coupled to the electric field resulting in a much lower Joule heating rate than might be anticipated. Overall, the neutral wind acts to reduce the approximated Joule heating rate under the conditions of this simulation.

Given a better understanding for the quantities $\vec{j} \circ \vec{E}$ (the electromagnetic energy flux) and $\vec{j} \circ \vec{E}'$ (the Joule heating rate), it is worth reviewing the approaches taken by many investigators in evaluating, empirically, the Joule heating rate in the high-latitude ionosphere. These investigations are mainly to quantify the height-integrated Joule heating rate to describe the change in the internal energy of the gas caused by the dissipation of electrical energy in the ionosphere. Because of the difficulty in determining the neutral wind with height, approximations to the neutral wind are typically made when calculating the Joule heating rate from measurements. However, the manner in which the approximation to the neutral wind is

treated can result in different interpretations for the evaluated Joule heating rate and subsequently the electromagnetic energy flux.

For the case when the height distribution of the conductivity and electric field (typically assumed independent of height) are known and the neutral wind is assumed to be zero, the form of the height-integrated Joule heating rate is $\vec{J} \circ \vec{E}' = \vec{J} \circ \vec{E} = \Sigma_p \vec{E}^2$. This form of the equation represents the electromagnetic energy flux and means that the kinetic energy of the gas is zero. Thus, electromagnetic energy from the magnetosphere described by the divergence in the Poynting flux is dissipated entirely into the ionosphere (acting purely as a resistive load described by the height-integrated Pedersen conductivity) as thermal or internal energy. This can be considered the standard approach used in many investigations of high-latitude energetics [e.g., Banks et al., 1981; Foster et al., 1983]. We have demonstrated in Figure 6 that this assumption can have significant consequences, particularly in the dusk sector and the central polar cap.

A different interpretation results for this case if the height distribution of the current density instead of the conductivity, is known. For instance, if the current distribution is determined by solving the expression $\vec{j} = en_e\left(\vec{V}_i - \vec{V}_e\right)$ from measurements at different altitudes, say from radar measurements, and the neutral wind is said to be zero, then the height-integrated Joule heating rate is not that at all but actually the total electromagnetic energy flux converted, dissipated, or generated in the ionosphere; that is, the quantity being determined is $\vec{j} \circ \vec{E}$ which is equal to $\vec{j} \circ \vec{E}' + \vec{u}_n \circ \left(\vec{j} \times \vec{B}\right)$. This can be seen more clearly by expressing the current density in the form $\vec{j} = \sigma \circ \left(\vec{E} + \vec{U}_n \times \vec{B}\right)$. This shows that height distribution of the neutral wind is implicit within the measurement of $\vec{j}$. Also, the Joule heating rate is a positive definite quantity, but the determination of $\vec{j} \circ \vec{E}$ could be of either sign, as discussed by Thayer and Vickrey [1992]. Therefore, for this case, the statement that the neutral wind is assumed zero is false and it is the total electromagnetic energy flux being calculated not the Joule heating rate. The same result occurs if the height-integrated current density and the electric field are determined from a satellite measurement using the expression $J = \nabla \times (\delta \vec{B}) / \mu_0$, exemplified by the recent DE-2 field-aligned Poynting flux results described by Gary et al. [1994].

In more general terms, if the neutral wind is contributing at all to the energetics, it is implicitly contained within the current density within the ionosphere or the electric field depending on the electrical coupling between the ionosphere and magnetosphere. Irrespective of whether it is contained in the current density or electric field, its contribution to the net electromagnetic energy flux is accounted for if both the current density and electric field are determined. Also, the measure of the electromagnetic energy flux is a more fundamental

quantity than the Joule heating rate and may be more accurately determined from a spacecraft capable of measuring the electric and magnetic field [Kelley et al., 1991].

Mechanical Energy Transfer Rate

The mechanical energy transfer rate is either a sink or source of electromagnetic energy flux depending on whether electromagnetic energy is converted into the bulk motion of the gas (sink) or generated by the motion of the neutral gas through dynamo action (source). In this steady-state model simulation, the conductivity-weighted neutral wind acts as an electrical source by contributing to the current distribution in the ionosphere. As a sink of electromagnetic energy, the conductivity-weighted neutral wind is powered by the $\vec{J} \times \vec{B}$ force. The sign of the mechanical energy transfer rate illustrates whether the neutral wind is opposite (negative) or in the direction of (positive) the $\vec{J} \times \vec{B}$ force. A negative mechanical energy transfer rate would indicate that the neutral winds are opposing the $\vec{J} \times \vec{B}$ force and energy is transformed from mechanical form to electrical form, and vice versa.

Figure 7 is a plot of the height-integrated mechanical energy transfer rate, Joule heating rate, and the total electromagnetic energy flux along the dawn-dusk plane, similar to Figure 3. The height-integrated Joule heating rate in Figure 7 (dashed line) accounts for much of the electromagnetic energy flux into the ionosphere (solid line), as was demonstrated by Figure 6. The mechanical energy transfer rate is positive in the dawn and dusk sectors and negative in the polar cap. The positive mechanical energy transfer rate in the dawn and dusk sectors, therefore, acts as a sink for electromagnetic energy as electrical energy is being converted to the mechanical energy of the gas. Figure 8 is a plot of the percent contribution from the Joule heating rate (dashed line) and the mechanical energy transfer rate (dotted line) to the net electromagnetic energy flux. In the dawn and dusk sectors, the contribution from the mechanical energy transfer rate varies between 10 and 30%. In the polar cap, where the mechanical energy transfer rate is negative, the contribution to the electromagnetic energy flux is also between about 10 and 30%. In the locations near the ion convection boundaries, the mechanical energy transfer rate can contribute as much as the Joule heating rate, allowing for the possibility of a net upward Poynting flux.

In steady state, a net upward (negative) electromagnetic energy flux can only be generated by a negative mechanical energy transfer rate that exceeds the Joule heating rate. However, a net electromagnetic energy flux directed downward into the ionosphere (positive) still allows for the generation of electrical energy in the ionosphere (i.e., the mechanical energy transfer rate may still be negative). This is because when the neutral wind opposes the $\vec{J} \times \vec{B}$ force resulting in a

negative mechanical energy transfer rate, the Joule heating rate is likely to increase and become more positive. This can be seen if we expand the expressions for the mechanical energy transfer rate

$$\int_z \vec{U}_n \circ \left(\vec{j} \times \vec{B}\right) dz = -\vec{E} \circ \int_z \sigma_p \left(\vec{U}_n \times \vec{B}\right) dz + \vec{E} \circ \int_z \sigma_h \vec{U}_n \left|\vec{B}\right| dz - \int_z \sigma_p \left(\vec{U}_n \times \vec{B}\right)^2 dz \quad . \qquad (12)$$

and the Joule heating rate

$$\int_z \vec{j} \circ \vec{E}' \, dz = \Sigma_p \vec{E}^2 + 2\vec{E} \circ \int_z \sigma_p \left(\vec{U}_n \times \vec{B}\right) dz + \int_z \sigma_p \left(\vec{U}_n \times \vec{B}\right)^2 dz \quad . \qquad (13)$$

The addition of (12) and (13) results in the expression for the electromagnetic energy flux given by (8). It can be seen from the two equations that any negative contribution to the mechanical energy transfer rate provided by the first and last terms of (12) result in a more positive Joule heating rate. The Hall term given by the second term in (12) is the only independent contributor in the mechanical energy transfer rate equation that would directly influence the net electromagnetic energy flux. However, the height-integrated Hall term was shown in Figure 3 to be a subsidiary contributor to the net electrical energy flux. As was shown earlier by (10), the only time the net electromagnetic energy flux can be upward is when the height-integrated, conductivity-weighted neutral wind exceeds the nonzero $\vec{E} \times \vec{B}$ drift velocity. This would cause Term 3 in the mechanical energy transfer rate equation to become more negative than the positive values of Term 1 and reduce the Joule heating rate such that a negative electromagnetic energy flux results. The offsetting terms in (12), the weak contribution from the Hall term, and the always positive Joule heating rate precludes the existence of a large upward Poynting flux under these modeled conditions and quite possibly in nature as well.

5 CONCLUSIONS

We investigated the exchange of electromagnetic energy in the high-latitude ionosphere using a steady-state, source-sink concept of Poynting's theorem to provide further insight into the M–I electrodynamic system. Poynting's theorem applied to the high-latitude M–I system and the theorem's relationship with the Joule heating rate and mechanical energy transfer rate has been elucidated and the consequences of this relationship evaluated through numerical modeling. Here, we used the VSH model to provide the necessary thermosphere–ionosphere parameters to evaluate and interpret the electromagnetic energy flux at high latitudes for moderate to quiet geomagnetic conditions during solar maximum. Although the model is coupled to the magnetosphere through the mapping of the magnetospheric electric field and particle precipitation, no direct feedback to the magnetosphere has been attempted. To this end, any neutral wind dynamo action in the model would be manifested in terms of currents, treating the magnetosphere as a pure voltage generator.

The analysis of the steady-state electromagnetic energy flux at high latitudes under the described model conditions leads to a number of conclusions.

- The electromagnetic energy flux, or field-aligned Poynting flux, is predominantly directed into the high-latitude ionosphere with weak regions of upward electromagnetic energy flux near the boundaries of the convection reversals. The distribution of electromagnetic energy flux at high latitudes is asymmetric with greater downward flux in the morning sector than in the evening sector by a factor of three for this simulation.
- The Joule heating rate accounts for much of the electromagnetic energy converted in the ionosphere with the conductivity-weighted neutral wind contributing significantly to the Joule heating rate and, thus, to the net electromagnetic energy flux in the ionosphere.
- On average, the mechanical energy transfer rate contributes about 20% to the net electromagnetic energy flux in the dawn, dusk, and polar cap regions, acting as a sink of electromagnetic energy flux in the dawn and dusk sectors and a source of electromagnetic energy flux in the polar cap.

- Weak upward electromagnetic energy flux is found in the regions near the convection reversal boundaries. This flux is due to the mechanical energy transfer rate exceeding the Joule heating rate. The upward electromagnetic energy flux was found to be small partly due to the relation of the conductivity-weighted neutral wind to the imposed electric field and partly due to the Joule heating rate increasing irrespective of the source of electromagnetic energy flux.

Acknowledgments. This work was supported by NASA, Contract NAS5-31214, NASA Grant NAGW-3508. We would like to thank Dr. Tim Killeen, Rob Raskin, and Alan Burns at the University of Michigan for the VSH model code.

6 REFERENCES

Banks, P.M., J.C. Foster, and J.R. Doupnik, Chatanika radar observations relating to the latitudinal and local time variations of Joule heating, *J. Geophys. Res., 86*, 6869-6878, 1981.

Brekke, A., and C.L. Rino, High-resolution altitude profiles of the auroral zone energy dissipation due to ionospheric currents, *J. Geophys. Res., 83*, A6, 2517-2524, 1978.

Cowley, S.W.H., Acceleration and heating of space plasmas: basic concepts, *Ann. Geophys., 9*, 176-187, 1991.

Deng, W., T.L. Killeen, A.G. Burns, R.G Roble, J.A. Slavin, and L.E. Wharton, The effects of neutral inertia on ionospheric currents in the high-latitude thermosphere following a geomagnetic storm, *J. Geophys. Res., 98*, 7775-7790, 1993.

Foster, J.C., J.-P. St.-Maurice, and V.J. Abreu, Joule heating at high latitudes, *J. Geophys. Res., 88*, 4885-4896, 1983.

Fraser, B.J., Observations of Ion Cyclotron waves near synchronous orbit and on the ground, *Space Sci. Rev., 42*, 357-374, 1985.

Gary, J.B., R.A. Heelis, W.B. Hanson, and J.A. Slavin, Field-aligned poynting flux observations in the high-latitude ionosphere, *J. Geophys. Res., 99*, 11417-11427, 1994a.

Gary, J.B., R.A. Heelis, J.P. Thayer, Summary of field-aligned poynting flux observations from DE-2, submitted to *Geophys. Res. Lett*, 1994b.

Gundlach, J.P., M.F. Larsen, and I.S. Mikkelsen, A simple model describing the nonlinear dynamics of the dusk/dawn asymmetry in the high-latitude thermospheric flow, *Geophys. Res. Lett., 15*, 307-310, 1988.

Heelis, R.A., J.K. Lowell, and R.W. Spiro, A model of the high-latitude ionospheric convection pattern, *J. Geophys. Res.*, 87, 6339-6345, 1982.

Heelis, R.A., and W.R. Coley, Global and local Joule heating effects seen by DE 2, *J. Geophys. Res., 93*, 7551-7557, 1988.

Hill, T.W., Solar-wind magnetosphere coupling, in *Solar-Terrestrial Physics*, pp. 261-302, R.L. Carovillano and J.M. Forbes, eds. (D. Reidel Publishing Company), 1983.

Kelley, M.C., D.J. Knudsen, and J.F. Vickrey, Poynting flux measurements on a satellite: a diagnostic tool for space research, *J. Geophys. Res.*, *96*, A1, 201-207, 1991.

Killeen, T.L., R.G. Roble, and N.W. Spencer, A computer model of global thermospheric winds and temperatures, *Adv. Space Res.*, *7*, 207-215, 1987.

Mikkelsen, I.S., and M.F. Larsen, A numerical modeling study of the interaction between the tides and the circulation forced by high-latitude plasma convection, *J. Geophys. Res.*, *96*, 1203-1213, 1991.

Roble, R.G., E.C. Ridley, A.D. Richmond, and R.E. Dickinson, A coupled thermosphere/ ionosphere general circulation model, *Geophys. Res. Lett.*, *15*, 1325-1328, 1988.

Thayer, J.P., and J.F. Vickrey, On the contribution of the thermospheric neutral wind to high-latitude energetics, *Geophys. Res. Lett.*, *19*, 3, 265-268, 1992.

Thayer, J.P., and T.L. Killeen, A kinematic analysis of the high-latitude thermospheric neutral circulation pattern, *J. Geophys. Res.*, *98*, 11549-11565, 1993.

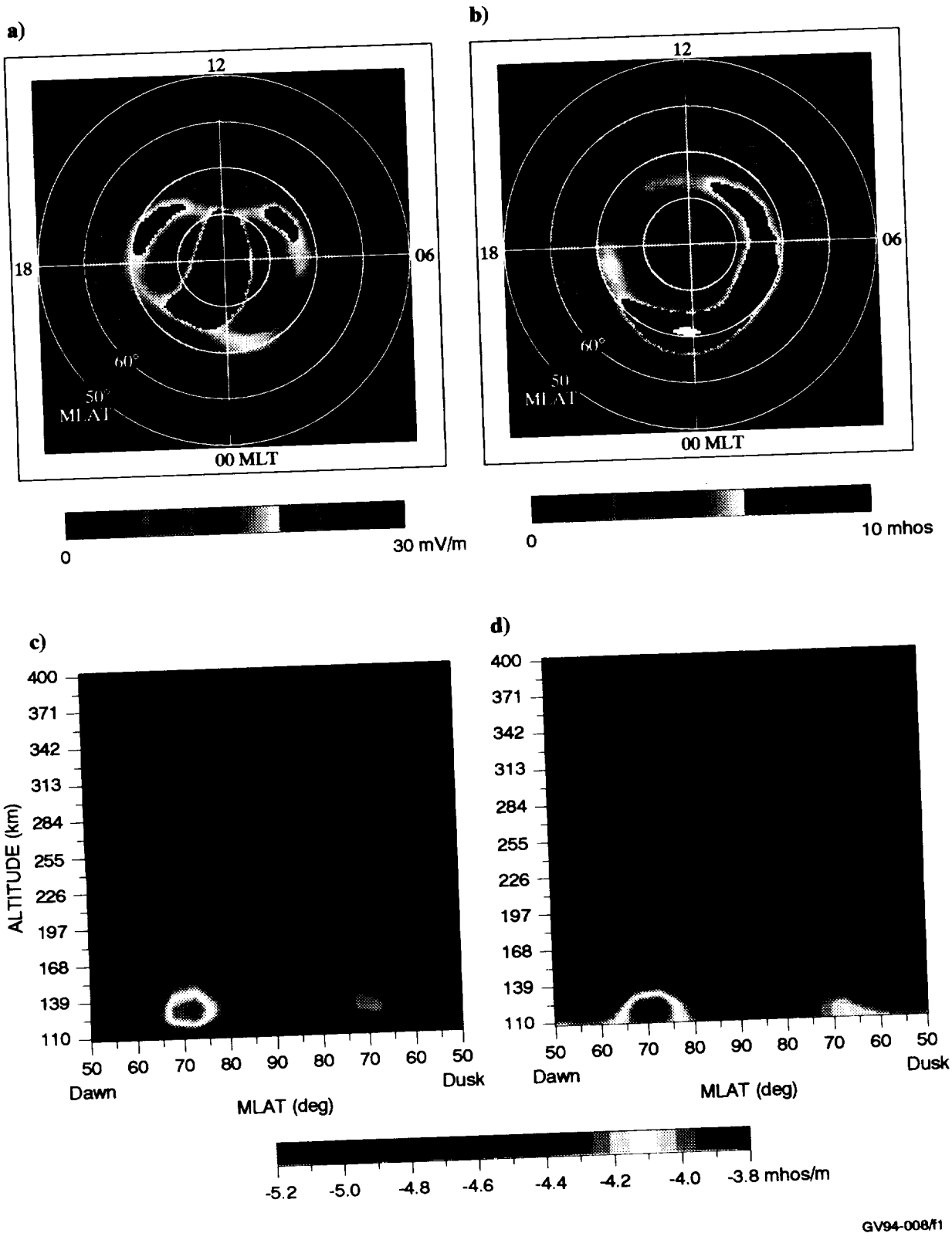

Fig. 1. Polar plots on a magnetic grid of a) electric field magnitude in mV/m b) height-integrated Pedersen conductivity in mhos. Altitude plots along the dawn-dusk magnetic plane of the local c) Pedersen and d) Hall conductivity in mhos/m.

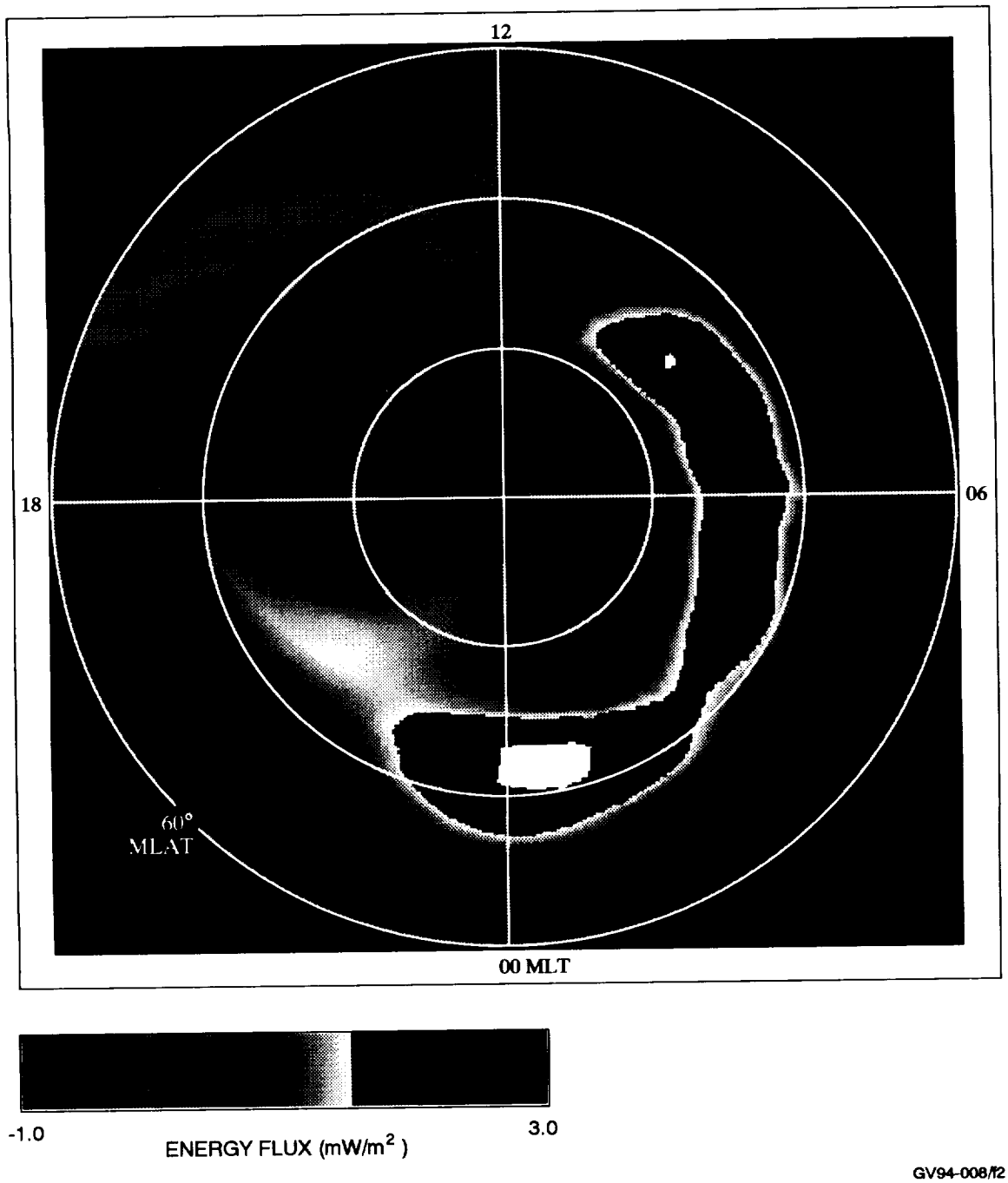

Fig. 2. Polar plots on a magnetic grid of the distribution of electromagnetic energy flux.

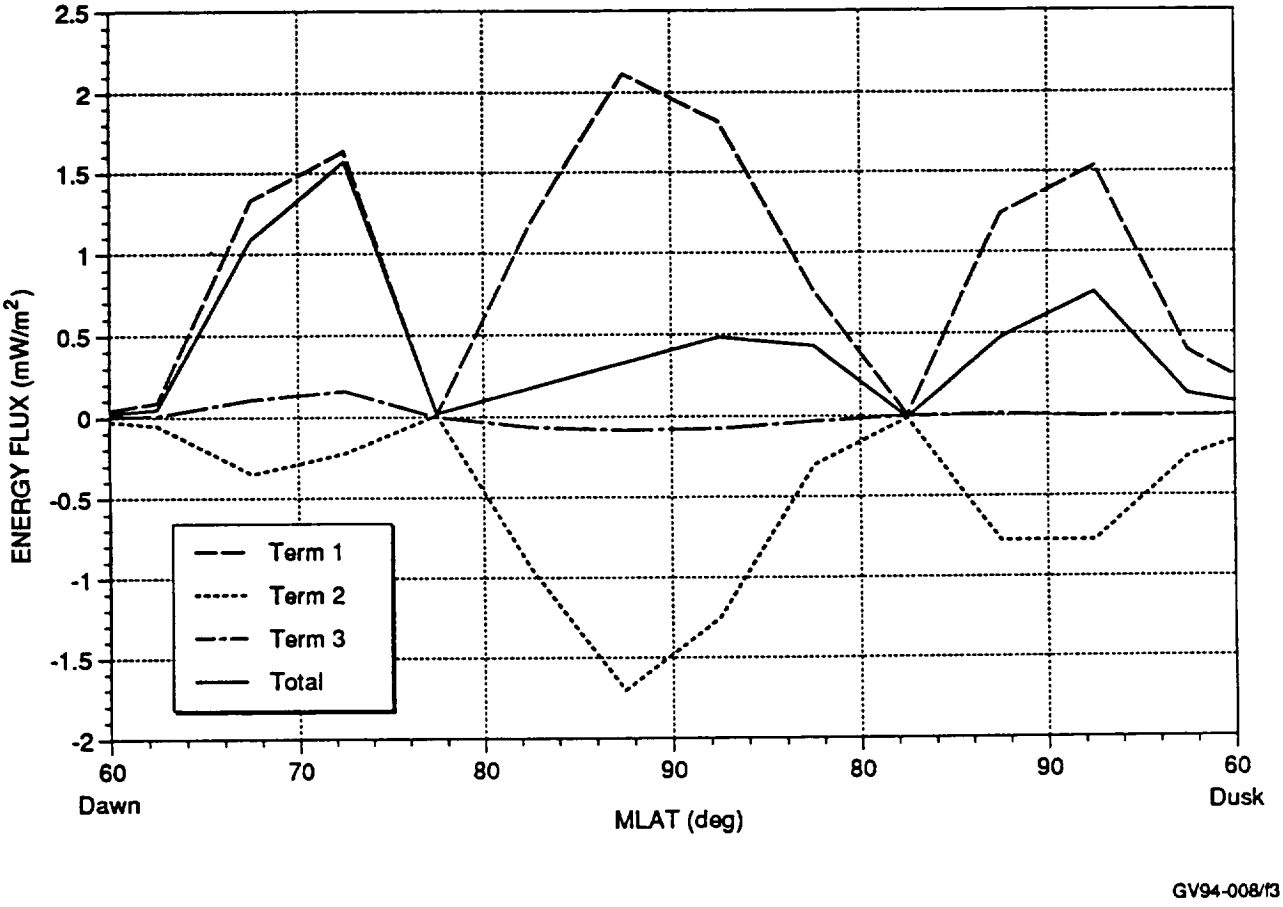

Fig. 3. Height-integrated terms given in Equation 8 along the dawn-dusk magnetic plane.

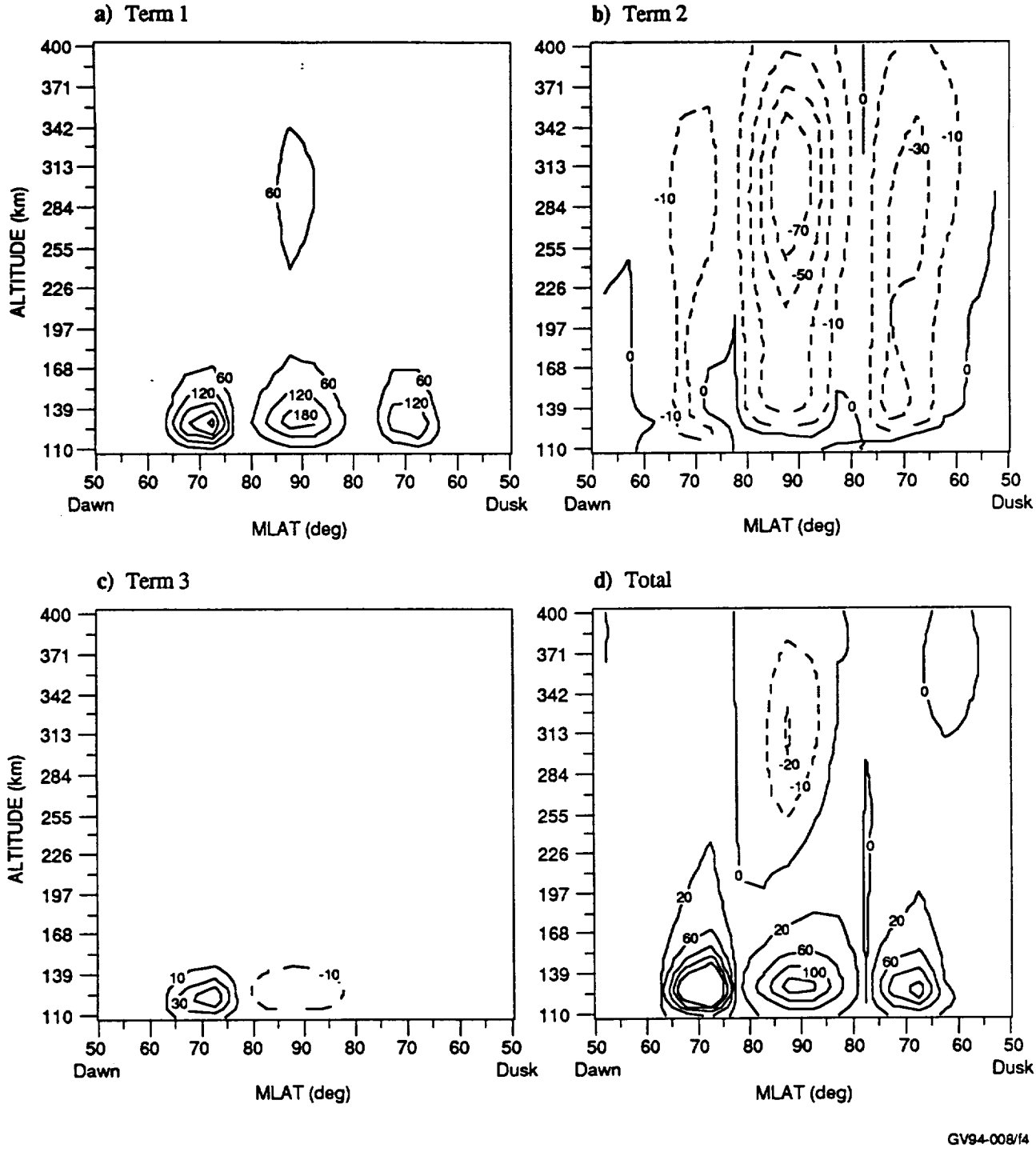

Fig. 4. Altitude distribution for each of the terms in Equation 8 along the dawn-dusk magnetic plane.

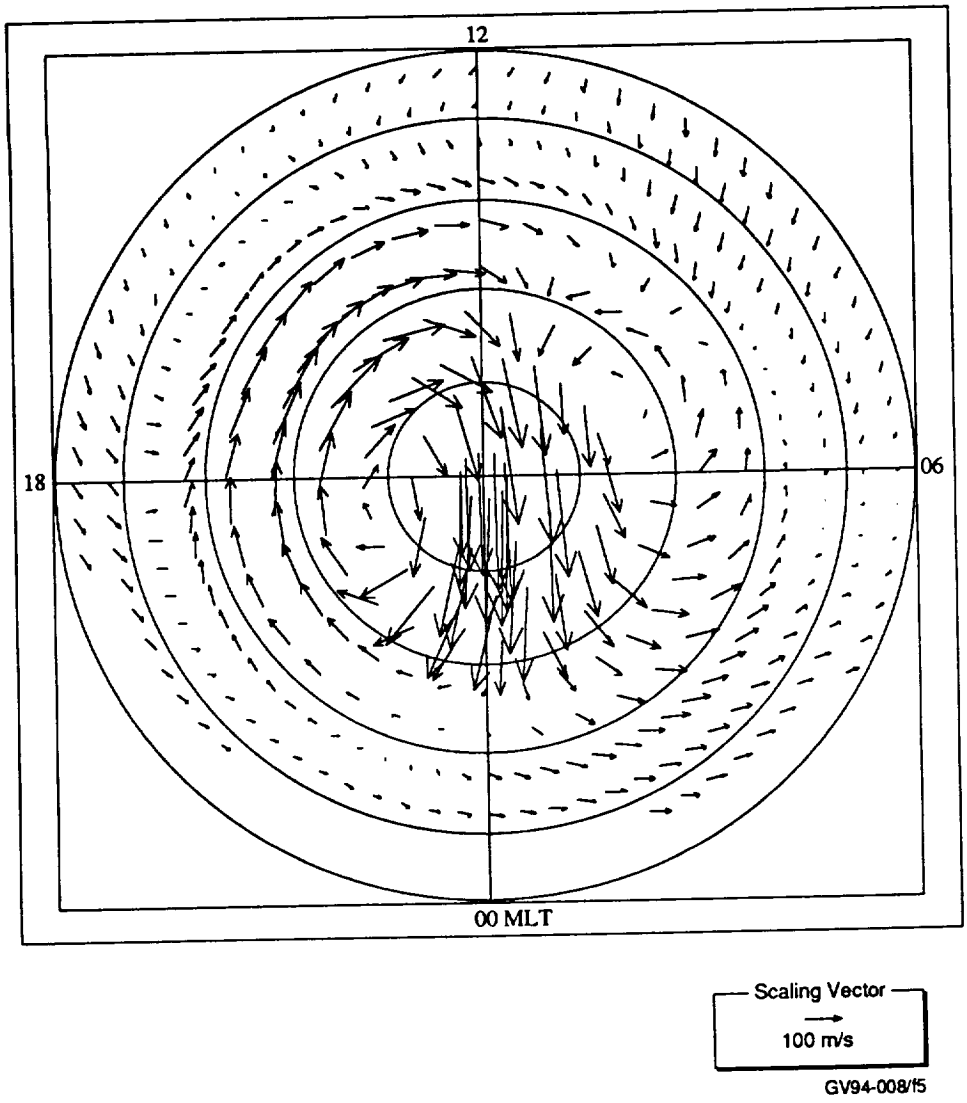

Fig. 5. Polar plot of the effective neutral wind (same format as Figure 2).

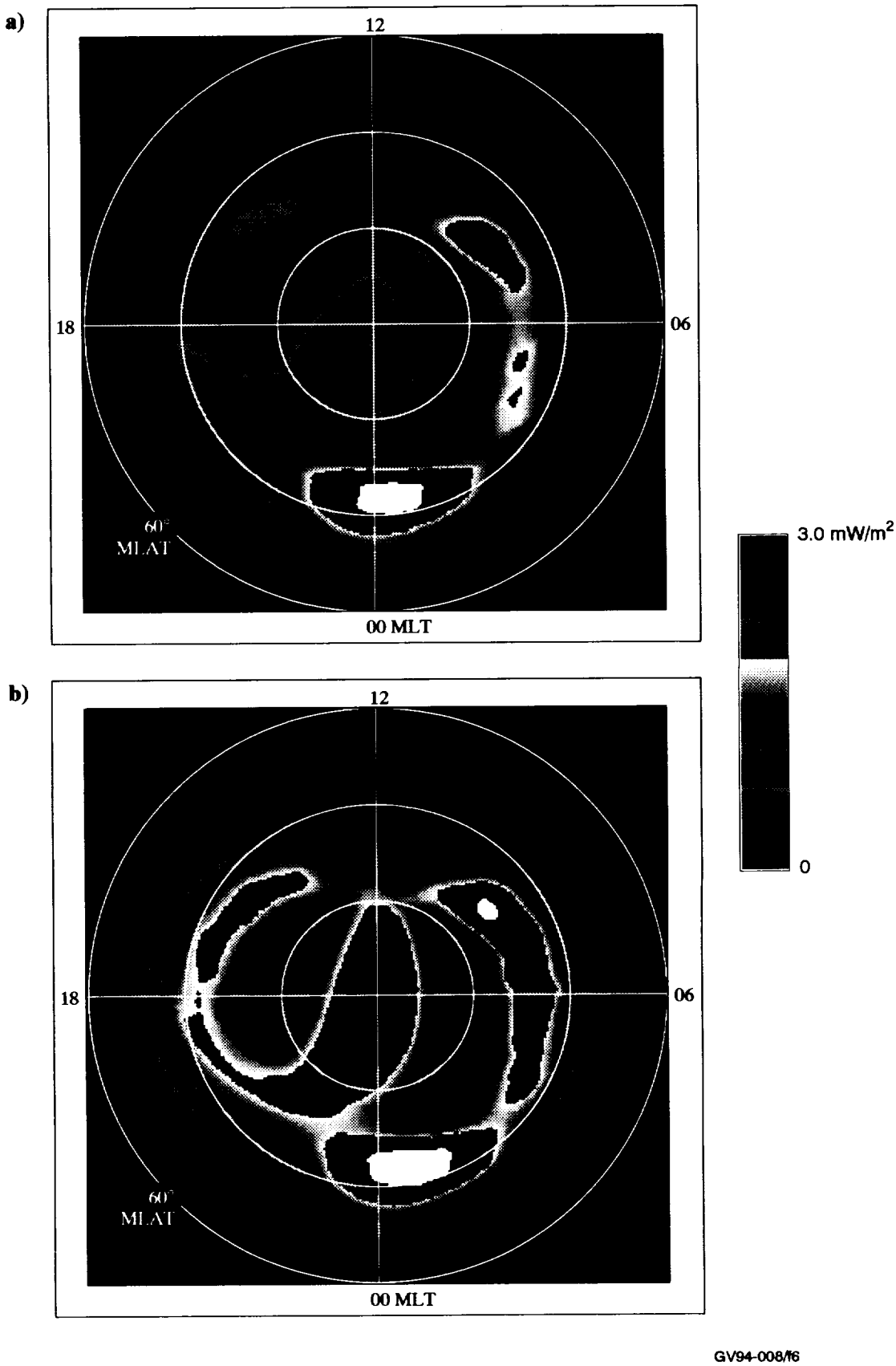

Fig. 6. Polar plots of a) the height-integrated Joule heating rate with neutral winds and b) height-integrated Joule heating rate without neutral winds (same format as Figure 2).

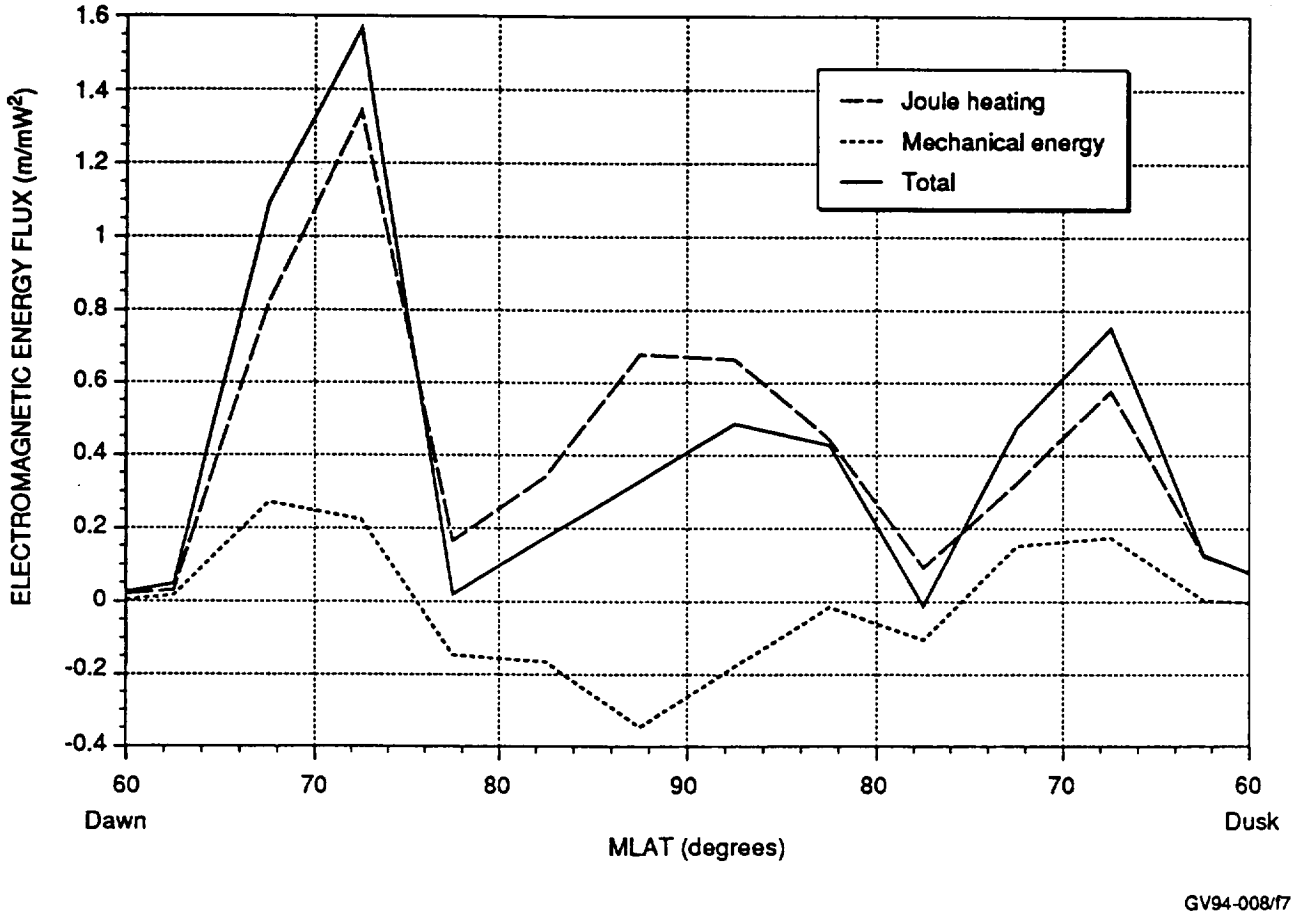

Fig. 7. Height-integrated mechanical energy transfer rate, Joule heating rate, and total electromagnetic energy flux along the dawn-dusk magnetic plane (same format as Figure 3).

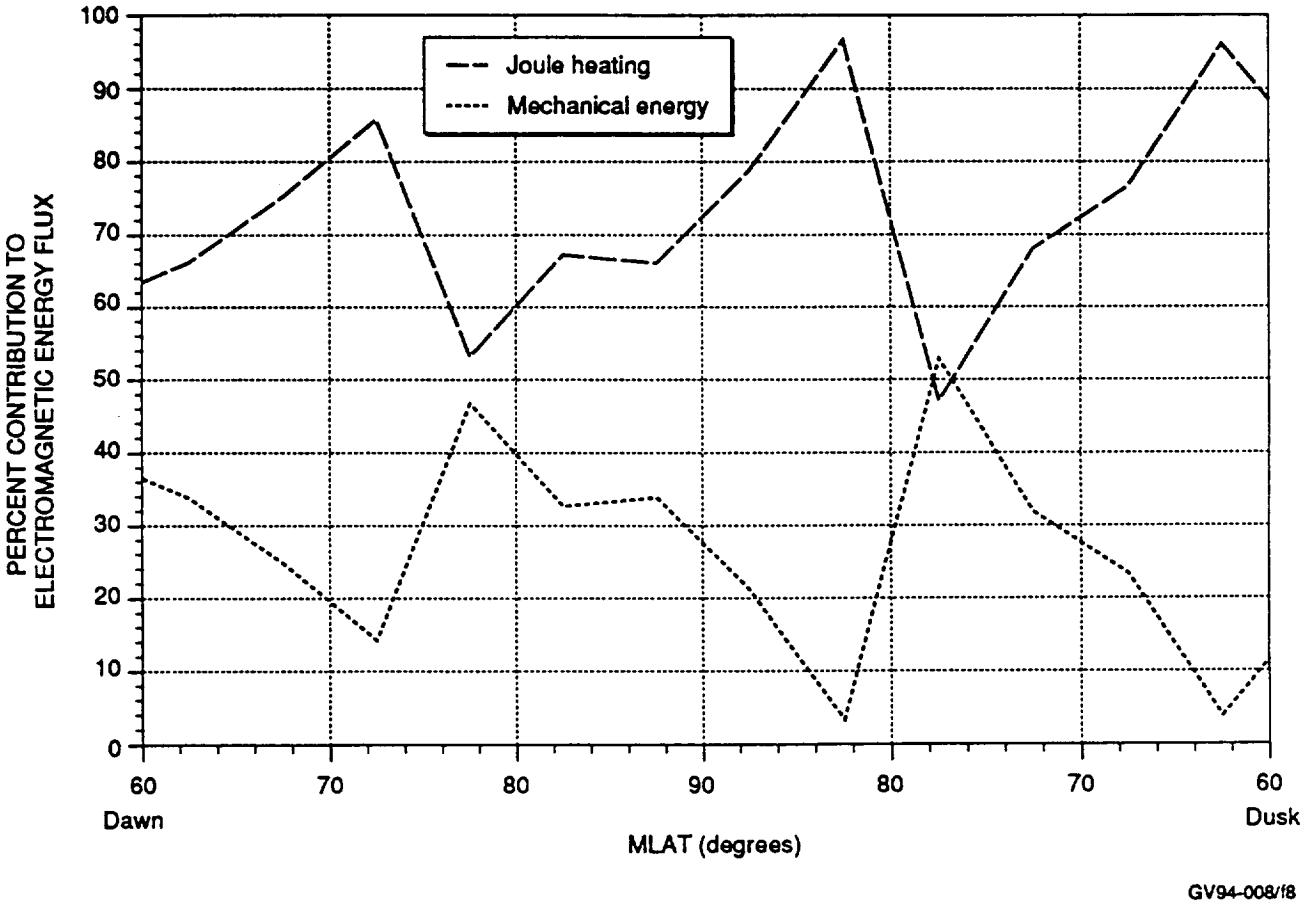

Fig. 8. Percent contribution from the Joule heating rate and the mechanical energy transfer rate to the net electromagnetic energy flux.

NASA
National Aeronautics and Space Administration

Report Documentation Page

1. Report No.	2. Government Accession No.	3. Recipient's Catalog No.

4. Title and Subtitle
Magnetospheric-Ionospheric Poynting Flux

5. Report Date
August 1994

6. Performing Organization Code

7. Author(s)
Jeffrey P. Thayer

8. Performing Organization Report No.
Final Report, SRI Project 2432

10. Work Unit No.

9. Performing Organization Name and Address
SRI International
333 Ravenswood Avenue
Menlo Park, California 94025-3493

11. Contract or Grant No.
NAS5-31214

13. Type of Report and Period Covered
Final Report

12. Sponsoring Agency Name and Address
National Aeronautics and Space Administration
Goddard Space Flight Center
Greenbelt, Maryland 20771

14. Sponsoring Agency Code

15. Supplementary Notes

16. Abstract

Over the past three years of funding, SRI, in collaboration with the University of Texas at Dallas, has been involved in determining the total electromagnetic energy flux into the upper atmosphere from DE-B electric and magnetic field measurements and modeling the electromagnetic energy flux at high latitudes, taking into account the coupled magnetosphere–ionosphere system. This effort has been very successful in establishing the DC Poynting flux as a fundamental quantity in describing the coupling of electromagnetic energy between the magnetosphere and ionosphere. The DE-B satellite electric and magnetic field measurements were carefully scrutinized to provide, for the first time, a large data set of DC, field-aligned, Poynting flux measurements. Investigations describing the field-aligned Poynting flux observations from DE-B orbits under specific geomagnetic conditions and from many orbits, were conducted to provide a statistical average of the Poynting flux distribution over the polar cap. The theoretical modeling effort has provided insight into the observations by formulating the connection between Poynting's theorem and the electromagnetic energy conversion processes that occur in the ionosphere. Modeling and evaluation of these processes has helped interpret the satellite observations of the DC Poynting flux and improve our understanding of the coupling between the ionosphere and magnetosphere.

17. Key Words [Suggested by Author(s)]	18. Distribution Statement
Poynting flux electrodynamics Joule heating mechanical energy transfer	

19. Security Classif. (of this report)	20. Security Classif. (of this page)	21. No. of pages	22. Price
UNCLASSIFIED	UNCLASSIFIED		